

2017

# Hemodynamic Regulation Of Cardiac Valve Development

Vinal Menon

*University of South Carolina*

Follow this and additional works at: <https://scholarcommons.sc.edu/etd>



Part of the [Medical Education Commons](#), and the [Other Medicine and Health Sciences Commons](#)

---

## Recommended Citation

Menon, V.(2017). *Hemodynamic Regulation Of Cardiac Valve Development*. (Doctoral dissertation). Retrieved from <https://scholarcommons.sc.edu/etd/4403>

This Open Access Dissertation is brought to you for free and open access by Scholar Commons. It has been accepted for inclusion in Theses and Dissertations by an authorized administrator of Scholar Commons. For more information, please contact [dillarda@mailbox.sc.edu](mailto:dillarda@mailbox.sc.edu).

HEMODYNAMIC REGULATION OF CARDIAC VALVE  
DEVELOPMENT

by

Vinal Menon

Bachelor of Technology  
Padmashree Dr. D.Y. Patil University, 2010

Master of Technology  
Padmashree Dr. D.Y. Patil University, 2010

Master of Science  
University of Central Florida, 2013

---

Submitted in Partial Fulfillment of the Requirements

For the Degree of Doctor of Philosophy in

Biomedical Science

School of Medicine

University of South Carolina

2017

Accepted by:

Jay Potts, Major Professor

Robert Price, Committee Member

John Eberth, Committee Member

Russell Norris, Committee Member

Gregorio Gomez, Committee Member

Cheryl L. Addy, Vice Provost and Dean of the Graduate School

© Copyright by Vinal Menon, 2017  
All Rights Reserved.

## ACKNOWLEDGEMENTS

I would like to express my sincere gratitude to the Biomedical Science program faculty and staff for their continuous motivation and inspiration throughout my graduate career.

Dr. Jay Potts, Principal Investigator and Major Professor, for his constant support and mentorship throughout my research endeavor.

Dr. Bob Price, Dr. John Eberth, Dr. Chip Norris and Dr. Greg Gomez, committee members, for giving direction to my research efforts. Dr. Eberth, for his assistance with analyzing ultrasound data and performing CFD analysis.

Ms. Lorain Junor, IRF Research Specialist, for performing the banding surgery and for equipment and software training and troubleshooting.

Dr. Katie Kathrein, Dr. Michael Jenkins, Dr. Diego Altomare, Dr. Susan Lessner and Dr. Mohamad Azhar, collaborators, for their valuable contributions.

Ms. Anna McNeal Harper, Mr. Benny Davidson, Ms. Sharon Cooper and Mr. Jeff Davis, IRF Research Specialists, for continued research support.

Dr. Wayne Carver, CBA departmental Chairman, for his motivation and encouragement. Ms. Heather Willingham, CBA Administrative Assistant, always ready to help.

Dr. Edie Goldsmith, IBS Program Director, and Graduate Office staff members, for guidance and assistance all through my graduate school years.

My parents, who taught me to be passionate and sincere in everything I do.

This study was funded in part by SPARC Graduate Research Grant, Research Development Fund grant, FirstString Research Inc., NIH INBRE grant for South Carolina P20GM103499.

## ABSTRACT

It is well established that valvulogenesis is a result of a complex interplay between genetic and environmental factors. Hemodynamics is one such environmental stimulus that is well documented to influence the development of heart valves. Using advanced imaging modalities, such as optical coherence tomography, investigators have better understood the effects of altering hemodynamic loads in the embryonic (avian) heart. However, the field of valvulogenesis is currently stagnant with a paucity of studies aiming to understand the molecular mechanisms influenced/affected by hemodynamic stimuli. Deciphering these pathways is critical from a valve development perspective, but also becomes vital as potential therapeutic targets, given the fact that several adult valve diseases have a congenital origin. Towards this end, we have developed a novel ex ovo method to alter hemodynamic stimuli through the chick embryonic heart by partially constricting the outflow tract (OFT). We acknowledge that the concept of banding a part of the developing heart has been exploited by several researchers; however, performing the banding intervention outside the eggshell not only highlights the novelty of our avian system, but also permits us to obtain sufficient tissue (from a statistical analysis standpoint) to carryout molecular biology experiments which was, until this point, impossible to achieve. Using this system, we have shown for the first time, that perturbation of intracardiac hemodynamics has consequences at the cellular and molecular level. Altered hemodynamics not only affected OFT cushion volume and expression of key players involved in valve development, but also led to a decrease in

epithelial-mesenchymal-transition, a pivotal process in valvulogenesis. The migratory capacity and secretory profile of atrioventricular cushions were also altered by changing intracardiac hemodynamics. Furthermore, when the constriction around the OFT was removed, anomalous cardiac phenotypes, resulting due to OFT banding, could not be rescued, while the expression of some genes returned to that observed in control tissue. Lastly, OFT banding seemed to have an influence on gene expression only if hemodynamics were altered at a certain developmental period. However, expression of collagen appeared sensitive to altered blood flow through the embryonic heart even at very early periods of embryonic development.

## TABLE OF CONTENTS

Acknowledgements.....	iii
Abstract.....	v
List of Tables .....	ix
List of Figures.....	x
Chapter 1: Introduction.....	1
Chapter 2: Materials and methods- molecular effects of altered intracardiac hemodynamics on OFT valve development .....	11
Chapter 3: Materials and methods- effects of releasing the constriction around the OFT .....	30
Chapter 4: Materials and methods (Preliminary study)- molecular responses to OFT banding at different developmental stages.....	33
Chapter 5: Results- molecular effects of altered intracardiac hemodynamics on valve development.....	34
Chapter 6: Results- effects of releasing the constriction around the OFT .....	58
Chapter 7: Results (Preliminary study)- molecular responses to oft banding at different developmental stages .....	71
Chapter 8: Discussion- molecular effects of altered intracardiac hemodynamics on valve development.....	72
Chapter 9: Discussion- effects of releasing the constriction around the OFT .....	84
Chapter 10: Discussion (Preliminary study)- molecular responses to oft banding at different developmental stages .....	89
Chapter 11: Conclusions.....	91
Chapter 12: Future studies .....	93

References.....	95
Appendix A: Permission to reprint .....	109

## LIST OF TABLES

Table 2.1: Reaction setup using iScript cDNA synthesis kit (BioRad) .....	20
Table 2.2: Run protocol for reverse transcription in the iCycler .....	20
Table 2.3: qPCR reaction set up .....	20
Table 2.4: Primer sequences used for qPCR.....	21
Table 2.5: Antibodies used for IF .....	26
Table 2.6: Immunofluorescence protocol .....	27
Table 2.7: Protocol for Herovici's collagen stain.....	28
Table 5.1: Differential expression of genes critical to valve development, upon OFT banding, in OFT cushion tissue of banded and control hearts .....	40
Table 5.2: Genes revealed in the microarray study validated by qPCR. Data represent changes in OFT from banded relative to that from control hearts .....	41

## LIST OF FIGURES

Figure 1.1: Early formation of heart valves .....	8
Figure 1.2: Endocardial cushions and heart valve leaflets .....	9
Figure 2.1: OFT banding .....	29
Figure 3.1: Schematic representation of our experimental paradigm .....	32
Figure 5.1: Our in vivo (ex ovo) chicken embryonic system .....	41
Figure 5.2: Ultrasound imaging .....	42
Figure 5.3: Velocity magnitude streamlines for (top) control chick hearts and (bottom) OFT banded chick hearts at the time-averaged flow velocity, peak flow conditions and late in the cardiac cycle during retrograde flow. V, ventricle; OVJ, OFT/ventricle junction; OFT, outflow tract .....	43
Figure 5.4: Wall shear stress magnitude for (top) control chick hearts and (bottom) OFT banded chick hearts at the time-averaged flow condition, during peak flow conditions and late in the cardiac cycle during retrograde flow. V, ventricle; OVJ, OFT/ventricle junction; OFT, outflow tract .....	44
Figure 5.5: Hemodynamic variables .....	45
Figure 5.6: 3D reconstructed OFT .....	46
Figure 5.7: Compensatory mechanisms for decreased OFT cushion volume and cell number .....	47
Figure 5.8: Transcriptome analysis upon OFT banding .....	48
Figure 5.9: Herovici's collagen stain .....	49
Figure 5.10: IF of OFT sections .....	50
Figure 5.11: Effect of OFT banding on mRNA levels of inhibitory smads .....	51
Figure 5.12: Downregulation of EMT/mesenchymal markers in OFT cushion from banded hearts relative to that of controls .....	52

Figure 5.13: Collagen gel assay with OFT explants .....	53
Figure 5.14: Effect of OFT banding on sert and tgm2 expression.....	53
Figure 5.15: Effect of OFT banding on htr1e and pERK1/2 .....	54
Figure 5.16: No apoptotic cells were observed in OFT cushion from banded or control hearts .....	54
Figure 5.17: IF of AV sections .....	55
Figure 5.18: Effect of OFT banding on expression of EMT markers in AV cushions.....	56
Figure 5.19: Collagen gel assay with AV cushion explants .....	56
Figure 5.20: Effect of OFT banding on proliferation of AV cushion mesenchyme with PCNA as a marker for cell proliferation.....	57
Figure 6.1: Bright field images of whole embryonic hearts illustrating the effect of OVJ band removal.....	63
Figure 6.2: Band removal did not have any significant difference in width of the outer wall of the OFT at 24 hr and 48 hr PBR time points .....	64
Figure 6.3: H&E stained heart sections obtained from stage matched controls and following band removal .....	64
Figure 6.4: qPCR analysis of the effect of band removal on relative expression of genes critical to EMT and valvulogenesis .....	65
Figure 6.5: Changes in OFT cushion volume in response to band removal .....	66
Figure 6.6: Calculation of Cushion and Cell volumes ( $\mu\text{m}^3$ ) in recovery hearts .....	67
Figure 6.7: Effect of band removal on heart rates .....	68
Figure 6.8: Effect of band removal on blood flow velocity.....	69
Figure 6.9: Effect of band removal on shear stress.....	70

# CHAPTER 1

## INTRODUCTION<sup>1</sup>

Valves in healthy adult four-chambered hearts allow for unidirectional flow of blood to both the pulmonary and systemic circuits. The fact that directionality of blood flow is a result of valves function was first observed by William Harvey who noted the importance of these structures by examining and calculating the amount of blood flowing in the body [1,2].

The adult heart has two sets of cardiac valves – semilunar (outlet) valves – aortic and pulmonary; and atrioventricular (inlet) valves – mitral and tricuspid. The tricuspid and pulmonary valves function to direct blood from the body to the lungs for oxygenation while the mitral and aortic valve function to maintain directionality of oxygenated blood flow to the body. The inlet valves have supporting structures, known as chordae tendineae, that connect the leaflets to the papillary muscle, which are absent in the semilunar valves [3].

Structure and function of cardiac valves are primarily determined during early embryonic development. Consequently, abnormally formed heart valves, especially

---

<sup>1</sup> Parts of this introduction have been excerpted from the following research articles  
(1) Menon V; Eberth JF; Goodwin RL; JD, P. Altered hemodynamics in the embryonic heart affects outflow valve development. *J Cardiovasc Dev Dis.* **2015**, 2, 108-124. (Open access)  
(2) Menon V; Eberth J; Junor L; Potts AJ; Belhaj M; DiPette DJ; Jenkins M; JD, P. Removing vessel constriction on the embryonic heart results in changes in valve gene expression, morphology, and hemodynamics. *Dev Dyn* **2017**.

defective outflow valves, are the most common type of congenital heart defects (CHDs) [4]. Abnormal cardiac valve structure may be present at birth; however, this may be asymptomatic and could subsequently predispose the individual to valve disease later in life. Thus, several adult valve diseases may be attributed to abnormal valve development which makes it imperative to understand the molecular basis of heart valve development and the effect that hemodynamics has on these processes.

### 1.1 EMBRYONIC DEVELOPMENT OF CARDIAC VALVES

The heart is the first organ to develop and function during embryogenesis. It initially forms as a tubular blood vessel comprised of endocardial endothelial cells (epithelial cell layer) surrounded by the myocardium [3] (figure 1.1a). Present between these two layers of the tubular heart is an acellular region known as the cardiac jelly (CJ); which is composed of extracellular matrix (ECM). [5]. This ECM, secreted by the myocardium, is primarily composed of glycosaminoglycans chondroitin sulfate and hyaluronan [6]. After the onset of rightward looping, the CJ expands at two distinct regions - the atrioventricular (AV) canal and the outflow tract (OFT) (figure 1.1b). These local CJ expansions are known as endocardial cushions (valve primordia) that eventually develop into the AV (inlet) and OFT (semilunar) valves [5,7]. The mechanisms of cushion development are conserved in both the AV canal and the OFT. In addition to the endocardially derived cells, neural crest cells also contribute to the OFT valves and OFT cushion epithelial-mesenchymal transition lags behind that occurring in AV cushions [3,8]. The endocardial cushions undergo differentiation, growth and remodeling to form the mature cardiac valves. The superior and inferior AV cushions fuse and remodel to form the anterior leaflet of the mitral valve and the septal leaflet of the tricuspid valve.

The left and right lateral AV cushions become the posterior mitral valve and the anterior and posterior tricuspid valve leaflets respectively [9]. The OFT cushions form the semilunar valves with the conotruncal cushions forming the right and left leaflets of the semilunar valves [10-12]. The intercalated OFT cushions form the posterior aortic and anterior pulmonic leaflets [10,12] (figure 1.2).

Epithelial-to-mesenchymal transition (EMT), a tightly regulated process, plays a crucial role in embryonic differentiation and development [13,14]. With respect to the embryonic heart, a subset of endocardial cells in the AV canal and OFT undergoes EMT in response to local signaling events thereby populating the CJ by adopting a migratory mesenchymal phenotype [7] (figure 1.1 c and d). Myocardium-derived signals induce EMT in the endocardial cells which hypertrophy, lose cell-to-cell contact and delaminate into the CJ. The endocardium then reforms a new cell layer [6,15]. Before the onset of EMT, the endocardial cells of the cushion exhibit a cobblestone appearance with undilated rough endoplasmic reticulum (RER) and underdeveloped Golgi [6]. Endocardial cells are activated immediately preceding EMT and have dilated RER and hypertrophied Golgi complexes. Mesenchymal cells, with filopodia, then migrate into the CJ.

In an *in vitro* model it was shown that chick AV canal explants (consisting of endocardial cushion cells and myocardium) cultured on collagen gels exhibit EMT [16]. Furthermore, it has been shown that only the endothelium of the AV canal and OFT, but not that of the ventricle, undergoes EMT to produce the mesenchyme; thus demonstrating a requirement for specialized spatial signaling to induce EMT [17,18]. While EMT is very active during valve development, this controlled process ceases and functions at

basal level, once mature valves have formed, to produce mesenchyme to maintain normal functionality of the valves. Failure of EMT downregulation in mature valves results in the production of excess ECM and fibrous diseased valves. While all aspects of cushion EMT are still not clearly understood, recent studies have identified key EMT players [19,20] some of which, we have shown, to be altered in response to changing intracardiac blood flow.

## 1.2 THE EFFECT OF HEMODYNAMIC STIMULI ON VALVE DEVELOPMENT

Cardiogenesis and valvulogenesis processes occur under flow conditions, as the embryonic heart beats and circulates blood soon after the primitive heart tube is formed. To meet the demands of the growing embryo, under normal conditions, the volumetric flow rates increase as does the ventricular pressure so as to pump larger blood volumes [21].

As blood flows through the embryonic tubular heart, it exerts pressure on the vessel wall. Shear stress is produced due to friction between the flowing blood and the heart wall [22]. It is known that endothelial cells sense and respond to hemodynamics by means of mechanotransducer proteins [23] and initiate rearrangement of the cytoskeleton leading to these cells being aligned parallel to the direction of flow [22]. Hemodynamics has been shown to play an important role in regulating embryonic cardiogenesis [22,24,25]. Mechanotransduction and hemodynamics are important for cushion EMT [26,27] with alterations leading to compromised valve development and pathological conditions.

Using a 3D tubular culture in vitro system in our laboratory, we have previously shown that shear stress influences the expression and deposition of fibrous ECM proteins

in both AV and OFT cushions [28,29]. However, it is not clearly understood how hemodynamics regulates (initiates and eventually terminates) EMT during heart valve development.

### 1.3 ALTERED HEMODYNAMICS AND CONGENITAL HEART DEFECTS

According to the Centers for Disease Control and Prevention (CDC), CHDs are the most common types of birth defects, affecting nearly 40,000 babies each year, and also are the leading cause of infant death in the U.S.A [30,31]. Though the incidence of CHDs is reported as 1 in every 100 live births, this percentage would be higher if embryos with CHDs were included in the statistics [32]. Abnormalities during embryonic heart development can result in miscarriages, and thus, these cases would not be reported as having a CHD [33-35].

Valvular defects are the most common type (20-30%) of CHDs [4] caused due to abnormally formed heart valves/septa. This is due to the fact that the structure and function of AV and outflow tract OFT valves are primarily determined during early embryogenesis [36]. However, many congenital valvular diseases remain asymptomatic until adulthood, thereby predisposing the patient to valve disease later in life. Treatment of diseased valves not only poses an economic constraint, but often requires valve replacement surgery [37]. The idea that several adult valve diseases can be attributed to abnormalities during development is highlighted by the fact that most of the replaced aortic valves have congenital abnormalities [38]. Valve insufficiency, valvular stenosis, ventricular septal defect, persistent truncus arteriosus, double outlet right ventricle, mitral valve prolapse, left heart hypoplasia are some of the CHDs resulting due to altered intracardiac hemodynamics [39].

Several studies have employed advanced imaging technologies to understand not only heart development but also the influence of hemodynamics on valvulogenesis [40-45]. However, till date, there have been limited studies pertaining to understanding the genetic regulation by hemodynamics on valvulogenesis. The fact that hemodynamic stimuli play a pivotal role in valvulogenesis is well documented by numerous studies which demonstrate that altering hemodynamics through the developing heart (in vivo), leads to a spectrum of congenital heart defects (CHDs) [25,46-58]. For example, insertion of glass beads in the heart tube of zebrafish obstructed blood flow at the inlet and outlet and prevented looping and proper formation of the heart chambers [25]. Vitelline vein ligation of the chick embryo was shown to affect cushion development and lead to ventricular septal defects and outflow valve defects [57]. Ligation of the left atrium of chick embryos were shown to result in hypoplastic left heart [58]. Only once underlining molecular pathways are well understood, can we develop therapeutic targets to treat congenital valve diseases that manifest even in adults. To bridge this gap, we have developed a novel in vivo (ex ovo) embryonic avian (chicken) system to alter intracardiac hemodynamics by partial OFT constriction (banding) [59]. Mammalian embryos cannot be surgically manipulated in the maternal environment, i.e., they need to be excised from the uterus. Moreover, genes controlling developmental pathways and processes in the chicken heart are similar to those in humans. In addition, the chick embryo is easily accessible to surgical manipulations and allows for downstream in vivo imaging [60,61].

The major advantage of our new banding system, compared to performing the intervention within the egg shell [62], is the ability to obtain a sufficient sample size (n) to carry out statistical analyses of key molecular biology experiments without any

compromise in embryo growth and development and cardiac physiology. Using this system, we recently reported on the genetic / cellular consequences of altering hemodynamics by increasing shear stress by banding in the embryonic chick heart [52,63] adding to the growing body of research that emphasizes the importance of maintaining normal hemodynamics during development.

The study described here aims to understand the role of blood, not as a ‘carrier’ fluid, but as a physical factor in the early development of both outlet and inlet valves. We hypothesized that altering intracardiac hemodynamic loads through the chicken embryonic heart influences both EMT and ECM production resulting in abnormal cardiac valve development.

The results described in this dissertation stem from experiments designed to answer three basic questions:

(1) What are the cellular responses to and molecular consequences of altered intracardiac hemodynamics (“Molecular effects of altered intracardiac hemodynamics on OFT valve development”)?

(2) Can the pathological phenotypes, resulting from perturbed hemodynamics through the embryonic heart, be rescued if the band around the OFT is removed (“Effects of releasing the constriction around the offt”)?

(3) Is there a period during embryonic development where the heart is more susceptible to changes in hemodynamics (“Molecular responses to OFT banding at different developmental stages”)?

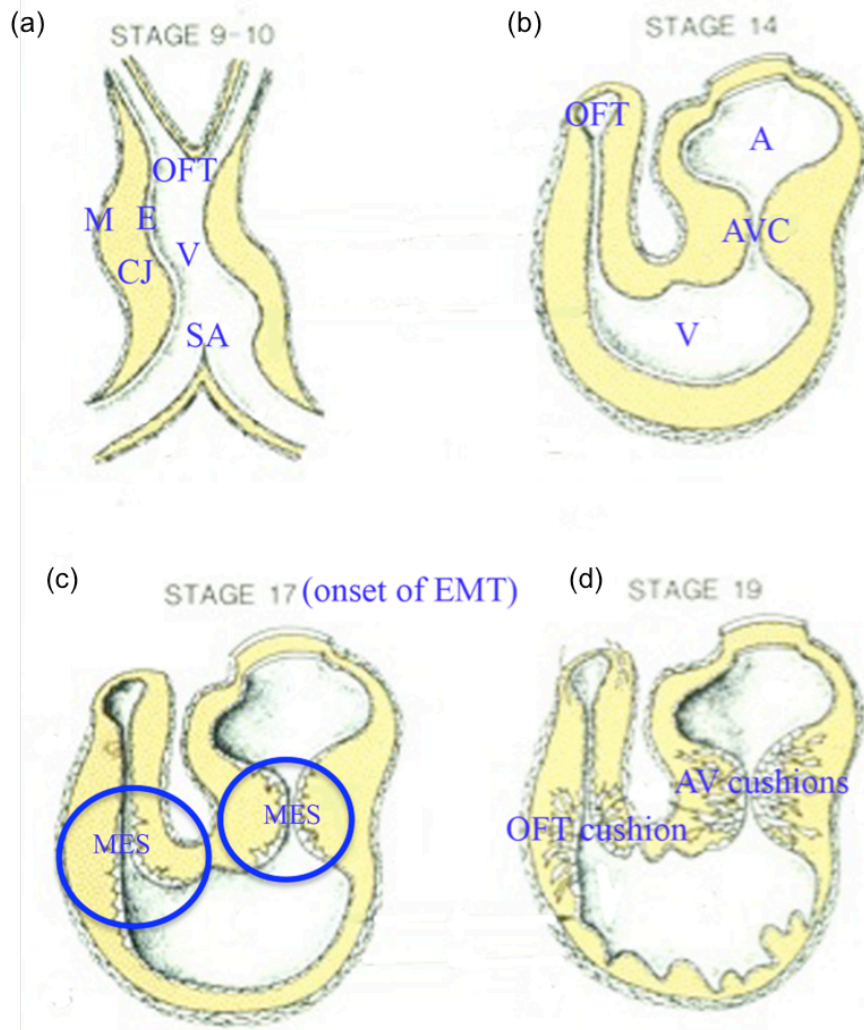


Figure 1.1: Early formation of heart valves. M: Myocardium, E: Endocardium, CJ: Cardiac jelly, OFT: Outflow tract, V: Ventricle, SA: Sinus arteriosus, AVC: Atrioventricular canal, MES: Mesenchyme

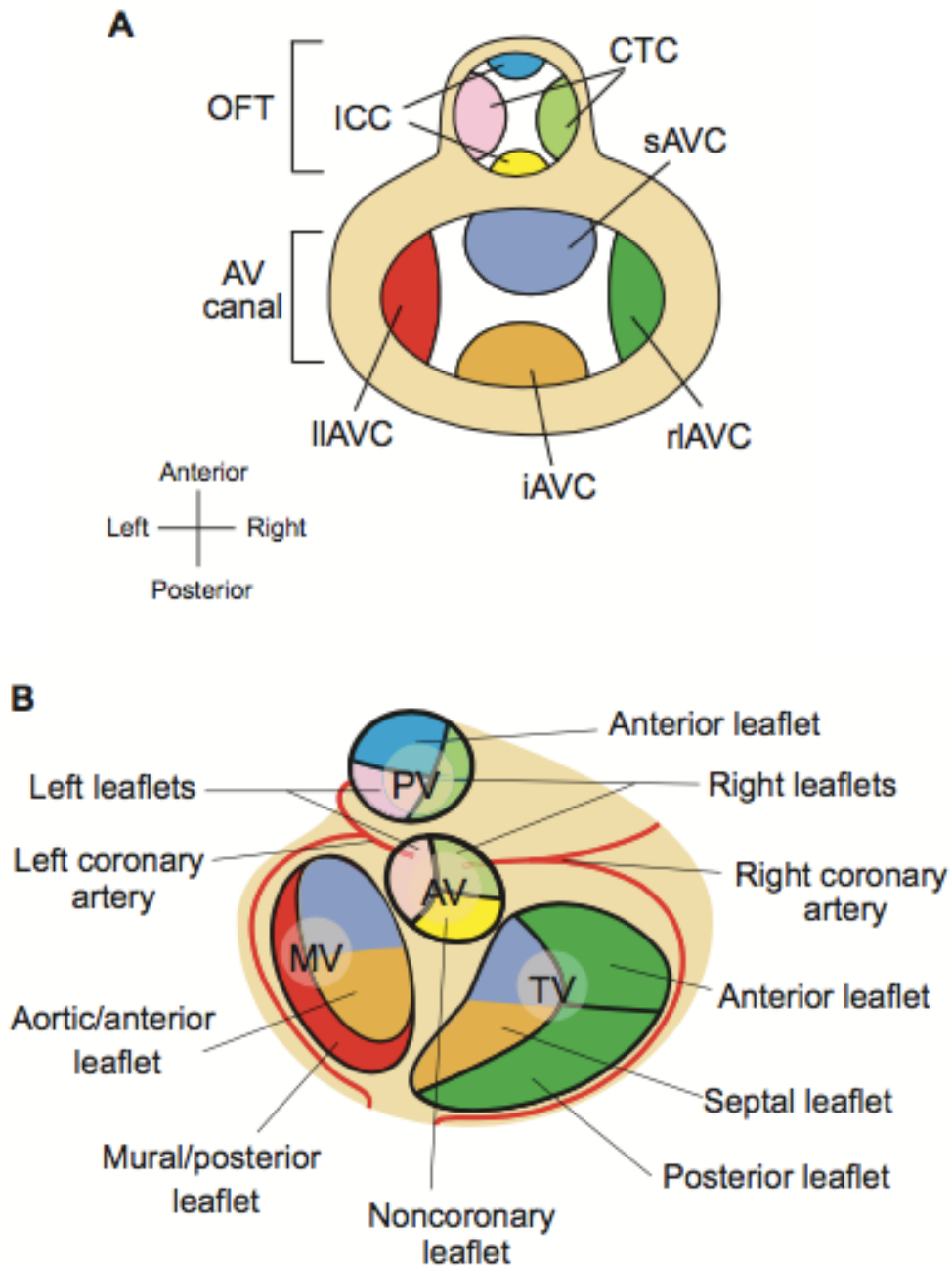


Figure 1.2: Endocardial cushions and heart valve leaflets. (A) Schematic of endocardial cushions in the atrioventricular (AV) canal and the outflow tract (OFT). The figure is a superior view of the heart with atria removed. The cushions are color coded to correspond to their derived valve leaflets illustrated in B. CTC. conotruncal cushions; ICC. intercalated cushions; sAVC. superior AV cushion; iAVC. inferior AV cushion; rIAVC. right lateral AV cushion; lIAVC. left lateral AV cushion. (B) Schematic (superior view) of atrioventricular and semilunar valve leaflets that develop from the

corresponding cushions color coded in A. PV, pulmonary valve; AV, aortic valve; TV, tricuspid valve; MV, mitral valve.

(reproduced with permission from Lin, C.; Lin, C.; Chen, C.; Zhou, B.; Chang, C. Partitioning the heart: Mechanisms of cardiac septation and valve development. *Development* **2012**, *139*(18), 3277-3299. doi: 10.1242/dev.063495 [64]).

## CHAPTER 2

### MATERIALS AND METHODS- MOLECULAR EFFECTS OF ALTERED INTRACARDIAC HEMODYNAMICS ON OFT VALVE DEVELOPMENT<sup>2</sup>

Results described in this dissertation were obtained by performing experiments on chicken embryonic hearts. Avian embryos are not considered vertebrate animals under IUCAC regulations.

#### 2.1 OBTAINING CHICKEN EMBRYOS FOR SURGERY

Fertilized Bovan chicken eggs (Morgan Poultry Center, Clemson, SC) were incubated (blunt end up) in a humidified rocker incubator at 40<sup>0</sup>C to obtain embryos at Hamilton and Hamburger (HH) stage 17 [65]. At this stage, the egg shell was sterilized with 70% ethanol and gently cracked, with a scalpel handle. The contents of the egg, with the embryo atop the yolk, were then carefully released into a deep petri dish containing warm Tyrode's buffer supplemented with 1g/L sodium bicarbonate. Embryos that appeared abnormal, not at the right embryonic stage, incorrectly oriented on the yolk and/or were bleeding were not used for any experiments.

---

<sup>2</sup> Parts of this chapter have been excerpted from the following research articles

- (1) Menon V; Eberth JF; Goodwin RL; JD, P. Altered hemodynamics in the embryonic heart affects outflow valve development. *J Cardiovasc Dev Dis.* **2015**, 2, 108-124. (Open access)
- (2) Menon V; Junor L; Balhaj M; Eberth JF; JD, P. A novel ex ovo banding technique to alter intracardiac hemodynamics in an embryonic chicken system. *J Vis Exp* **2016**, 13.

## 2.2 OFT BANDING TO ALTER INTRACARDIAC HEMODYNAMICS

Embryos were randomly divided into two groups: control and banded. Those in the banded group had their OFT partially constricted, at the OFT/ventricular junction (OVJ) as mentioned below (figure 2.1). Control embryos were not subjected to the banding intervention.

1 cm-long threads were tweezed out from a single 11/0 nylon surgical suture and were tied into individual knots which were then UV sterilized. Before surgery, about 6ml of warm Tyrode's buffer was pipetted onto the embryo. The suture was then positioned at the OVJ and the free end was then passed through the knot, thereby constricting the OFT at the OVJ. After surgery, another 6ml of warm Tyrode's buffer was pipetted onto the embryo and yolk surface. Banding caused a 28% luminal constriction of the OFT, on average, as determined by optical coherence tomography (OCT).

Control and banded embryos were incubated, *ex ovo*, at 40°C in a humidified incubator for a period of 24 hr. (For all experiments in this dissertation, banding was performed on HH 17 chick embryos and studies were performed 24 hr post-surgery, unless otherwise stated).

## 2.3 ANALYSIS OF CHANGE IN BLOOD FLOW VELOCITY

Changes in blood flow velocity at the OVJ of banded (n=5) and control (n=5) embryos were determined by ultrasound using the Vevo 770 imaging system (VisualSonics, Toronto, ON, Canada). The petri dish containing the embryo to be imaged was placed on a heating pad and carefully filled to the brim with warm Tyrode's buffer, making sure that the yolk sac was intact. A 708 scanhead, operating in B mode, was used to obtain a 2D image of the beating heart and the stage was moved till the OVJ was

clearly visible. The PW mode, at a pulse repetition frequency of 20 kHz, was used to obtain a waveform. For each embryo, peak velocities at the OVJ were measured for ten heartbeats. From the resulting data, the heart rate in beats-per-minute (BPM) was calculated by measuring the foot-to-foot time of the velocity wave so that  $HR=60/T$ . Time-dependent centerline and spatially averaged velocities were measured from the PW Doppler waveforms using built-in software algorithms and these waveforms were digitized using the ImageJ figure calibration plugin so that the time-averaged and peak velocities could be found [66]. Embryos with a slowing heart rate during the test were not used for analysis.

#### 2.4 THREE DIMENSIONAL (3D) OFT RECONSTRUCTION AND DETERMINATION OF EXTENT OF EMT

Banded (n=3) and control (n=3) embryos were carefully excised from the yolk and fixed overnight in 2% paraformaldehyde (PFA). Extra embryonic membranes were left intact so as to prevent sectioning artifacts. Fixed embryos were dehydrated through an alcohol series, cleared with xylene, and penetrated with and embedded in paraffin. 5  $\mu\text{m}$  serial sections were obtained on a microtome and stained with hematoxylin & eosin (H&E). Individual nuclei were counted from the H&E images of banded and control OFTs to determine the number of cells that invaded the cushions by EMT. TIFF images of the complete OFT were captured using a Nikon Optiphot-2 light microscope at a total magnification of 40X and loaded into the AMIRA software package (FEI Visualization Science Group, Burlington, MA, USA). All sections were aligned and the OFT and myocardium were segmented. A 3D model of the OFT was then generated from which the volume of the OFT cushion was determined. Models were reduced to 2,500 faces to improve manageability and exported as Stereolithography (.stl) files to Geomagic Studio

(Rock Hill, SC, USA) for smoothing and anatomical measurements of cross-sectional area and perimeter at the OVJ. These reconstructions were then converted into the Initial Graphics Exchange Specification (IGES) file format for finite element analysis.

## 2.5 COMPUTATION FLUID DYNAMICS (CFD)

IGES files were imported as a continuous geometry into COMSOL Multiphysics 4.3b (Comsol, Burlington, MA, USA). In COMSOL, faces perpendicular to the axis of blood flow were generated at the proximal (ventricle) and distal (OFT) sides to act as inlet and outlet conditions. A single representative 3D model was generated for the control, and a single representative 3D model was generated for the banded hearts. From these models, the cross-sectional areas at the OVJ were measured using Geomagic (Control:  $A = 14,491$ ; Banded:  $A = 1714 \mu\text{m}^2$ ). Unique volumetric flow inlet boundary conditions were applied for each of the control ( $n = 5$ ) and banded hearts ( $n = 5$ ). At a given cross-section, the time-averaged, peak and late retrograde flow velocities were calculated from the spatially-averaged velocity and used to calculate the inlet time-averaged, peak and late retrograde volumetric flow rates. A zero-pressure boundary condition was applied at the distal location for all samples. Despite the importance of a changing geometry during the cardiac cycle, our analyses are limited by the available imaging modalities to tissue arrested under physiological loading. Accordingly, a rigid wall assumption and no-slip boundary conditions were assigned for the remaining surfaces. Using a hematocrit of 19.4% for HH Stage 16–17 chick embryos, we assumed that blood, at high shear rates, behaved as a Newtonian fluid; therefore, the density  $\rho = 1025 \text{ kg/m}^3$  and apparent dynamic viscosity  $\mu = 0.0015 \text{ Pa}\cdot\text{s}$  remained constant in our simulations. Accordingly, the lowest time-averaged shear rate from our simulations was  $\gamma$

=  $424 \pm 113 \text{ s}^{-1}$ . Similarly, low peak Reynolds numbers ( $Re = 7.08 \pm 1.06$ ) indicated laminar flow behavior, while a rough estimate of the Womersley numbers ( $\alpha = 0.18 \pm 0.02$ ), a metric used to relate pulsatile-inertial to viscous effects, yields a low value, as well. Collectively, these results suggest that quasi-static conditions are sufficient for analysis [67]. Wall shear stresses were calculated on the surface of the blood-tissue interfaces and spatially averaged for each of the flow conditions (time-averaged, peak and late cardiac cycle retrograde flow). The time-averaged pressure drop across the stenosis was calculated as the difference between the inlet and outlet ( $P = 0 \text{ mmHg}$ ) pressures.

## 2.6 EXTRACTION OF TOTAL RNA FROM OFT CUSHIONS

OFT cushions (including the myocardial sleeve) were dissected after whole hearts were carefully excised from banded and control embryos. Each sample ( $n=3-4$ ) consisted of OFT cushions from about 20-22 pooled hearts. Total RNA was extracted using the GeneJET RNA purification kit (Thermo Scientific, Waltham, MA, USA) according to the manufacture's protocol. RNA was eluted from the columns with 50ul of nuclease-free (NF) water (provided in the kit). After RNA extraction, the purity and concentration of the isolated RNA were determined spectrophotometrically using the NanoPhotometer Pearl (Implemen, GmbH, Munich, Germany). All RNA samples had A260/280 and A260/230 ratios  $> 1.9$ . RNA samples were stored at  $-80^{\circ}\text{C}$  until further analysis.

## 2.7 COMPLEMENTARY DNA (cDNA) SYNTHESIS

cDNA was synthesized from total RNA using the iScript cDNA Synthesis Kit (BioRad, Hercules, CA, USA). Five hundred nanograms of RNA was used in each reaction. Reverse transcription was carried out in the iCycler thermal cycler (BioRad,

Hercules, CA, USA). Each cDNA sample was diluted 5X with NF water before being used for qPCR.

## 2.8 QUANTITATIVE REAL-TIME POLYMERASE CHAIN REACTION (qPCR)

qPCR was carried out using Fast SYBR Green Master Mix (Applied Biosystems Foster City, CA, USA) on a BioRad CFX connect system (BioRad, Hercules, CA, USA). The following run conditions were used: enzyme activation at 95<sup>0</sup>C for 3min, denaturation at 95<sup>0</sup>C for 10 sec, and annealing/extension at 60<sup>0</sup>C for 30 sec (40 cycles). Water-only negative control was included for each gene. A melt curve analysis was performed on each run. Each sample was run in triplicate and qPCR was repeated three times per gene. Relative gene expression was quantified using the Pfaffl method [68] with *arbp* as the housekeeping (normalizing) gene. Target-specific primers were designed using the Primer-BLAST software tool [69]. Primer sequences used for qPCR are listed in table 2.4.

## 2.9 MICROARRAY

Total RNA was extracted from OFT tissue from control and banded hearts as in 2.6. Each sample (n=6) consisted of pooled OFT tissue from 25 hearts. RNA quality was assessed using an Agilent 2100 Bioanalyzer and RNA Integrity Numbers ranged from 9.3 to 10.0. Microarray experiments were performed using Affymetrix's platform. Total RNA samples were amplified and biotinylated using GeneChip WT PLUS Reagent Kit (Affymetrix, Santa Clara, CA). Briefly, 100 ng of total RNA per sample was reverse transcribed into ds-cDNA using NNN random primers containing a T7 RNA polymerase promoter sequence. T7 RNA polymerase was then added to cDNA samples to amplify RNA, and then RNA was copied to ss-cDNA and degraded using RNase H. ss-cDNA

molecules were then fragmented and terminally labelled with biotin. Amplified and labeled samples were hybridized to ChiGene-1\_0-st arrays (Affymetrix, Santa Clara, CA) for 16 h at 45°C using a GeneChip Hybridization Oven 640 and a GeneChip Hybridization, Wash, and Stain Kit (Affymetrix, Santa Clara, CA). Hybridized arrays were washed and stained using GeneChip Fluidics Stations 450 (Affymetrix, Santa Clara, CA). Arrays were then scanned using a GeneChip Scanner 3000 7G system and computer workstation equipped with GeneChip Command Console 4.0 software (Affymetrix, Santa Clara, CA).

Following completion of array scans, probe cell intensity (CEL) files were imported into Expression Console Software (Affymetrix, Santa Clara, CA) and processed at the gene-level using the Robust Multichip Analysis (RMA) algorithm to generate CHP files. After confirming data quality within Expression Console, CHP files containing log<sub>2</sub> expression signals for each probe were imported into Transcriptome Analysis Console Software version 3.0.0.466 (Affymetrix, Santa Clara, CA) to perform differential gene expression analysis between the experimental groups. A one-way between-subject analysis of variance statistics and p-value of 0.05 and a fold change of 1.5 were used as cutoff parameters.

## 2.10 IMMUNOFLUORESCENCE (IF)

Five-micron paraffin-embedded heart sections containing OFT and AV cushions were stained by IF probing for targets listed in table 5. Appropriate secondary antibodies were used. Slides were deparaffinized by immersion in xylene and rehydrated by immersion in decreasing concentrations of ethanol. Staining was performed as in table 6. Images were captured on the Zeiss LSM 510 META confocal scanning laser microscope

under identical settings for control and banded heart sections.  $n > 4$  for each experiment. Each experiment included a no-primary negative control.

### 2.11 HEROVICI'S COLLAGEN STAIN

Five-micron paraffin-embedded heart sections containing OFT cushions were stained with Herovici's collagen stain (American MasterTech, Lodi, CA) to determine the level of young collagen in cushions from banded vs. control hearts. Slides were deparaffinized as mentioned in section 2.10 and then stained as in table 7 ( $n > 3$  for each group). Images were captured using the Invitrogen EVOS FL Auto Cell Imaging System. Images from control and banded section were collected under identical microscope settings.

### 2.12 TUNEL ASSAY

The DeadEnd Fluorometric TUNEL System (Promega, Maddison, WI) was used to investigate the effect of altered hemodynamics on apoptosis in OFT cushion tissue from banded vs. control hearts. Paraffin-embedded heart sections were deparaffinized as mentioned in 2.10. Sections were then permeabilized with 0.2% Triton for 5 min. After rinsing in PBS, slides were equilibrated with equilibration buffer for 10 min at RT. The TdT reaction mix was then added to sections followed by incubation at  $37^{\circ}\text{C}$  for 60 min. After labeling, reaction was stopped by immersing slides in SSC for 15 min and rinsed in PBS. Nuclei were labeled with DAPI. Slides were mounted with DABCO and images captured with the Nikon E600 Widefield Epifluorescence and Darkfield Microscopy System. Control and banded samples were capture with identical microscope settings.  $n=3$ .

### 2.13 COLLAGEN GEL ASSAY

OFT and AV cushion tissues were dissected from control (n=3, 5 respectively) and banded (n=3, 4 respectively) hearts and seeded onto a PureCol (Advanced BioMatrix, Carlsbad, CA) collagen gel in a 24-well plate (1 explant/well).

Collagen gels were prepared by mixing chilled PureCol (3mg/ml) with MEM and HEPES in a ratio of 8:1:1. 400  $\mu$ l of gelation solution was dispensed into wells of a 24-well plate and allowed to solidify at 37<sup>0</sup>C.

Cushion explants were then seeded on formed collagen gels. Explants were allowed to attach for 24 hr at 37<sup>0</sup>C, after which DMEM, containing 10% FBS, penicillin/streptomycin and Amphotericin B, was added to each well and then cultured for another 24 hr. Then, culture media was aspirated, gels were fixed with 2% PFA and nuclei stained with DAPI. Z-stacks were captured on the Invitrogen EVOS FL Auto Cell Imaging System under identical settings, which were then imported into AMIRA, from which the number of mesenchymal cells invading the gel and the depth of gel invaded (bounding box) were determined.

### 2.14 STATISTICAL ANALYSIS

Student's t-test was used for in-between group analysis with alpha = 0.05. Statistics and graphs were generated using Prism 5 (GraphPad Software, San Diego, CA, USA). Data are reported as mean  $\pm$  SEM.

Table 2.1: Reaction setup using iScript cDNA synthesis kit (BioRad)

<b>Component</b>	<b>Volume per reaction</b>
5X iScript reaction mix	4 $\mu$ l
iScript Reverse Transcriptase	1 $\mu$ l
RNA template	Scaled to 500 ng
NF water	Adjusted to 20 $\mu$ l
Total volume	20 $\mu$ l

Table 2.2: Run protocol for reverse transcription in the iCycler

<b>Reaction step</b>	<b>Temperature</b>	<b>Duration</b>
Priming	25 <sup>0</sup> C	5 min
Reverse transcription	46 <sup>0</sup> C	20 min
Enzyme inactivation	96 <sup>0</sup> C	1 min
Hold	4 <sup>0</sup> C	$\infty$

Table 2.3: qPCR reaction set up

<b>Component</b>	<b>Volume per reaction</b>
Fast SYBR Green Master Mix (2X)	10 $\mu$ l
Forward primer (10 $\mu$ m)	0.3 $\mu$ l
Reverse primer (10 $\mu$ m)	0.3 $\mu$ l
Nuclease-free water	7.4 $\mu$ l
cDNA	2 $\mu$ l

Total volume	20 $\mu$ l
--------------	------------

Table 2.4: Primer sequences used for qPCR

Gene	Forward (F) and reverse (R) primers
<i>arbp</i>	F: 5'-GCTTTGCTTCGGTCTTTGAG- 3' R: 5'-AACAACTTTCCGATCACCAC- 3'
<i>klf2</i>	F: 5'-GCTTCTACCAGACAAACCCG- 3' R: 5'- CAGGACTGGCCCATAACTGT-3'
<i>rhoA</i>	F: 5'-CAGCACCTGCACTTGAGTA- 3' R: 5'GCATCCTGTGAGTGCAGAAA- 3'
<i>collagen 1</i>	F: 5'- TACCACTGCAAGAACAGCGT-3' R: 5'- TCGGTGACCCCATAGGTGAA-3'
<i>collagen VI</i>	F: 5'- AGCAGGTTTTCTTGCTGAA- 3' R: 5'-TGCCAAGGATTTTCATCATCA-

	3'
<i>vinculin</i>	F: 5'-CAGGTAGTATCGGCTGCTCG- 3' R: 5'-CCACCAGCCCTGTCATCTTT- 3'
<i>elastin</i>	F: 5'-GTATCCCATCAAAGCTCCCA- 3' R: 5'-CAGCTCCGTATTTAGCTGCC- 3'
<i>periostin</i>	F: 5'- GGATGGTATGAGAGGATGTC-3' R: 5'GCAAAGAAAGTGAATGAACC-3'
<i>tenascin</i>	F: 5'- AGGACACAGCCTCTGCAAGT-3' R: 5'-TACTGCCCTGAGAGCTGAT- 3'
<i>cdh11</i>	F: 5'- AAGACACTGGACCGAGAGGA-3' R: 5'- TTCTGAGGGCGGTTCCAAAG-3'
<i>filamen A</i>	F: 5'- CGGCGACTACACCATCAACA-3'

	R: 5'-GTCAC TTTGGTGGGGTCGAA- 3'
<i>tgfβrIII</i>	F: 5'-CTCTTACCGTCGTGGGCATT- 3' R: 5'-CTGCTTCCCCTGTGTGAGAG- 3'
<i>tgfβ2</i>	F: 5'- GAGAAAGCCAACCACAGAGC-3' R: 5'-GGTACAGCTCTATCCGCTGC- 3'
<i>tgfβ3</i>	F: 5'-CACAATGAGTTGGGCATTG- 3' R: 5'- GGA ACTCTGCTCGAAACAGG-3'
<i>snai2</i>	F: 5'-CACGCTCCTTCCTGGTCAAG- 3' R: 5'- GGCTGCGGTATGATAGGGAC-3'
<i>has2</i>	F: 5'-CACCGCTGCTTACATTGTGG- 3' R: 5'- TGTGATGCCAGGATAGCACC-3'
<i>mmp2</i>	F: 5'-

	TGATGATGACCGCAAGTGGG-3' R: 5'- TGTAGATCGGGGCCATGAGA-3'
<i>aqp1</i>	F: 5'- AAAATGTTCTGGAGGGCGGT-3' R: 5'-CTGAGTTGCTGATGTCCCGT- 3'
<i>smad 6</i>	F: 5'- TGCGAATGTCAGAGGTTGGG-3' R: 5'- CTCGTCGTTAGGAGACAGCC-3'
<i>smad 7</i>	F: 5'-CCAGACCGACGACGCAG-3' R: 5'- ATACCTGGAGTAGGGCGGAG-3'
<i>htrel</i>	F: 5'-CACCGACAGCCAAAACCTCCT- 3' R: 5'- CAGCCAGGTCCAAGTCATTCT-3'
<i>thsd7a</i>	F: 5'- TGTGTGGAGGTGGCATTCAAA-3' R: 5'- GCCTTGAGGCTTCTTTTCCTTG-3'
<i>pdgfa</i>	F: 5'-

	<p>GTGTCAAGGTGGCAAAAGTG-3'</p> <p>R: 5'-</p> <p>CCCTAGGCCTTCCAGTTTCTT-3'</p>
<i>tbx18</i>	<p>F: 5'-ACTAGCCAGCTCTGTAGCCT-</p> <p>3'</p> <p>R: 5'-TTGGGGGTGCAAATGTCTCA-</p> <p>3'</p>
<i>icf21</i>	<p>F: 5'-</p> <p>TAACAAAGAGTTCGGGGCGT-3'</p> <p>R: 5'- CCTTCCTGGCTCACACCATT</p> <p>-3'</p>
<i>aldha12</i>	<p>F: 5'-</p> <p>TGAATGTGGGGGTAAAGGGC -3'</p> <p>R: 5'-</p> <p>CAGGCCCAAAAATCTCCTCCT -3'</p>
<i>cdh6</i>	<p>F: 5'-</p> <p>GGGCGGATTATCAGGAACCA-3'</p> <p>R: 5'-</p> <p>TGAGTCAGGTGGCGTAGACT-3'</p>
<i>wt1</i>	<p>F: 5'-</p> <p>TGAAACGGCACCAAAGACGA-3'</p> <p>R: 5'-</p> <p>GGCTTTTCACTTGTTTTACCTGT -</p>

	3'
<i>cd44</i>	F: 5'- TCATTCTTCTGGAGGAGGTGAA-3' R: 5'- ACGTAGACCTAGTACTTGCAGGA- 3'
<i>bmp10</i>	F: 5'-TGAAGACCTTGCTTCCCACC- 3' R: 5'-GTGTAGAGTCTCAGCTCCGC- 3'
<i>tgm2</i>	F: 5'- AGAGCGAAGGGGTTTACTGC-3' R: 5'- TTGACCTCCGCAAAGACGAA-3'
<i>sert</i>	F: 5'-TGGTTCTACGGCATCACCCA- 3' R:5'- GACAGAAAGCTGCAAGTGACAA- 3'

Table 2.5: Antibodies used for IF

Target	Host species	Company
Type I Collagen	Rabbit	Millipore

Periostin	Rabbit	Abcam
IST-9	Mouse	Abcam
PCNA	Mouse	Novus Biologicals
Vimentin	Mouse	Sigma
Fibronectin	Rabbit	Santa Cruz Biotechnology
Phospho-ERK1 (pThr <sup>202</sup> /pTyr <sup>204</sup> ) and ERK2 (pThr <sup>185</sup> /pTyr <sup>187</sup> )	Rabbit	Sigma
N cadherin	Mouse	Developmental Studies Hybridoma Bank
TGM2	Rabbit	Neomarkers

Table 2.6: Immunofluorescence protocol

<b>Step</b>	<b>Reagent</b>	<b>Time/duration</b>
Permeabilize	PBS/ 0.1% Triton – X	3x – 15 min each
Glycine wash	0.3M Gly	30 min RT
Rinse	PBS	3x – 5 min each
Block	2% BSA/PBS	1h @ 37 <sup>0</sup> C
Rinse	PBS	3x – 5 min each
Probe with 1 <sup>0</sup>	Primary ab (1:100) in 1% BSA/PBS	Overnight at 4 <sup>0</sup> C

Rinse	1% BSA/PBS	2x – 15 min each
Rinse	PBS	3x – 5 min each
Probe with 2 <sup>0</sup>	Secondary Ab (1:100) in 1% BSA/PBS	1 h @ 37 <sup>0</sup> C
Rinse	1%BSA/PBS	2x - 15 min each
Rinse	PBS	3x – 5 min each
Nuclear stain	DAPI (1:5000)	20 min @ RT
Rinse	PBS	2x 15 – min each
Mount	DABCO	

Table 2.7: Protocol for Herovici's collagen stain

<b>Step</b>	<b>Duration</b>
Immerse in Wigert's Hematoxylin	5 min
Rinse with tap water	45 sec
Immerse in Herovici's working solution	2 min
Immerse in 1% acetic acid	2 min
Dehydrate with absolute alcohol	3 changes, 1 min each
Clear with xylene	3 changes, 1 min each

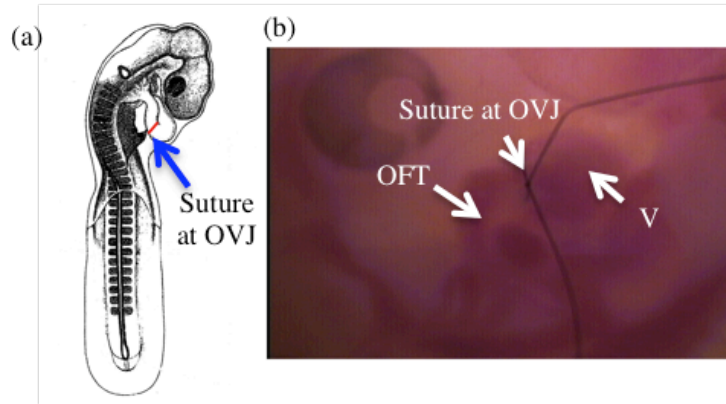


Figure 2.1: OFT banding. (a) Schematic representation of banding site. (b) Ex ovo banded embryo imaged 24h after surgery. OVJ: OFT/Ventricle junction; V: ventricle

## CHAPTER 3

### MATERIALS AND METHODS- EFFECTS OF RELEASING THE CONSTRICTION AROUND THE OFT<sup>3</sup>

#### 3.1 REMOVAL OF THE BAND AROUND THE OFT

After correct staging and visualization of intact blood islands and embryo posture, the OFT of HH 17 chick embryos was banded at the junction of the OFT and ventricle (OVJ) using surgical suture as mentioned in 2.2. Embryos in the control group were not subjected to OFT banding. Both cohorts of embryos were then allowed to develop, ex ovo, for 24 hr in a humidified incubator. 24 hr after banding, embryos in the banded group had the suture surgically removed by carefully cutting the knot. Any embryos that showed signs of bleeding were not used in the study. Following band removal, embryos were maintained ex ovo for two time points: 24 hr post-band removal (PBR) and 48 hr PBR. Control embryos were stage-matched with PBR embryos. Thus, embryos were divided into the following four groups: (1) 24 hr PBR Control, (2) 24 hr PBR Recovery, (3) 48 hr PBR Control and (4) 48 hr PBR Recovery (figure 3.1).

#### 3.2 ULTRASOUND-MEDIATED ANALYSIS OF BLOOD FLOW VELOCITY

Embryos from all four groups were subjected to 2D ultrasound imaging using the Vevo 3100 imaging system (VisualSonics, Toronto, ON, Canada) and velocity data were

---

<sup>3</sup> Parts of this chapter have been excerpted from the following research articles  
(1) Menon V; Eberth J; Junor L; Potts AJ; Belhaj M; DiPette DJ; Jenkins M; JD, P.  
Removing vessel constriction on the embryonic heart results in changes in valve  
gene expression, morphology, and hemodynamics. *Dev Dyn* **2017**.

analyzed as detailed in 2.3. Embryos that demonstrated a decreased heart rate or signs of bleeding during imaging were excluded from analysis. (24 hr PBR control: n = 9; 24 hr PBR recovery: n = 6; 48 hr PBR control: n = 7; 48 hr PBR recovery: n = 7)

### 3.3 TOTAL RNA EXTRACTION, cDNA SYNTHESIS AND qPCR

Total RNA was extracted from OFT cushion tissue using the GeneJET RNA purification kit and quantified as mentioned in 2.6. Each sample (n = 3 for each group) consisted of OFT tissue pooled from 15 – 20 hearts. Five hundred nanograms of RNA were converted into cDNA using the iScript cDNA Synthesis Kit (BioRad, Hercules, CA, USA) as described in 2.7. Before performing qPCR, each cDNA sample was diluted five times with NF water. qPCR was performed using SYBR green chemistry and data analyzed as mentioned in 2.8.

### 3.4 DETERMINATION OF OFT CUSHION AND CELL VOLUME AND CFD ANALYSIS

OFT cushion and cell volumes were determined from AMIRA 3D models generated using H&E stained TIFF images of the entire OFT as in 2.4 (n = 3 for each group). Cell volume was determined using the same AMIRA software on the same images following the segmenting of the nuclei of cells in the OFT cushion. Every fourth slice was taken for cell volume calculation as we assumed that taking every fourth slice would not contain the same cells. Cushion volumes and cell volumes were determined and used in determining the ratios of cell volume to cushion volume.

From AMIRA, 3D reconstructed OFT from each of the four groups, was reduced to 2,500 faces and exported as a stereolithography (.stl) file. The .stl files were then imported into Geomagic Design X (3D Systems, Rock Hill SC, USA) where 3D reconstructions were smoothed, re-meshed, and surfaced. The final model was exported

as an Initial Graphics Exchange Specification (IGES) file format and imported into COMSOL Multiphysics 4.3b (Comsol, Burlington, MA, USA) for CFD analysis. Planar faces perpendicular to the inlet and outlet were created and 20  $\mu\text{m}$  thick sections of the OFT, just distal to the ventricle but proximal to OFT septation, were chosen for analysis. CFD analysis was performed as detailed in 2.5.

### 3.5 STATISTICAL ANALYSIS

As in 2.14, Student's t-test was used for in-between group analysis with alpha = 0.05.

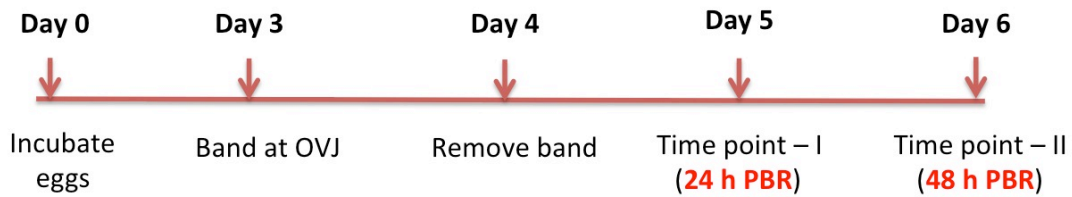


Figure 3.1: Schematic representation of our experimental paradigm. The OFT of HH 16/17 chick embryos was banded at the OVJ and allowed to develop for 24 hr; after which the band was surgically removed. Embryos were then allowed to develop for two time points post band removal (PBR): 24 hr PBR and 48 hr PBR. Control embryos were stage-matched to embryos that had the OFT constriction removed

## CHAPTER 4

### MATERIALS AND METHODS (PRELIMINARY STUDY)- MOLECULAR RESPONSES TO OFT BANDING AT DIFFERENT DEVELOPMENTAL STAGES

#### 4.1 OFT BANDING AT DIFFERENT DEVELOPMENTAL STAGES

Fertilized Bovan chicken eggs were incubated as mentioned in 2.1 to obtain embryos at HH 14 and HH 20 [65]. At the appropriate stage, embryos were randomly divided into control and banded groups, with the banded embryos undergoing OFT banding as detailed in 2.2. Both groups of embryos (control and banded) were allowed to develop for another 24 hr, after which OFT cushion tissue was dissected and used for gene expression profiling by qPCR.

#### 4.2 RNA EXTRACTION, REVERSE TRANSCRIPTION AND qPCR

Total RNA was extracted from HH 14 control (n = 3) and banded (n = 3) OFT tissue and HH 20 OFT tissue from control (n = 3) and banded (n = 3) hearts at the 24 hr time point as described in 2.6. cDNA synthesis and qPCR was performed exactly as stated in 2.7 and 2.8 respectively.

#### 4.3 STATISTICAL ANALYSIS

As in 2.14, Student's t-test was used for in-between group analysis with alpha = 0.05.

## CHAPTER 5

### RESULTS- MOLECULAR EFFECTS OF ALTERED INTRACARDIAC HEMODYNAMICS ON VALVE DEVELOPMENT<sup>4</sup>

#### 5.1 EFFECT OF OFT BANDING ON BLOOD FLOW VELOCITY

Ultrasound imaging was performed to investigate whether the constriction of the OFT (figure 5.1 a, b) resulted in a change in flow velocity across the OVJ. The suture placed around the OVJ was clearly visible in a B-mode 2D image of the beating heart (figure 5.2 a). As expected, centerline flow velocity, measured with PW Doppler (figure 5.2 b, c), yielded higher time-averaged (control =  $2.54 \pm 0.68$  cm/s, banded =  $17.6 \pm 6.32$  cm/s;  $p = 0.002$ ) and peak velocities (control =  $8.57 \pm 2.54$  cm/s, banded =  $51.5 \pm 17.16$  cm/s;  $p = 0.0018$ ) at the banded OVJ relative to the control OVJ (figure 5.2 d). No statistical differences were found between heart rates of control ( $95.8 \pm 21.4$  BPM) and banded ( $108 \pm 23.0$  BPM) embryonic chick hearts (figure 5.2 e) ( $p = 0.19$ ) or between the late cycle retrograde flow velocities (control =  $-1.44 \pm 1.55$  cm/s, banded =  $-2.74 \pm 2.43$  cm/s;  $p = 0.44$ ) (figure 5.2 d)

---

<sup>4</sup> Parts of this chapter have been excerpted from

- (1) Menon V; Eberth JF; Goodwin RL; JD, P. Altered hemodynamics in the embryonic heart affects outflow valve development. *J Cardiovasc Dev Dis.* **2015**, 2, 108-124. (Open access).
- (2) Menon V; Junor L; Eberth J; ford SM; McPheeters M; Jenkins M; Belhaj M; JD, P. Molecular consequences of cardiac valve development as a result of altered hemodynamics. *Microsc. Microanal.* **2017**, 23

## 5.2 EFFECT OF OFT BANDING ON COMPUTED HEMODYNAMICS

A 3D streamline velocity plot was generated from computational fluid dynamics (CFD) simulations to show the path and velocity magnitude within the developing embryonic chick heart. Consistent with the Doppler studies, the highest velocity occurred at the OVJ banding site (figure 5.3). Consequently, this location experienced the highest time-averaged and peak wall shear stresses (figure 5.4).

When spatially averaged, significant differences were found between the time-averaged control ( $0.97 \pm 0.26$  Pa) and banded ( $6.1 \pm 2.19$  Pa) wall shear stresses ( $p = 0.002$ ) (figure 5.5 a). Peak spatially-averaged wall shear stresses were also found to be significantly different between control ( $3.30 \pm 0.50$  Pa) and banded ( $17.8 \pm 5.96$  Pa) hearts ( $p = 0.002$ ) (figure 5.5 a). No statistical differences in shear stresses were found at the late retrograde flow condition (control =  $-0.71 \pm 0.49$  Pa, banded =  $-0.95 \pm 0.88$  Pa;  $p = 0.32$ ). Banding generated a  $5.32 \pm 1.19$ -mmHg pressure gradient across the banding site, whereas normal hearts experienced a pressure drop of  $0.20 \pm 0.05$  mmHg through this section (Figure 5.5 b) ( $p < 0.001$ ). Overall, no statistical differences were found between the volumetric flow rates in the control ( $0.18 \pm 0.05$  mm<sup>3</sup>/s) and banded ( $0.15 \pm 0.05$  mm<sup>3</sup>/s) embryonic chick hearts ( $p = 0.32$ ) (Figure 5.5 c).

## 5.3 EFFECT OF OFT BANDING ON OFT CUSHION VOLUME AND EXTENT OF EMT

To determine whether the alteration in hemodynamics in the embryonic heart caused any change in the volume of the OFT cushions, the OFT of banded and control hearts were 3D reconstructed from H&E TIFF images of the OFTs (figure 5.6 a) using AMIRA (figure 5.6 b). A comparison of the AMIRA-generated volume data revealed a

significant decrease in the OFT cushion volume of banded hearts compared to the control hearts (figure 6.6 c) ( $p = 0.01$ ).

Individual nuclei that invaded the OFT cushions were counted from H&E images (figure 5.6 a) which revealed that OFT banding led to a significant decrease in the number of cells that entered the OFT cushion tissue, by means of EMT, in the banded relative to control OFT (figure 5.6 d) ( $p=0.002$ ).

Transcript levels of the water channel *aqp1* were significantly upregulated in OFT cushion tissue from banded hearts relative to that of controls (figure 5.7 a) ( $p=0.043$ ). Mesenchymal cells in the OFT cushion from banded hearts exhibited an increase in proliferative capacity compared to control OFT cushion as revealed by PCNA staining (figure 5.7 b).

#### 5.4 EFFECT OF OFT BANDING ON RELATIVE EXPRESSION OF GENES INVOLVED IN VALVE DEVELOPMENT

Real-time PCR was carried out to investigate the effects of constricting the OFT on the expression of a selected panel of genes that are critical to valve development (table 5.1). Transcript levels of the mechanotransducer *rhoA* were significantly lower in the OFT cushion from banded hearts relative to OFT cushions of control hearts ( $p = 0.02$ ). No significant differences were observed in the mRNA expression of shear-responsive *klf2* between OFT cushions of banded and control hearts ( $p = 0.12$ ).

The OFT cushions of banded hearts exhibited significantly decreased mRNA levels of collagen1 $\alpha$ 1 (*coll*) ( $p = 0.01$ ) and increased transcript levels of *periostin* ( $p = 0.01$ ) compared to OFT cushion tissue of the control hearts. Though there was a downregulated trend in the expression of *tenascin C* ( $p = 0.08$ ) in OFT cushion from

banded hearts, there were no significant differences in the mRNA levels of *elastin* ( $p = 0.19$ ) and *vinculin* ( $p = 0.12$ ) in the OFT cushion of banded vs. control hearts.

The expression of *tgfbRIII* mRNA and that of *tgfb3* were significantly upregulated ( $p = 0.004$  and  $p = 0.02$  respectively) in OFT cushions of banded vs. control hearts; however, there were no differences in the expression levels of *tgfb2* ( $p = 0.25$ ) in OFT tissue from hearts in these two groups. Moreover, no significant differences were observed in the transcript levels of *snai2* ( $p = 0.14$ ) and *has2* ( $p = 0.1$ ), while mRNA expression of *mmp2* was significantly upregulated ( $p = 0.03$ ) in the OFT cushion from the banded hearts compared to OFT tissue from controls. Though the mRNA expression levels of *cdh11* were significantly downregulated ( $p = 0.02$ ) in OFT cushions of banded hearts there were no significant changes in transcript levels of *filamen A* ( $p = 0.34$ ) between OFT cushions of banded vs. control hearts.

About 116 genes were differentially expressed, at the mRNA level, in banded OFT cushion tissue compared to controls as revealed by microarray analysis. From these, the expression of 11 genes, that have specific roles in valvulogenesis, was validated by qPCR.

### 5.5 EFFECT OF OFT BANDING ON EXPRESSION OF ECM PROTEINS

Herovici's collagen staining was performed to determine the level of type I collagen in OFT cushions (figure 5.9). There appeared to be a decrease in type I collagen in OFT cushion of banded hearts compared to that of control. As expected, no mature collagen was detected in heart sections from banded or control embryos.

IF revealed that OFT cushion from banded hearts had a decreased collagen type I expression relative to that from the controls (figure 5.10 a). Periostin was expressed more

in the myocardium of OFT than control hearts while OFT from banded hearts had increased periostin localization in the cushion (figure 5.10 b). IST-9 (fibronectin splice variant expressed in mesenchyme) expression was higher in the cushion of banded OFT compared to the OFT of control hearts (figure 5.10 c).

#### 5.6 EFFECT OF OFT BANDING ON SIGNALING PATHWAYS

In addition to upregulation of *tgfb3* and *tgfrIII*, banded OFT cushion tissue also showed an increase in message levels of the inhibitory smads – smad6 (p=0.0493) and smad7 (p=0.0435) (figure 5.11). OFT cushions from banded hearts exhibited a decrease in the expression of mesenchymal markers- N cadherin, fibronectin and vimentin, as seen by IF of heart sections containing OFT (figure 5.12).

The number of mesenchymal cells that invaded the collagen gel were significantly less in OFT explants from banded vs. control hearts (p=0.0300), though there was no significant difference in the depth of the gel invaded by these cells from both groups (p=0.3217) (figure 5.13).

The expression of *htr1e*, at the transcript level, was significantly downregulated (p=0.0003, while mRNA levels of *tgm2* (p=0.0009) and *sert* (p=0.0378) were significantly upregulated in banded OFT tissue compared to control. There was also an increase in *tgm2* at the protein level in OFT cushion from banded hearts relative to that from control, as revealed by IF (figures 5.14 and 5.15).

#### 5.7 EFFECT OF OFT BANDING ON APOPTOSIS

There was no significant incidence apoptosis in the OFT cushion mesenchyme from control or banded hearts as revealed by TUNEL staining (figure 5.16).

## 5.8 EFFECT OF OFT BANDING ON EXPRESSION OF ECM / EMT PROTEINS AND ON PROLIERATION OF MESENCHYME IN AV CUSHIONS

IF was performed on AV sections. There appeared to be increased collagen type I in AV cushions from control hearts compared to those from banded hearts (Fig 5.17 a). Periostin (Fig 5.17 b) and IST-9 (Fig 5.17 c) expression was much higher in the control myocardium and endocardium compared to these regions in the AV cushions of the banded heart. There appeared to be an increase in intensity of signal of fibronectin and vimentin from AV cushions of banded hearts compared to that from AV cushions of control hearts (figure 5.18). PCNA was used as a marker for proliferation. There seemed to be an increase in the proliferative status of mesenchyme in AV cushions of banded vs. control hearts (figure 5.20). Furthermore, a gap was observed between the two AV cushions in the banded heart sections (indicated by arrowheads).

## 5.9 EFFECT OF OFT BANDING ON AV CUSHION EXPLANT MIGRATION ON COLLAGEN GEL

A collagen gel assay was performed with AV cushion explants to investigate if altered hemodynamics induced by OFT banding had any effect on AV cushion cell migration (figure 5.19). There was no significant difference in the number of cells that invaded the collagen gel ( $p=0.4684$ ). However, the cells from AV explants of OFT banded hearts, showed a significant decrease in the depth of the gel invaded ( $p=0.0294$ ).

Table 5.1: Differential expression of genes critical to valve development, upon OFT banding, in OFT cushion tissue of banded and control hearts



Gene	Relative expression in OFT cushions of banded hearts	P-value
<b>Shear/flow-responsive</b>		
RhoA	↓	0.02
KLF2	—	0.12
<b>ECM</b>		
Collagen 1 $\alpha$ 1	↓	0.01
Periostin	↑	0.01
Tenascin C	↘	0.08
Elastin	—	0.19
Vinculin	—	0.12
<b>EMT / cell migration</b>		
TGF $\beta$ RIII	↑	0.004
TGF $\beta$ 2	—	0.25
TGF $\beta$ 3	↑	0.02
Snai2	—	0.14
Has2	—	0.1
MMP2	↑	0.03
CDH11	↓	0.02
Filamen A	—	0.34

Table 5.2: Genes revealed in the microarray study validated by qPCR. Data represent changes in OFT from banded relative to that from control hearts.

Gene name	Gene symbol	Role in valve development	Gene expression
5-hydroxytryptamine receptor 1E	HTR1E	Activation of TGF $\beta$ signaling → ECM production	Downregulated
Thrombospondin Type 1 Domain Containing 7A	THSD7A	Endothelial cell migration	Downregulated
Platelet Derived Growth Factor Subunit A	PDGFA	Ventricular development and morphogenesis	Downregulated
T-box 18	TBX18	Early cardiac lineage determination, chamber specification, valvoseptal development, and diversification of the specialized conduction system	Downregulated
Transcription factor 21	TCF21	Differentiation of epicardium-derived cells into SMC, fibroblasts	Downregulated
Aldehyde dehydrogenase 1 family, member A2	ALDH1A2	Formation of valve leaflets	Downregulated
Cadherin 6	CDH6	EMT	Downregulated
Wilms tumor 1	WT1	EMT	Downregulated
	CD44	Valve leaflet development	Upregulated
Bone morphogenetic protein 10	BMP10	Cardiac growth and chamber maturation	Upregulated
Transglutaminase 2	TGM2	ECM organization	Upregulated

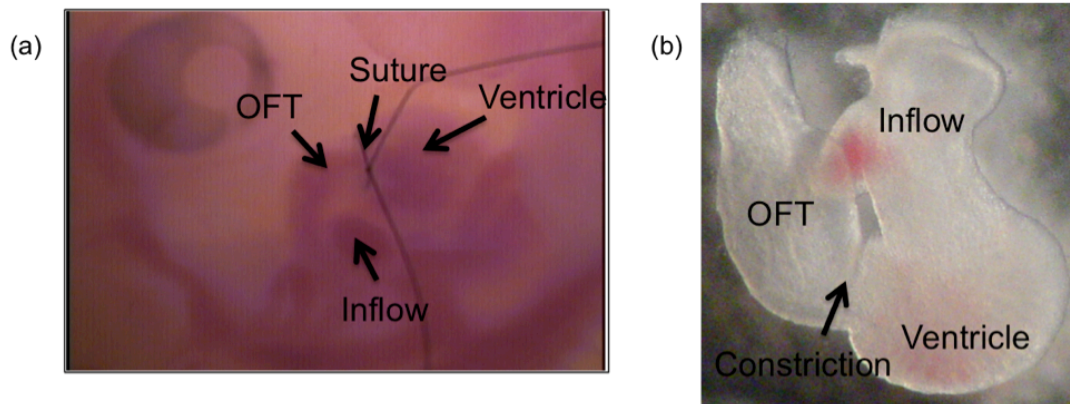


Figure 5.1: Our in vivo (ex ovo) chicken embryonic system. (a) Whole chicken embryo with OFT banded, imaged after 24h. (b) Isolated chick embryonic heart, 24h after OFT banding

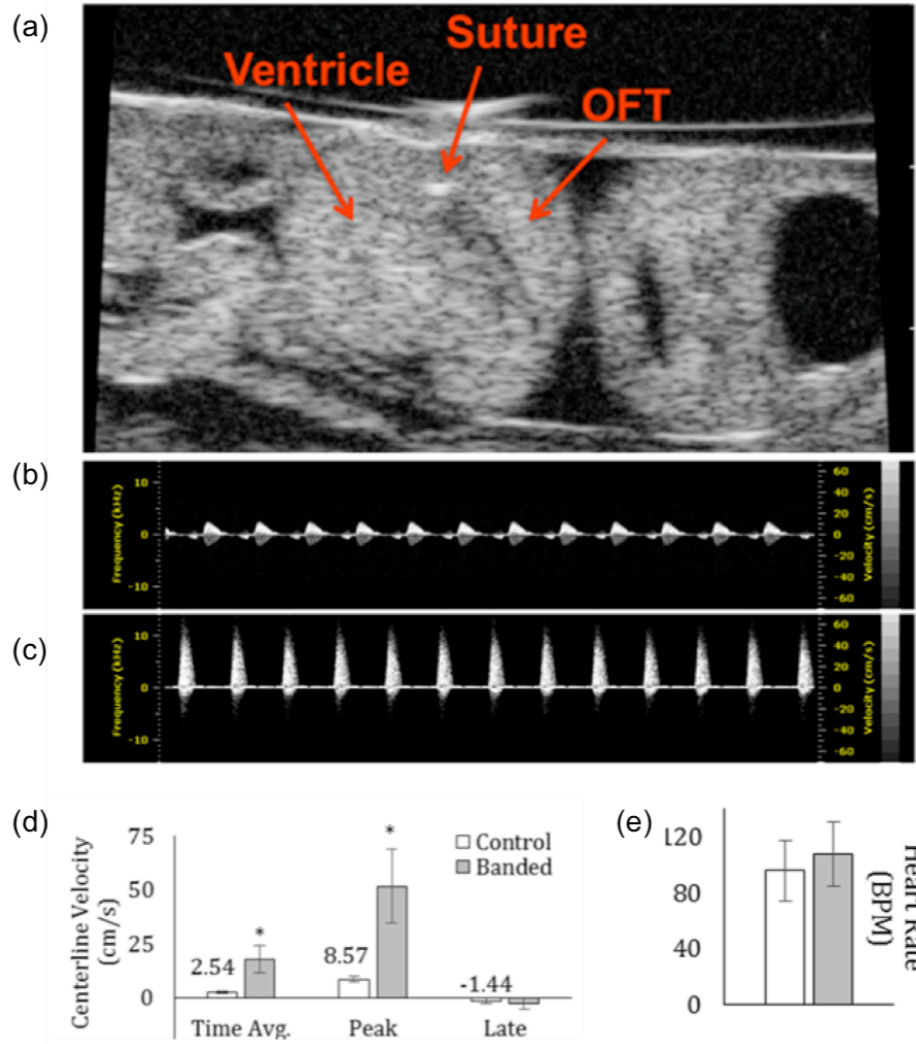


Figure 5.2: Ultrasound imaging. (a) B mode of a banded embryo showing the suture at the OVJ. Pulsed Wave Velocity (PWV) at the OVJ for the (b) control and (c) banded hearts. (d) OFT banding causes significant changes in the time averaged and peak centerline velocities measured at the OVJ. (e) Heart rate remains unchanged between controls and banded chick hearts

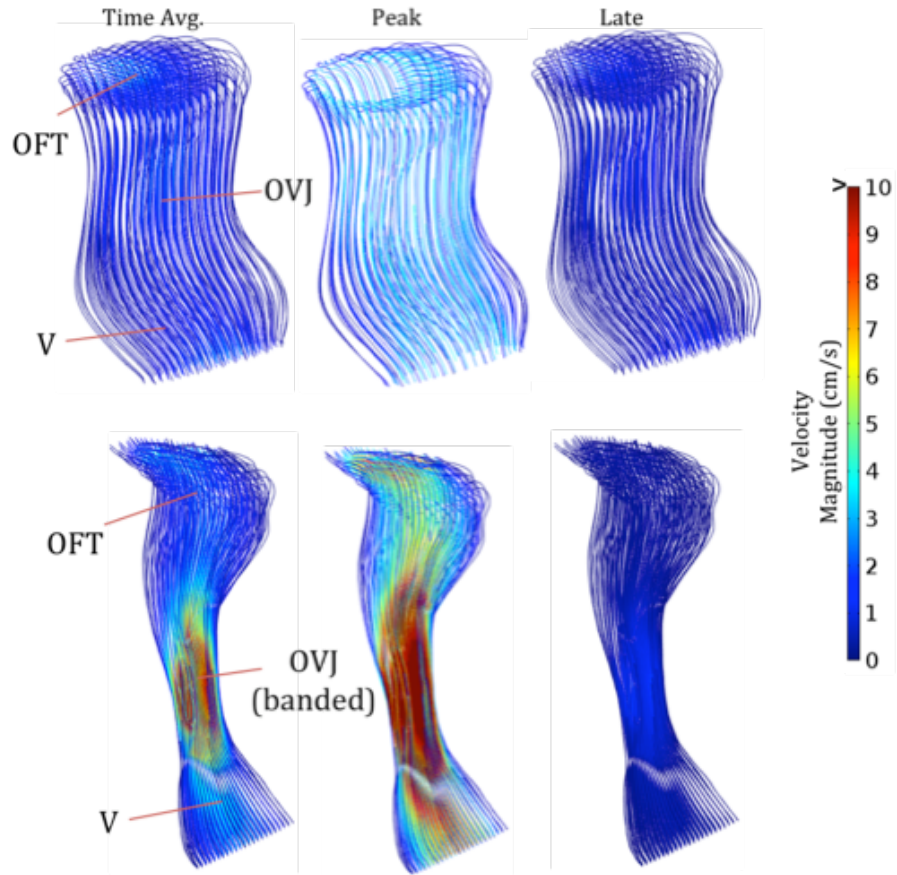


Figure 5.3: Velocity magnitude streamlines for (top) control chick hearts and (bottom) OFT banded chick hearts at the time-averaged flow velocity, peak flow conditions and late in the cardiac cycle during retrograde flow. V, ventricle; OVJ, OFT/ventricle junction; OFT, outflow tract

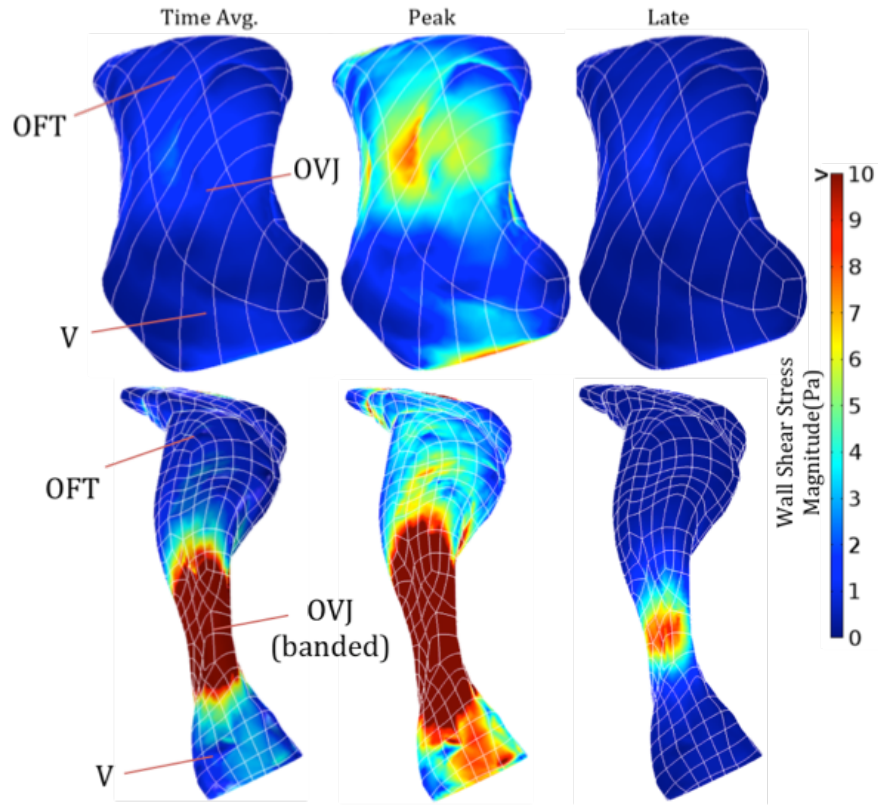


Figure 5.4: Wall shear stress magnitude for (top) control chick hearts and (bottom) OFT banded chick hearts at the time-averaged flow condition, during peak flow conditions and late in the cardiac cycle during retrograde flow. V, ventricle; OVJ, OFT/ventricle junction; OFT, outflow tract

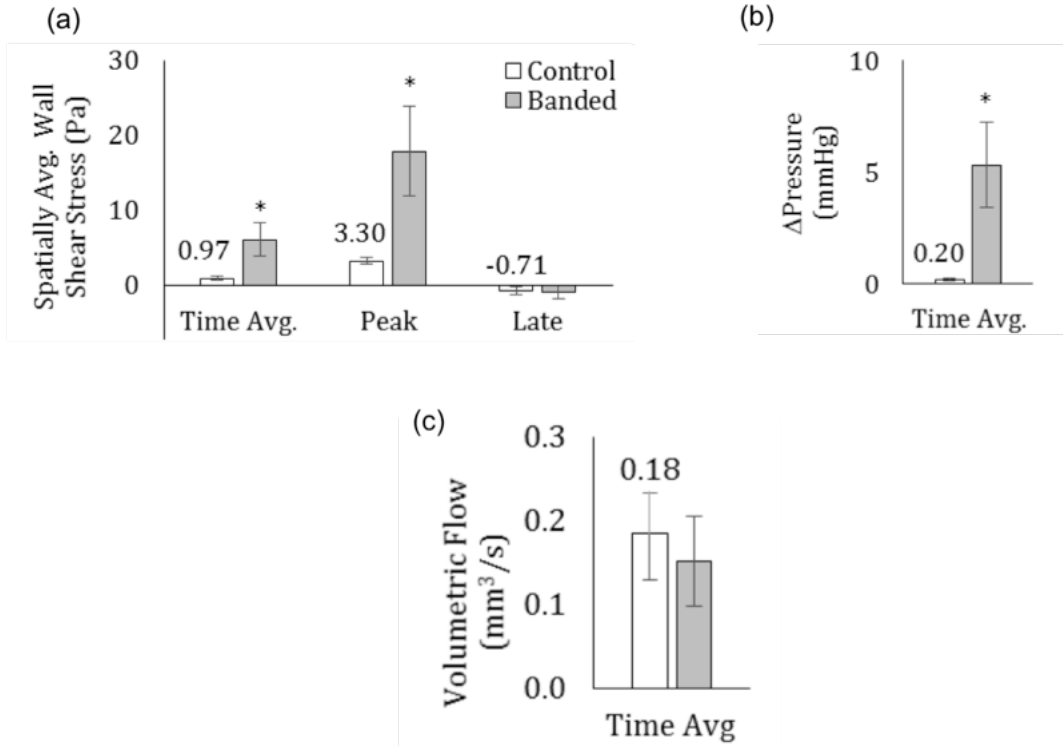


Figure 5.5: Hemodynamic variables. (a) the spatially-averaged wall shear stress at the time-averaged flow condition, during peak flow conditions and late in the cardiac cycle during retrograde flow, (b) time-averaged pressure gradient and (c) the volumetric flow rate. \*  $p < 0.05$ .

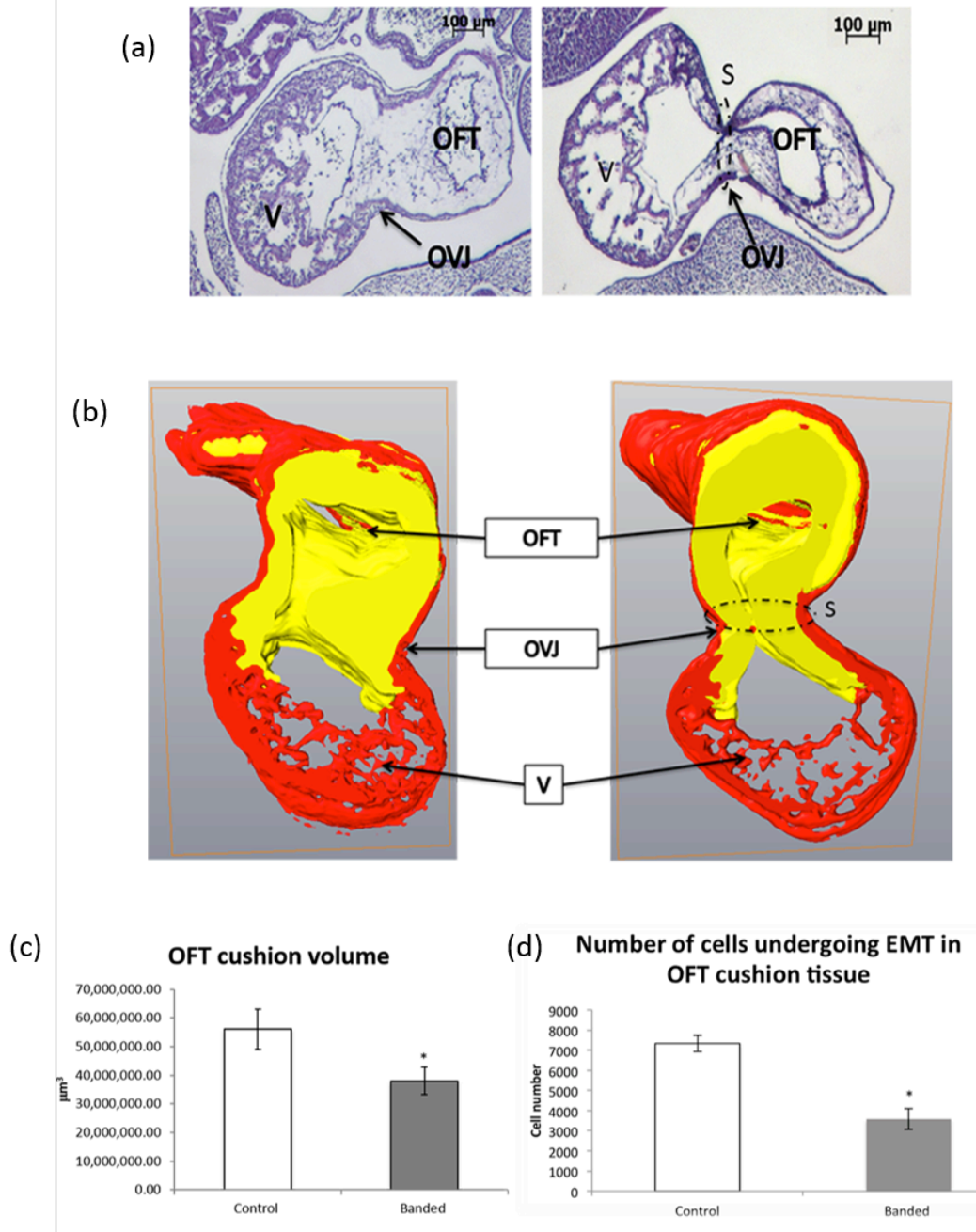


Figure 5.6: 3D reconstructed OFT.(a) Representative H&E stained images of a control (left) and banded OFT (right). (b) Cut-away view of a control (left) and banded (right) OFT showing cushion (yellow) and myocardium (red). Effect of OFT banding on (c) OFT cushion volume and (d) number of cells undergoing EMT. V: ventricle, S: position of suture

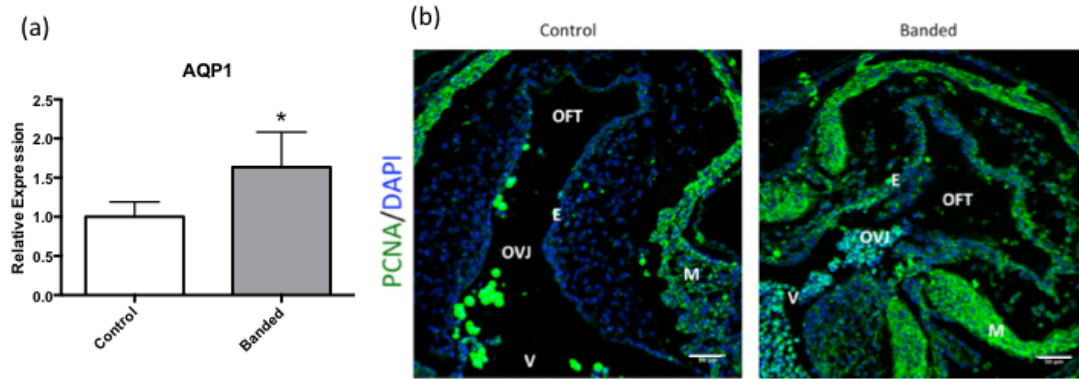


Figure 5.7: Compensatory mechanisms for decreased OFT cushion volume and cell number. Increase in AQP1 transcript level and increase in proliferation (PCNA staining) could potentially be compensatory mechanisms to counteract decreased cushion volume and reduced cell number resulting due to altered hemodynamics. Bars = 50 microns. M: Myocardium, E: endocardium, V: Ventricle

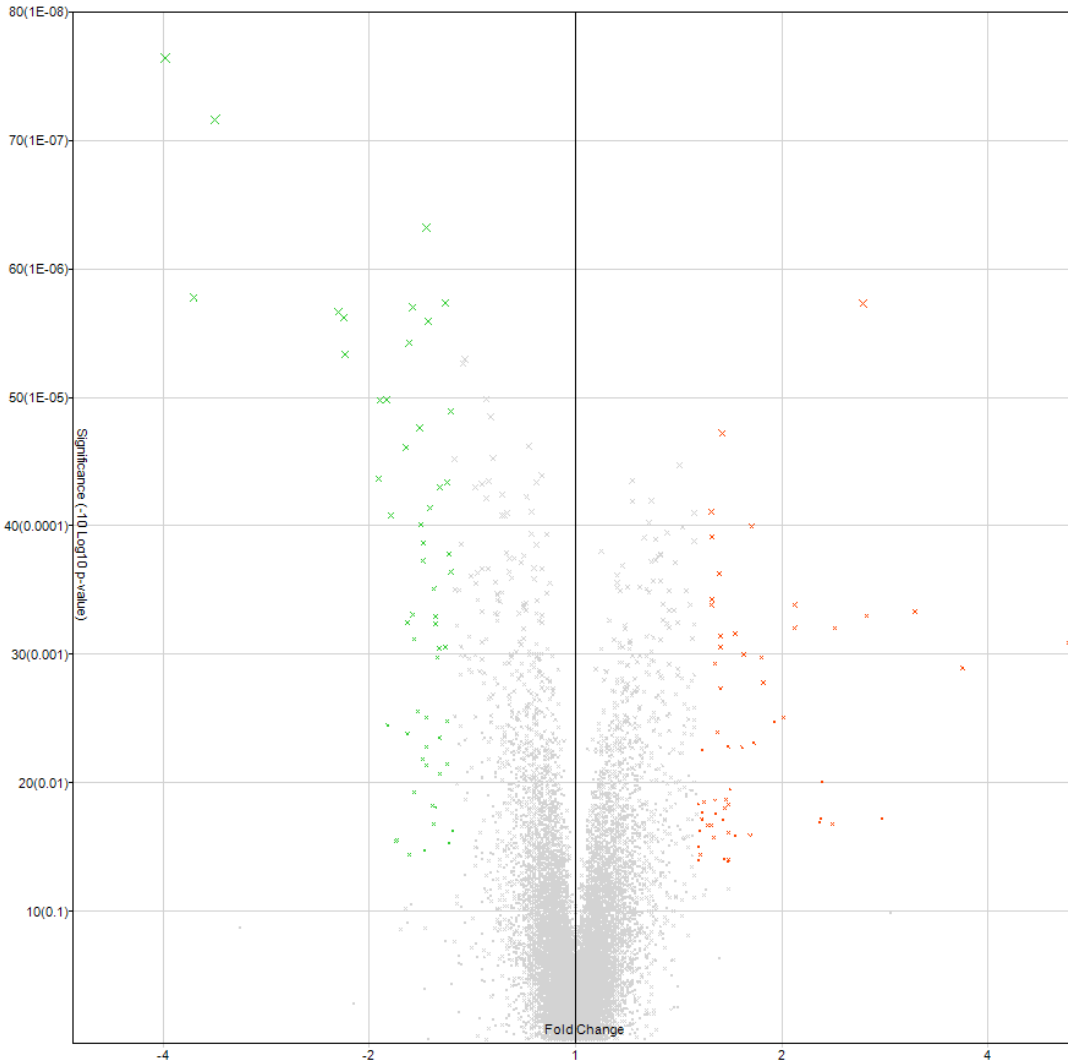


Figure 5.8: Transcriptome analysis upon OFT banding. Volcano plot resulting from microarray analysis of banded vs control OFT showing 116 transcripts exhibiting  $\geq 1.5$  fold change (red: upregulated, green: downregulated). Data represent changes in OFT from banded relative to that from control hearts.

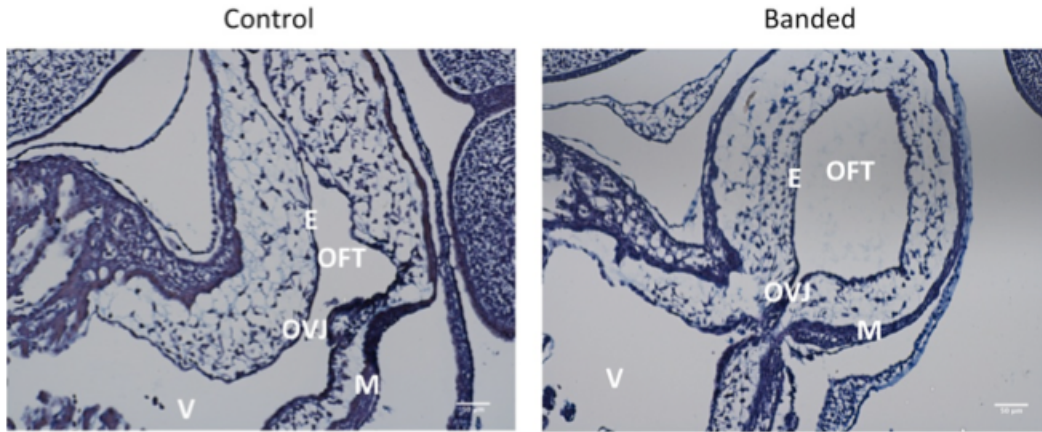


Figure 5.9: Herovici's collagen stain. A decrease was observed in the localization of type I collagen in the OFT cushion from banded vs. control hearts. Bars = 50 microns. M: Myocardium, E: endocardium, V: Ventricle

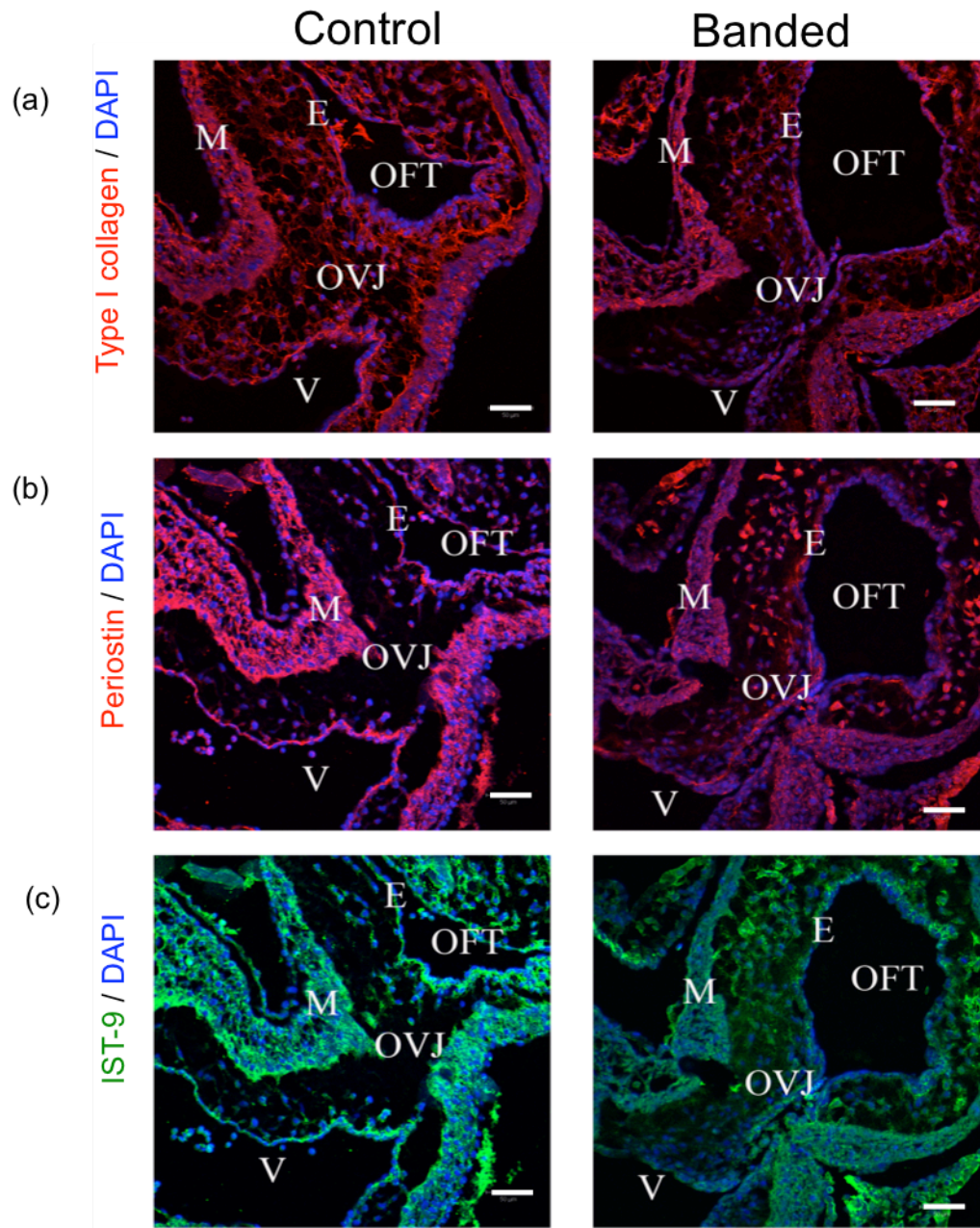


Figure 5.10: IF of OFT sections. OFT sections were probed for (a) Type I collagen, (b) Periostin and (c) IST-9 by IHC-P. Bars = 50 microns. M: Myocardium, E: endocardium, V: Ventricle

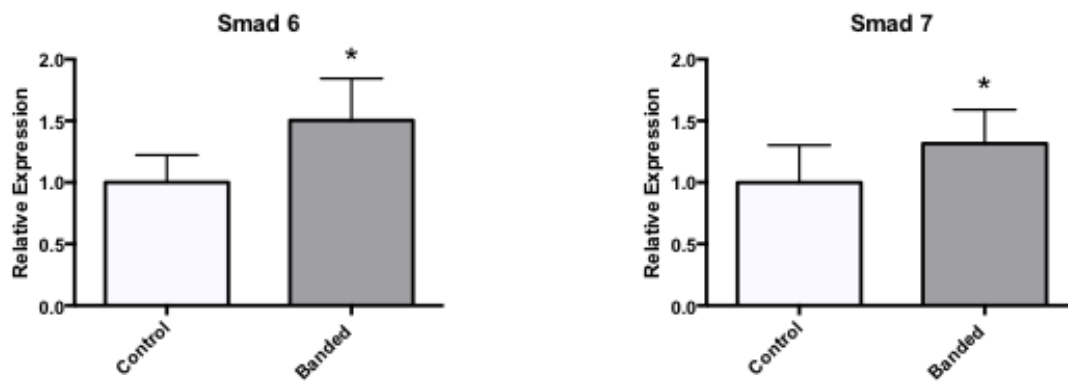


Figure 5.11: Effect of OFT banding on mRNA levels of inhibitory smads. \* indicates statistical significance.

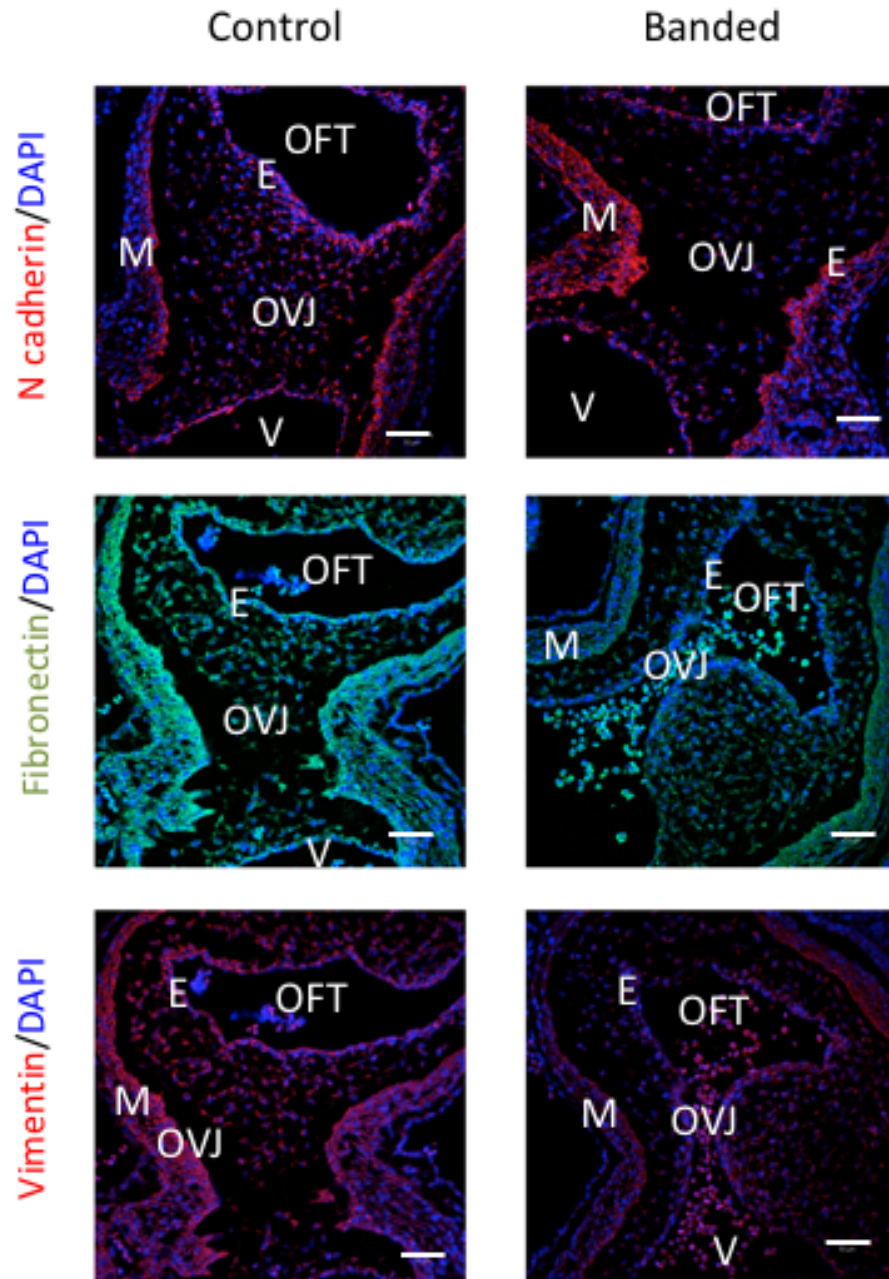


Figure 5.12: Downregulation of EMT/mesenchymal markers in OFT cushion from banded hearts relative to that of controls. Bars = 50 microns. M: Myocardium, E: endocardium, V: Ventricle

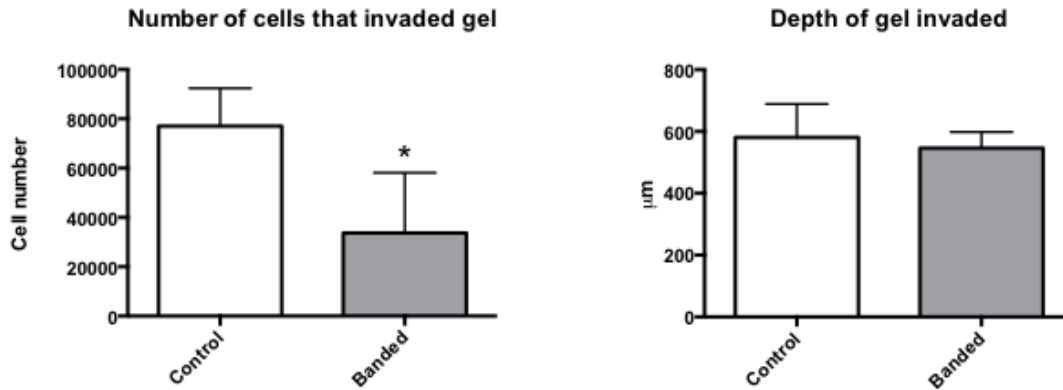


Figure 5.13: Collagen gel assay with OFT explants. There was a significant decrease in the number of cells that invaded the gel from OFT explants excised from banded hearts relative to that of control hearts, though there was no significant difference in the depth of the collagen invaded by cells derived from explants in both groups.

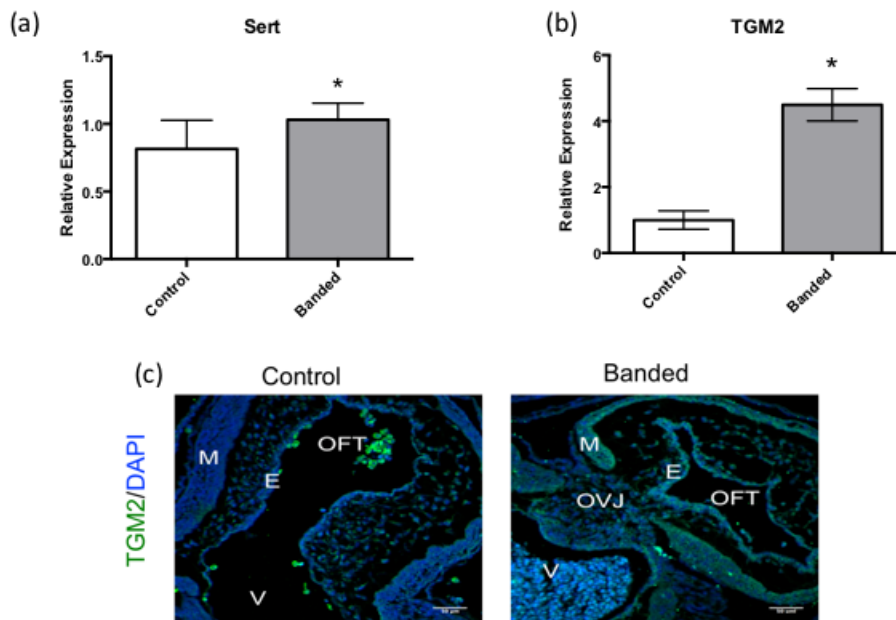


Figure 5.14: Effect of OFT banding on *sert* and *tgm2* expression. Expression of *sert* (a) and *tgm2* (b) were upregulated at the transcript level in response to OFT banding. (c) OFT from banded hearts showed increased protein expression of TGM2 relative to that from controls. Bars = 50 microns. M: Myocardium, E: endocardium, V: Ventricle.

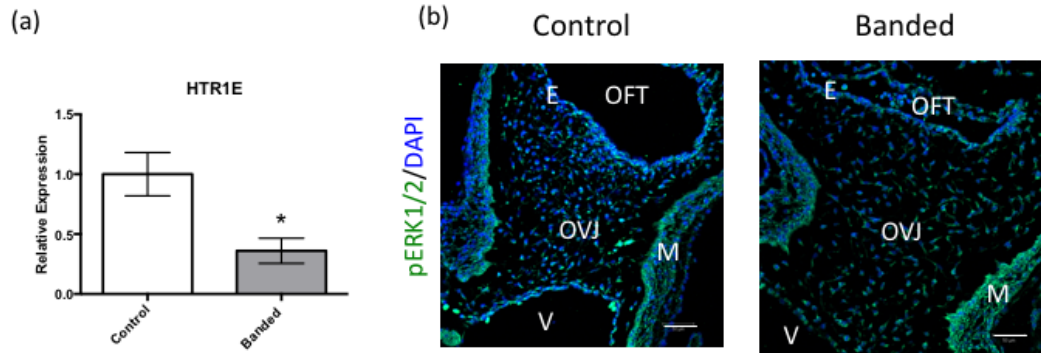


Figure 5.15: Effect of OFT banding on *htr1e* and pERK1/2. Altered hemodynamics due to OFT banding caused a decrease in mRNA levels of *htr1e* (a); although there was no noticeable difference in protein expression of phospho ERK 1/2 in OFT cushion from banded vs. control hearts. Bars = 50 microns. M: Myocardium, E: endocardium, V: Ventricle.

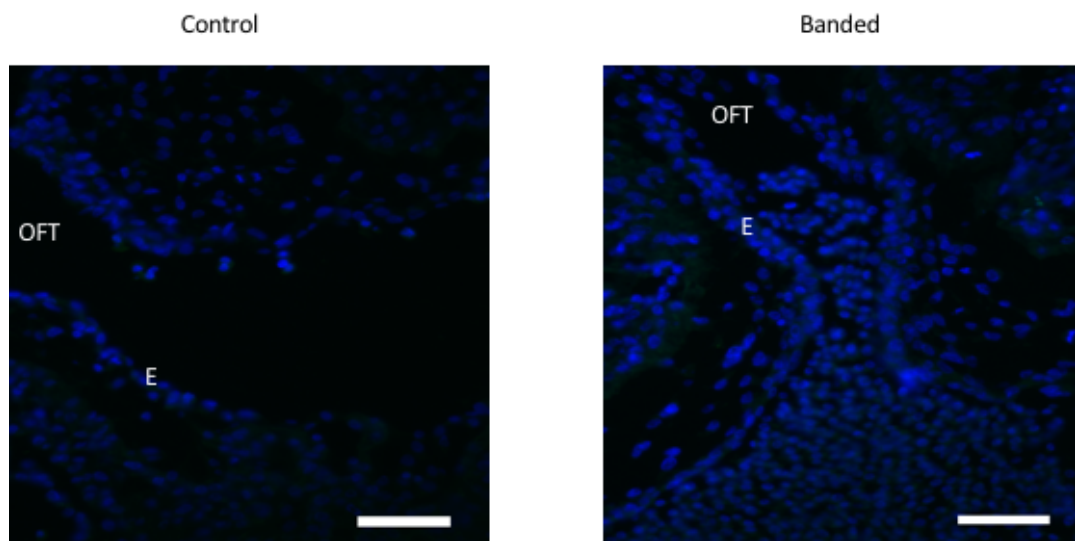


Figure 5.16: No apoptotic cells were observed in OFT cushion from banded or control hearts. E: endocardium. Bars = 50 microns.

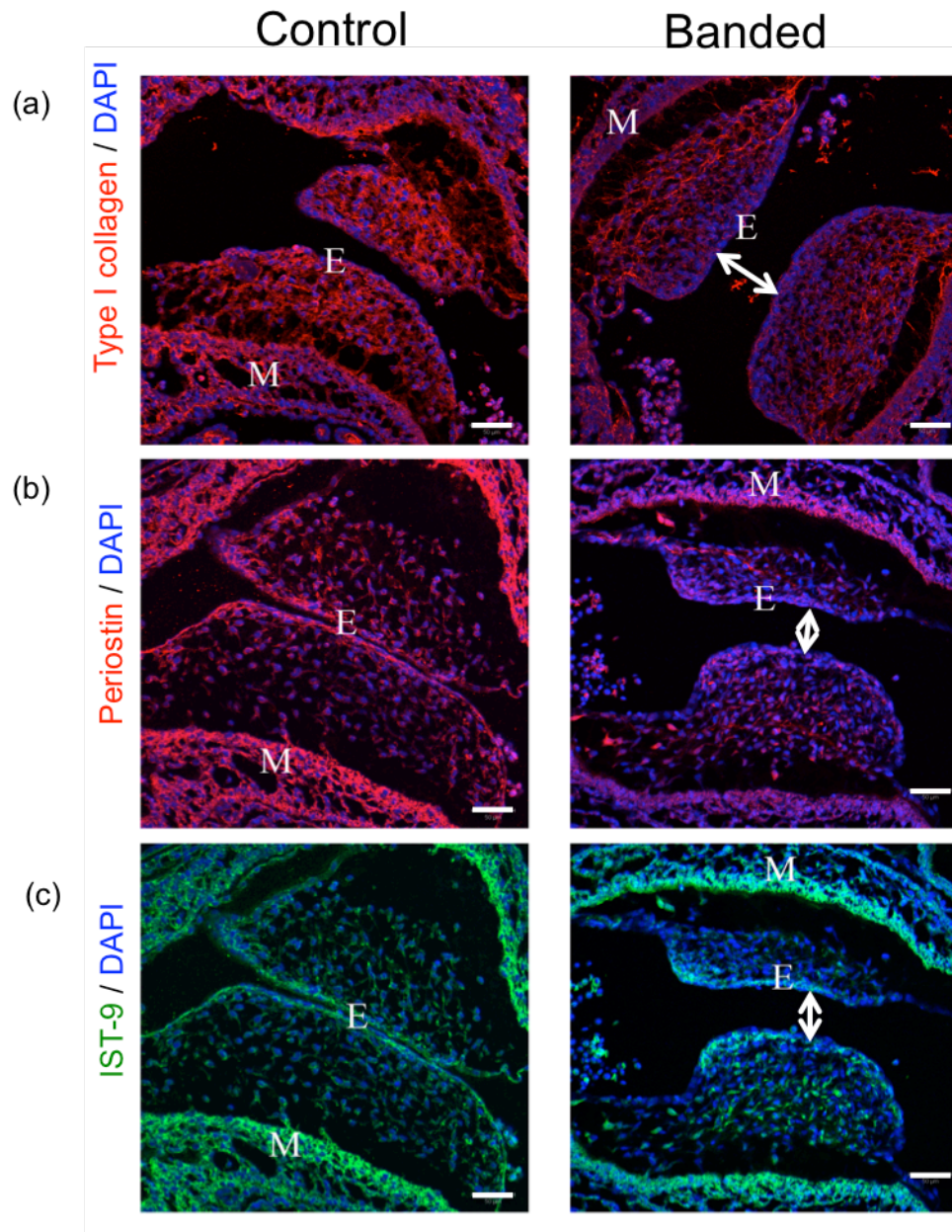


Figure 5.17: IF of AV sections. AV sections were probed for (a) Type I collagen, (b) Periostin and (c) IST-9 by IF. Arrowheads indicate a gap between AV cushions from banded hearts. Bars = 50 microns. M: Myocardium, E: endocardium.

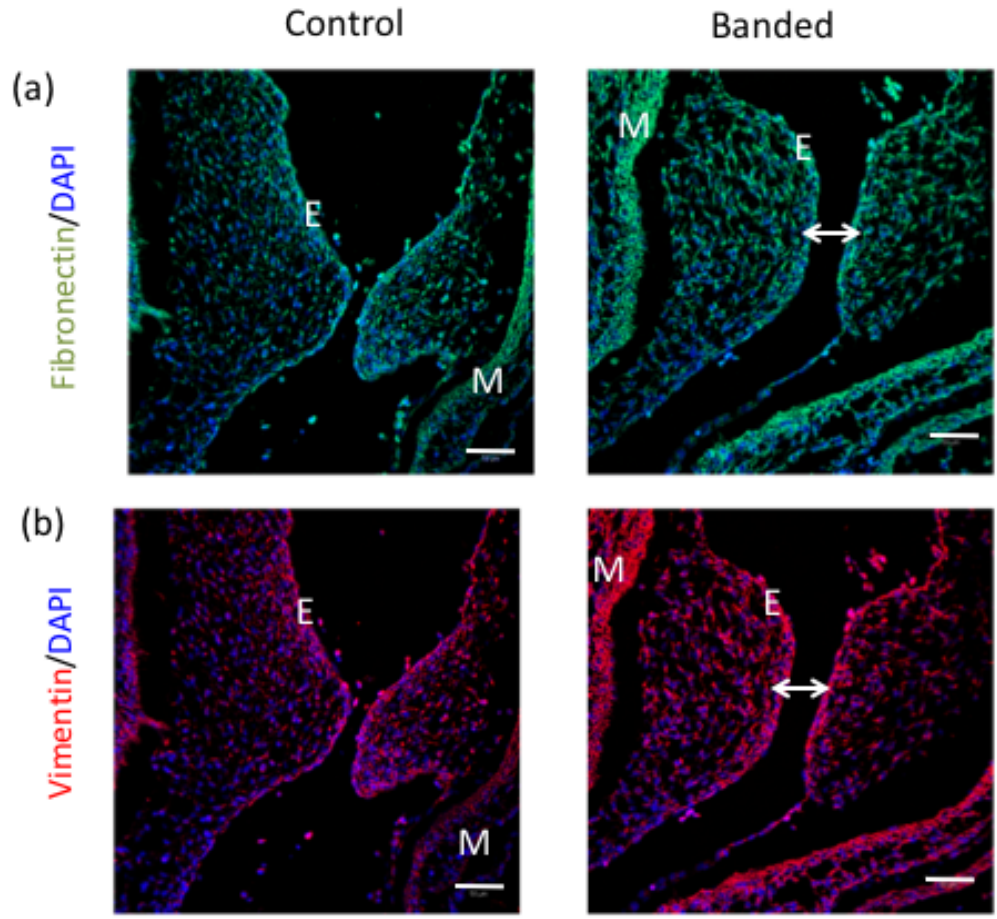


Figure 5.18: Effect of OFT banding on expression of EMT markers in AV cushions. AV sections were probed for (a) fibronectin and (b) vimentin by IF. Arrowheads indicate a gap between AV cushions from banded hearts. Bars = 50 microns. M: Myocardium, E: endocardium.

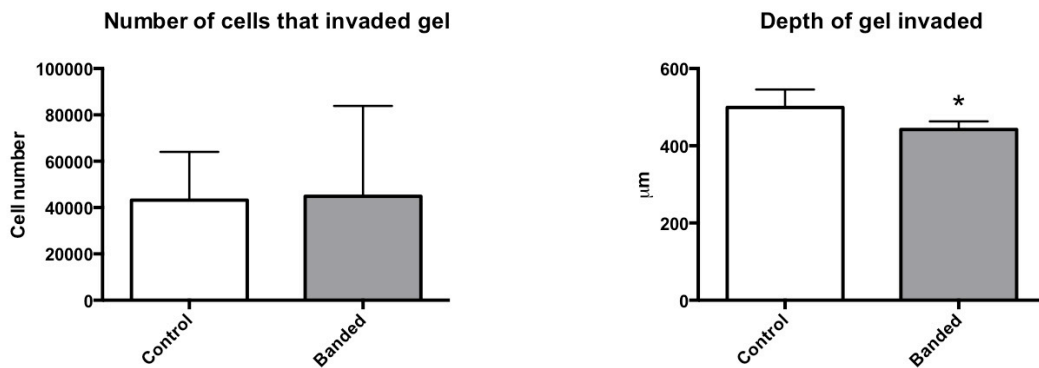


Figure 5.19: Collagen gel assay with AV cushion explants. There was no significant difference in cell number from AV cushion explants from both groups seeded on collagen

gels, although the depth of the gel invaded was significantly decreased in AV cushion explants from banded hearts relative to that of controls.

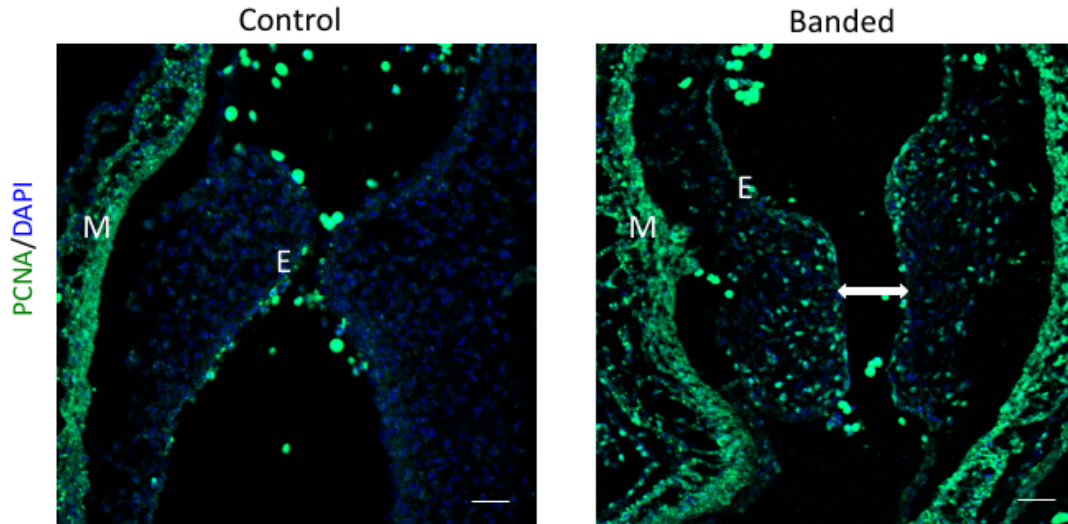


Figure 5.20: Effect of OFT banding on proliferation of AV cushion mesenchyme with PCNA as a marker for cell proliferation. Arrowheads indicate a gap between AV cushions from banded hearts. Bars = 50 microns. M: Myocardium, E: endocardium.

## CHAPTER 6

### RESULTS- EFFECTS OF RELEASING THE CONSTRICTION AROUND THE OFT<sup>5</sup>

#### 6.1 EFFECT OF BAND REMOVAL ON THE PHENOTYPE OF THE DEVELOPING HEART

As described in the experimental procedures and shown in figure. 3.1, embryos were banded at HH16-17 and incubated for 24 hr; after which the band was removed and embryos were further incubated until two post-band-removal (PBR) time points were reached: 24 hr PBR and 48 hr PBR. Four groups of tissues were therefore analyzed in the present work: 24 hr stage matched control, 24 hr PBR recovery, 48 hr stage matched control and 48 hr PBR recovery (controls were stage-matched with the recovery embryos). At the appropriate time points, embryos from each of the four groups were excised from the yolk, hearts dissected, and images captured under a dissection scope. At the 24 hr PBR time point, hearts of the embryos in the recovery group (figure 6.1 b) had a deformed OFT relative to that of the control hearts (figure 6.1 a). At the 48 hr PBR time point, the early septation of the OFT into the aorta and pulmonary artery could be clearly seen in the control hearts (figure 6.1 c). However, hearts in the recovery group continued to exhibit abnormal phenotypes (figure 6.1 d). H&E stained heart sections revealed a

---

<sup>5</sup> Parts of this chapter have been excerpted from Menon V; Eberth J; Junor L; Potts AJ; Belhaj M; DiPette DJ; Jenkins M; JD, P. Removing vessel constriction on the embryonic heart results in changes in valve gene expression, morphology, and hemodynamics. *Dev Dyn* **2017**

continuity of the OFT and AV cushions in the 24 hr PBR control hearts (figure 6.3 a), as is expected during normal heart/valve development. However, in the recovery group at this time point, the OFT remained separate from the AV cushions (figure 6.3 b). 48 hr after band removal, the recovery hearts exhibited OFT and AV cushions similar to that in the control group (figure 6.3 c and d), however the OFT of the 48 hr PBR recovery hearts (figure 6.3 d) appeared elongated relative to the controls at this time point.

## 6.2 EFFECT OF BAND REMOVAL ON RELATIVE EXPRESSION OF GENES INVOLVED IN EMT AND VALVE DEVELOPMENT

Genes selected in the current study are those that previously showed significant differential expression 24 hr after OFT banding (i.e., 24 hr post-surgery – PS; table 5.1). Shown in figure. 6.4 are the mRNA expression patterns of these transcripts in the OFT tissue from the recovery hearts relative to those in the control group at the respective time-points. Gene expression data reported here are transcript levels in the recovery group relative to that of the controls (i.e., 1.000). 24 hr PBR mRNA level of the mechanotransducer rhoA, in the recovery group, was similar to that of the controls ( $0.8689 \pm 0.05687$ ,  $p=0.1040$ ). However, 48 hr after band removal, rhoA expression was downregulated ( $0.7154 \pm 0.03212$ ,  $p=0.0072$ ). We analyzed the relative expression of genes coding for three important ECM proteins – collagen type I, periostin and collagen type VI. 24 hr PS, transcript levels of collagen VI were significantly downregulated relative to controls ( $0.4510 \pm 0.08549$ ,  $p=0.0040$ ). At the 24 hr PBR time point, message levels of collagen I and collagen VI were both upregulated ( $1.259 \pm 0.001197$ ,  $p=0.0063$  and  $2.499 \pm 0.1714$ ,  $p=0.0049$ , respectively). However, 48 hr after removing the band, expression of these targets was normalized ( $1.038 \pm 0.03153$ ,  $p=0.3622$  and  $0.9642 \pm 0.07846$ ,  $p=0.3746$ ). Periostin gene expression was upregulated 24 hr PBR ( $1.916 \pm$

0.1474,  $p=0.0092$ ), but then downregulated at the 48 hr PBR time point ( $0.2397 \pm 0.04456$ ,  $p=0.0106$ ). We further analyzed the expression of genes involved in EMT and cell migration. Transcript levels of *tgfbRIII* (Type III TGF beta receptor) were normalized at the 24 hr PBR time point ( $1.054 \pm 0.1831$ ,  $p=0.4015$ ), but 48 hr after band removal, levels were significantly lower relative to stage- matched controls ( $0.7688 \pm 0.03122$ ,  $p=0.0069$ ). However, mRNA levels of the type III TGF beta ligand (*tgfbIII*) continued to be upregulated 24 hr PBR and were then normalized 48 hr PBR ( $1.674 \pm 0.005772$ ,  $p=0.0078$  and  $0.9494 \pm 0.08052$ ,  $p=0.3301$ ). Expression of *mmp2* and *cadherin-11* (*cdh11*) were normalized 24 hr PBR ( $1.109 \pm 0.05288$ ,  $p=0.1766$  and  $1.023 \pm 0.1173$ ,  $p=0.4538$ ) and continued to be similar to controls even 48 hr after the band was removed ( $0.9642 \pm 0.07846$ ,  $p=0.3746$  and  $0.9849 \pm 0.07089$ ,  $p=0.4682$ ).

### 6.3 EFFECT OF BAND REMOVAL ON OFT CUSHION AND CELL VOLUME

Our previous studies demonstrated that following 24 hr of banding the OFT cushions showed a significant volume reduction. To that end, we examined the hearts and OFTs following band removal to assess any changes that were created. AMIRA-generated 3D models of the OFT were used to determine the volume of the OFT cushions after band removal. 24 hr PBR cushion volume of the OFT in the recovery group was significantly lower compared to that of the control group ( $p=0.0262$ ) (figure 6.5 a). However, in contrast, cushion volume of OFT 48 hr after removing the band showed no significant reduction in volume to that of the control group at this time point ( $p=0.3027$ ) (figure 6.5 b). That finding prompted us to examine whether there was a corresponding change in the cellular volume as well within the cushion. Using the AMIRA program, we examined every fourth 5  $\mu\text{m}$  section through the cushion and collected the cell

volumes for cells within the cushions analyzed above. This was done to assure that we did not count a cell multiple times. Assuming that our cell volume measurements were taken at similar thresholds throughout and that all mesenchymal cells have a similar volume, the cell volumes are reflective of the cell number in each cushion analyzed. At both time points, 24 and 48 hr PBR, there were no significant increases in the cell volume within the cushions ( $p=0.1238$ ;  $p=0.4836$  respectively) (figure 6.6 a). However, when we took into consideration the volume of the cushion itself and calculated a ratio of cushion volume to cell volume we found a significant decrease in the ratio at 24 hr. ( $p=0.0237$ ) (figure 6.6 b). This significance observed at 24 hr. PBR was subsequently lost when we examined the 48 hr. PBR ratio of cushion to cell volume ( $p=0.1976$ ).

#### 6.4 HEMODYNAMIC CHANGES IN RESPONSE TO BAND REMOVAL

Overall no significant differences were found in the heart rate at either time point (24hr stage matched control= $154.9 \pm 10.52$  BPM; 24hr PBR recovery= $135.8 \pm 10.04$ ; 48hr control= $168.5 \pm 14.44$ ; 24hr PBR= $166.3 \pm 18.51$ ;  $p=0.4635$ ; figure 6.7). In our prior work, we demonstrated that the application of a fixed diameter band around the outflow tract of the HH-stage 16-17 embryonic chick heart resulted in localized increases in time averaged (control =  $2.54 \pm 0.68$ ; banded =  $17.6 \pm 6.32$  cm/s) and peak (control =  $8.57 \pm 2.54$ ; banded =  $51.5 \pm 17.16$  cm/s) centerline velocity. These increased velocities resulted in higher levels of time averaged (control= $0.97 \pm 0.26$ ; banded  $6.1 \pm 2.19$  Pa) and peak wall shear stress (control= $3.30 \pm 0.50$ ; banded= $17.8 \pm 5.96$  Pa) in the OFT. In this study, our recovery groups showed similar velocities to the time-matched controls 24 hrs after band removal, in terms of time-averaged (24hr PBR control= $13.63 \pm 1.337$ ; 24hr PBR recovery =  $16.36 \pm 1.734$  cm/s;  $p=0.1146$ ; figure 6.8 a), peak (24hr PBR control= $53.07 \pm$

5.536; 24hr PBR recovery =  $61.72 \pm 7.957$  cm/s;  $p=0.1864$ ; figure 6.8 b), and retrograde (24hr PBR control= $-6.264 \pm 1.447$ ; 24hr PBR recovery= $-3.819 \pm 2.044$  cm/s;  $p=0.1663$ ; figure 6.8 c) velocity. Likewise, similar velocities were observed at the 48 hr PBR time point in terms of time-averaged (48hr PBR control= $16.99 \pm 1.176$ ; 48hr PBR recovery= $16.06 \pm 1.914$  cm/s;  $p=0.3437$ ; figure 6.8 d), peak (48hr PBR control= $63.82 \pm 4.752$ ; 48hr PBR recovery= $63.06 \pm 3.130$  cm/s;  $p=0.4483$ ; figure 6.8 e), and retrograde (48hr PBR control= $-10.52 \pm 1.784$ ; 48hr PBR recovery= $-11.59 \pm 3.191$  cm/s;  $p=0.3708$ ; figure 6.8 f) velocity.

No statistically significant differences were found 24 hr after removing the band for time averaged wall shear stress (24hr PBR control= $1.067 \pm 0.1107$ ; 24hr PBR recovery= $0.9780 \pm 0.1128$  Pa;  $p=0.2993$ ; figure 6.9 a), peak wall shear stress (24 hr PBR control= $53.07 \pm 5.536$ , 24 hr PBR recovery= $61.72 \pm 7.957$ ;  $p=0.1864$ ; figure 6.9 b) or retrograde wall shear stress (24 hr PBR control= $-6.264 \pm 1.447$ , 24 hr PBR recovery = $-3.819 \pm 2.044$ ;  $p=0.1663$ ; figure 6.9 c). However, time averaged (48 hr PBR control= $1.227 \pm 0.08780$ , 48 hr PBR recovery= $1.688 \pm 0.1118$ ;  $p=0.0035$ ; figure 6.9 d) and peak (48 hr PBR control= $3.709 \pm 0.3103$ , 48 hr PBR recovery= $4.815 \pm 0.2244$ ;  $p=0.0068$ ; figure 6.9 e) wall shear stress were increased in the recovery group 48 hr after band removal, although retrograde wall shear stress (48 hr PBR control= $-0.4691 \pm 0.1062$ , 48 hr PBR recovery= $-0.7163 \pm 0.1266$ ;  $p=0.0803$ ; figure 6.9 f) appeared different but did not reach statistical significance at this sample size.

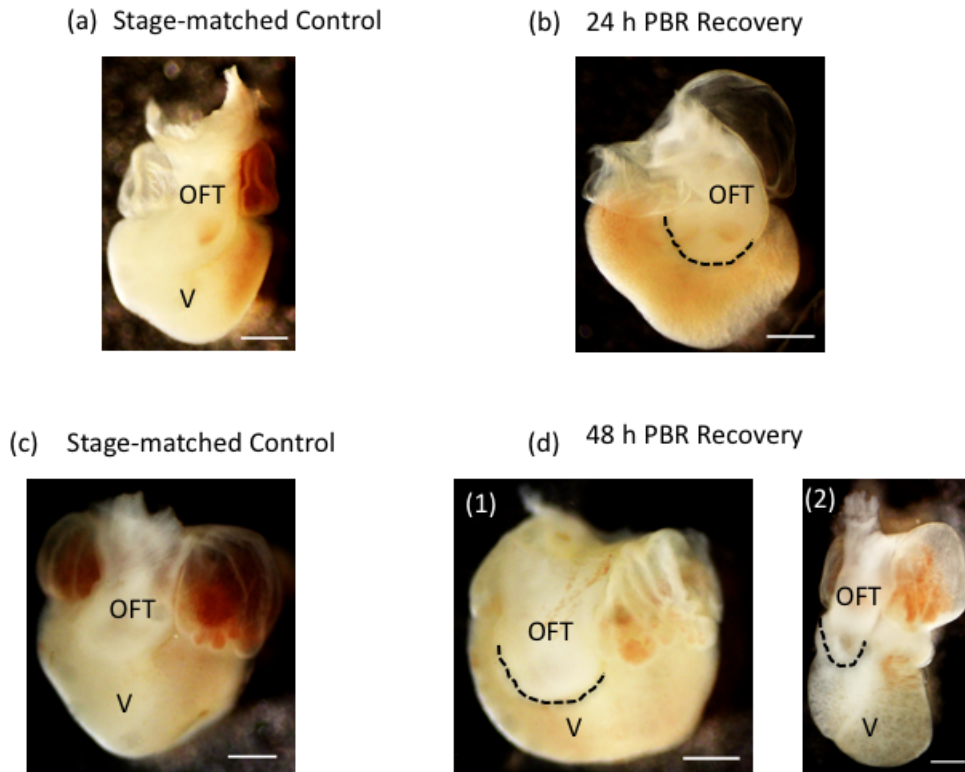


Figure 6.1: Bright field images of whole embryonic hearts illustrating the effect of OVJ band removal. (a), (c) show representative images of stage-matched control hearts at 24 and 48 hr respectively. (b), (d) illustrate the altered morphology observed from 24 and 48hr PBR. The two predominant observed phenotypes are shown in (d) 1-2. Both show OFT changes. Ventricle (V) and outflow tract (OFT) are designated. The hashed line represents the area that the band is placed. Bar=500 microns.

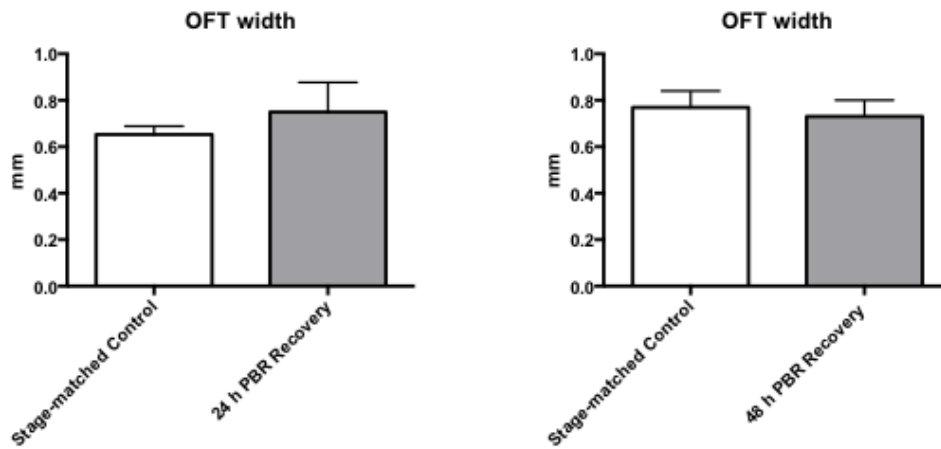


Figure 6.2: Band removal did not have any significant difference in width of the outer wall of the OFT at 24 hr and 48 hr PBR time points.

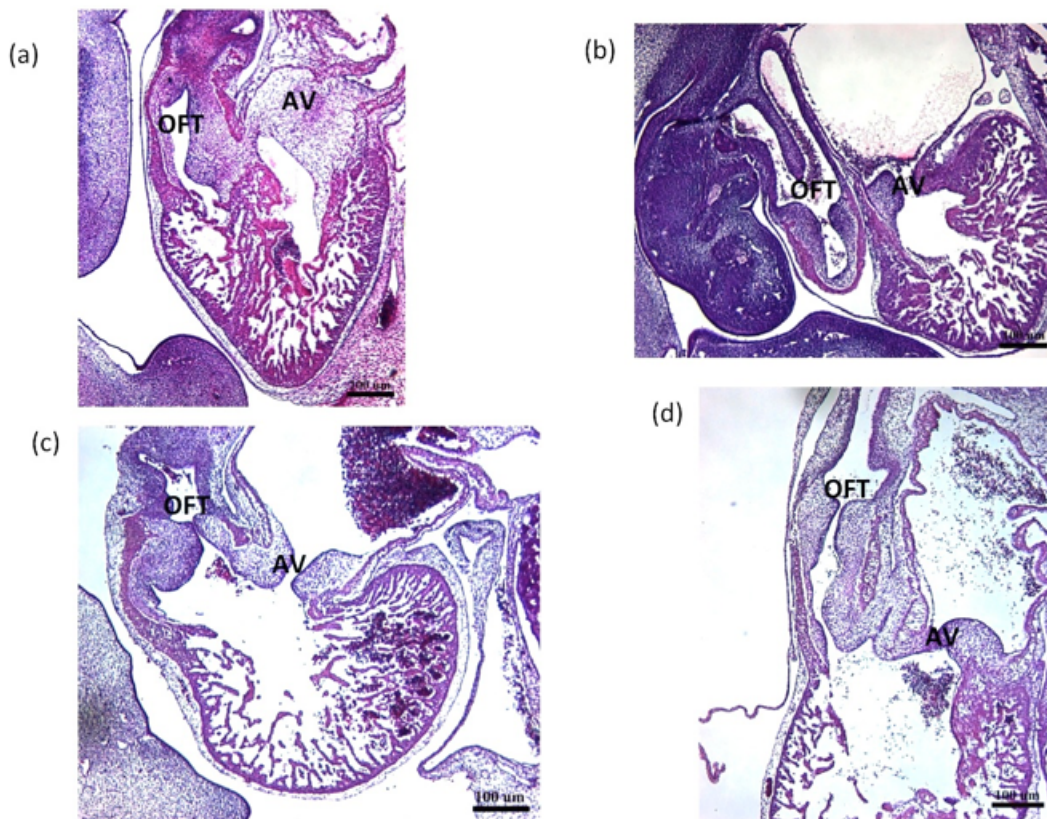


Figure 6.3: H&E stained heart sections obtained from stage matched controls and following band removal. 24 hr PBR control (a), and 48 hr PBR control (c) show normal phenotypes in both sets of cushions. In contrast, both 24 hr PBR recovery (b), and 48 h PBR recovery (d) hearts show altered phenotypes. An elongated OFT (d) is one of the

phenotypes observed in the 48 hr PBR hearts. Outflow tract (OFT), atrioventricular (AV) and ventricle (V). Bar = 100 microns

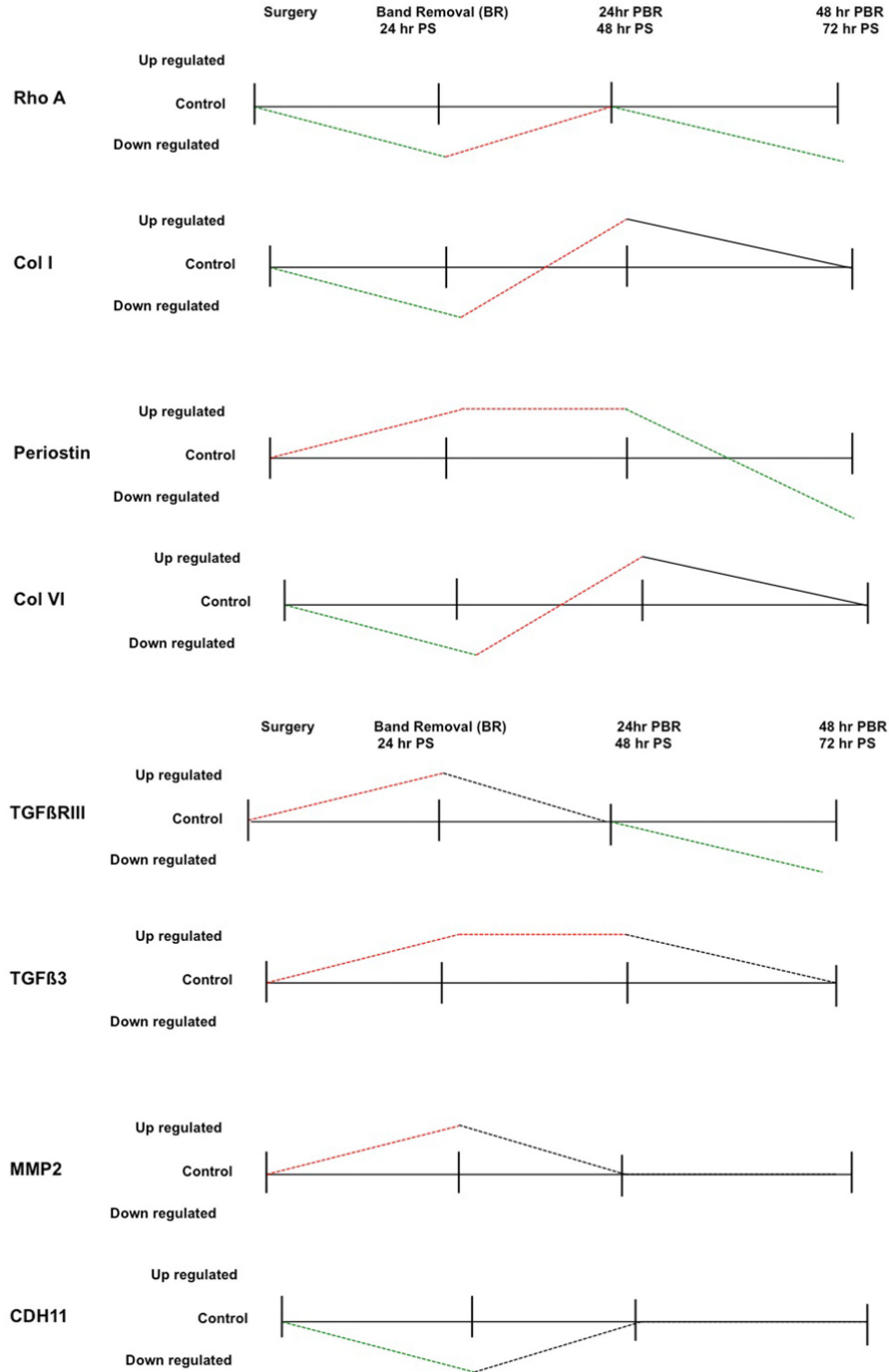


Figure 6.4: qPCR analysis of the effect of band removal on relative expression of genes critical to EMT and valvulogenesis. OFTs were excised from heart at the appropriate time

frames and ran for changes in gene expression. A variety of outcomes were observed for the various genes. Each up or down regulated time point was given its designation if it was statistically significant. As was previously described by us all of the genes chosen were altered immediately upon band removal. Some genes returned to returned to baseline levels at 24 hr PBR (48 hr PS) e.g. Rho A, MMP2 and CDH11. Others were upregulated at that time and several showed a downregulation at the 48 hr PBR time point (RhoA, Periostin, and TGF $\beta$ RIII). Post band removal (PBR), Post surgery (PS). \* indicates  $p < 0.05$

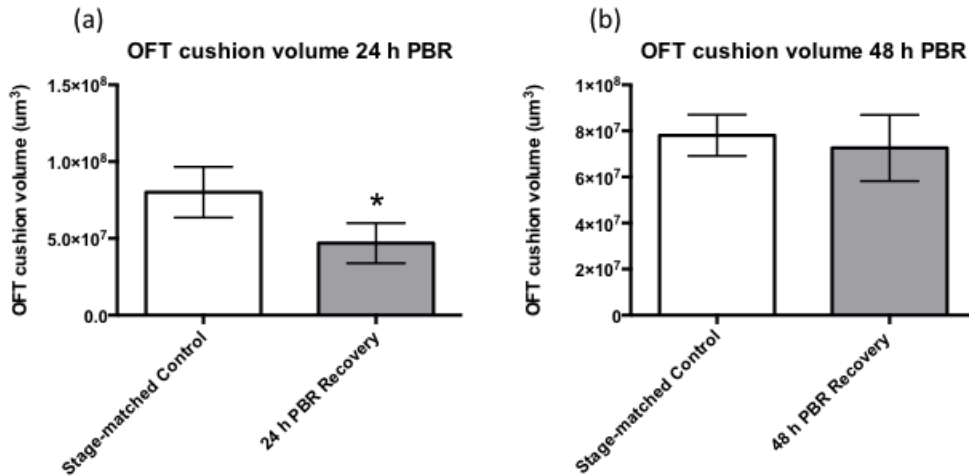


Figure 6.5: Changes in OFT cushion volume in response to band removal. Cushion volumes were determined from Amira reconstruction of hearts from both control and PBR recovery hearts at 24 and 48 hr PBR. Cushion volume showed a significant decrease in the 24 hr PBR hearts compared to stage- matched controls (a). However, by the 48 hr PBR time point, there was no significant volume change when compared to stage matched controls (b). \* indicates  $p < 0.05$

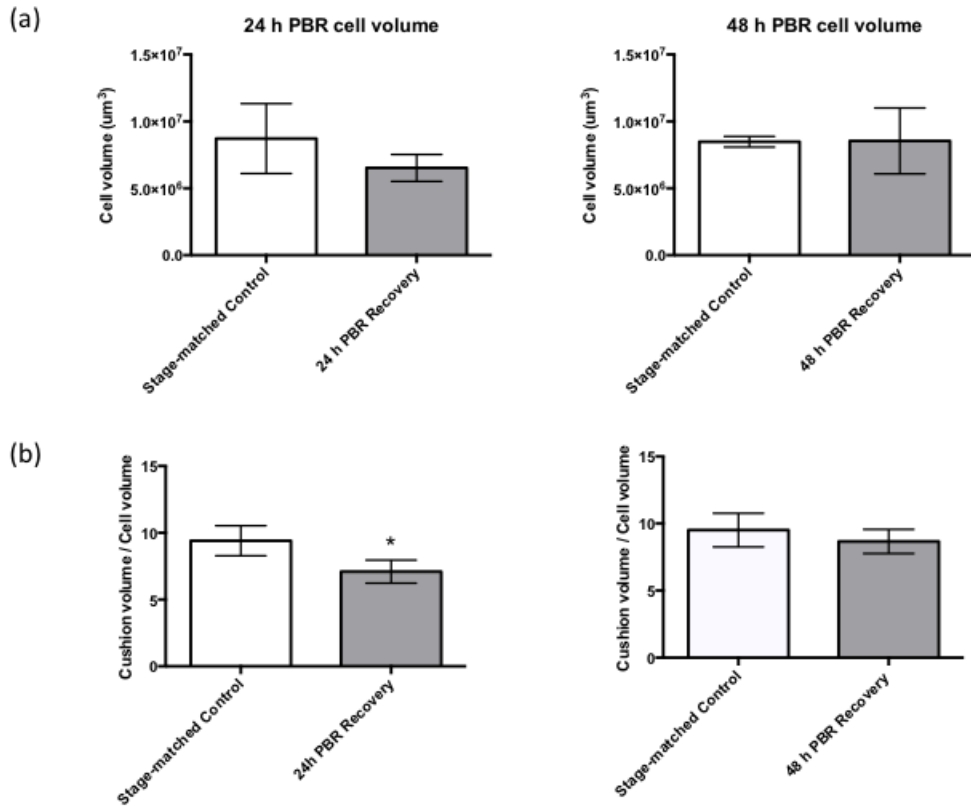


Figure 6.6: Calculation of Cushion and Cell volumes ( $\mu\text{m}^3$ ) in recovery hearts. Recovery hearts at 24 and 48 hr PBR were serial-sectioned and images collected for analysis using AMIRA software. At both time points following band removal, no significant volume changes were observed compared to control cushion volume. However, at 24 hr PBR, there was a significant decrease in the cell volume/cushion volume ratio. By 48 hr PBR there was no longer any significance in the ratio

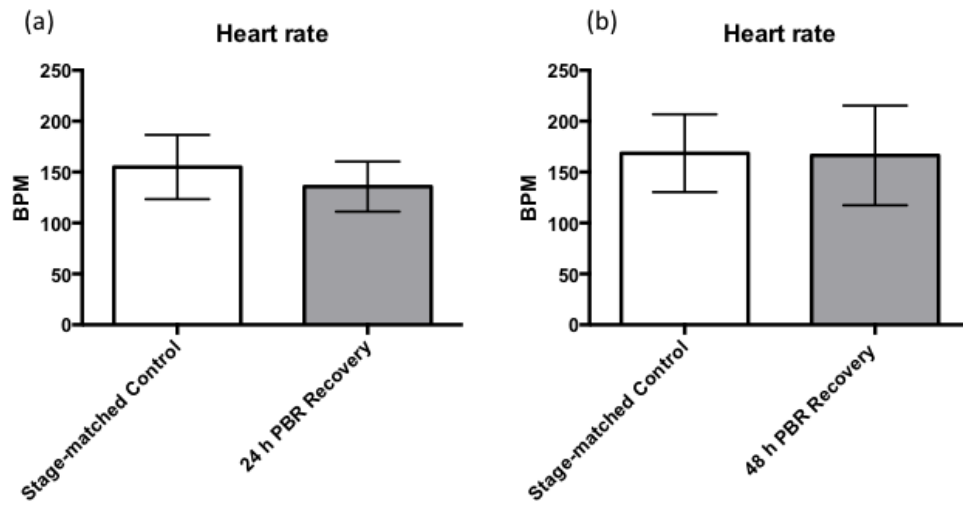


Figure 6.7: Effect of band removal on heart rates. Embryonic heart rates (a) 24 hr PBR and (b) 48 hr PBR with age-matched controls. Ultrasound data was acquired from the hearts and used to obtain heart rates. There were no statistically significant differences found at either time point (24 hr PBR (a), 48 hr PBR (b)) compared to controls.

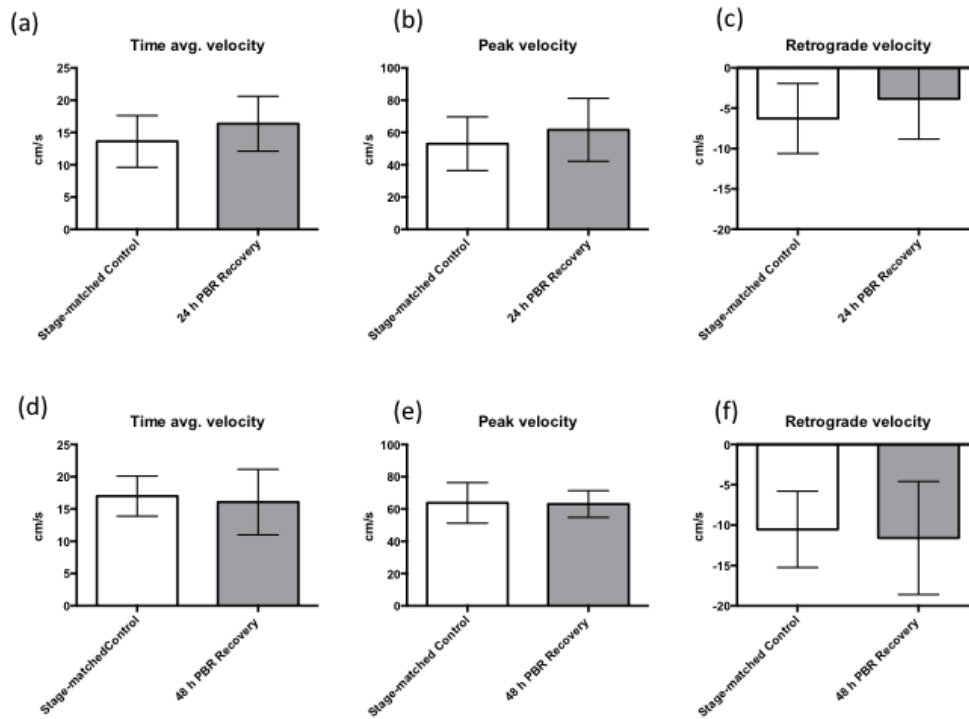


Figure 6.8: Effect of band removal on blood flow velocity. Measured time averaged, peak, or retrograde flow velocity (a-c) 24 hr post band removal (PBR) or (d-f) 48 hr PBR with age matched controls. No statistically significant differences were found at either time point or during any stage in the cardiac cycle

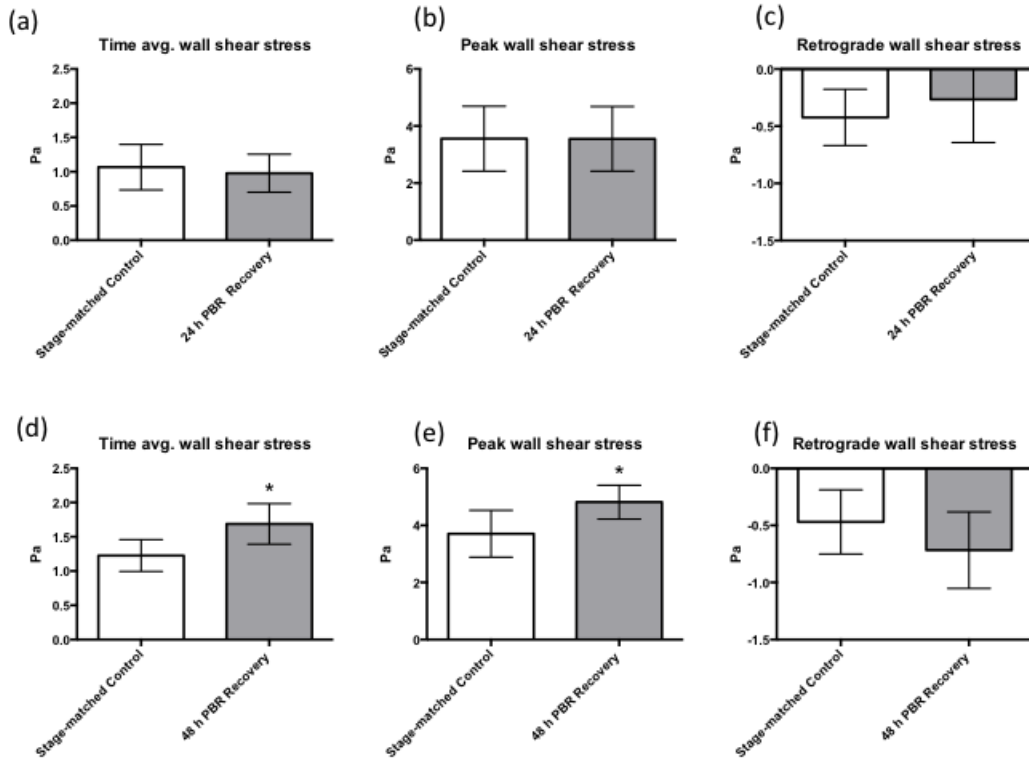


Figure 6.9: Effect of band removal on shear stress. Computed time averaged, peak, or retrograde shear stress (a-c) 24 hr post band removal (PBR) and (d-f) 48 hr PBR with age matched controls. (\*) indicates statistical significance between the 48 hr PBR and the 48 hr control.

## CHAPTER 7

### RESULTS (PRELIMINARY STUDY)- MOLECULAR RESPONSES TO OFT BANDING AT DIFFERENT DEVELOPMENTAL STAGES

qPCR was carried out to investigate if there exists a window of time during embryonic development during which altered hemodynamics through the embryonic heart has any effect on the expression of those transcripts that were shown to be affected 24 hr after banding HH 17 OFTs (5.4).

#### 7.1 EFFECT OF OFT BANDING AT HH 14 ON RELATIVE EXPRESSION OF GENES INVOLVED IN VALVE DEVELOPMENT

The expression of collagen type I was significantly upregulated in OFT tissue of banded relative to that from control hearts ( $p=0.0121$ ). However, there was no significant change in expression of other genes between OFT tissue from banded vs. that from control hearts. ( $\rho A$   $p=0.4904$ , collagen type VI  $p=0.2015$ , periostin  $p=0.2592$ ,  $tgfbRIII$   $p=0.4030$ ,  $tgfbIII$   $p=0.4984$ ,  $mmp2$   $p=0.4729$ ,  $cdh11$   $p=0.3247$ ).

#### 7.2 EFFECT OF OFT BANDING AT HH 20 ON RELATIVE EXPRESSION OF GENES INVOLVED IN VALVE DEVELOPMENT

Of all the genes analyzed, only the expression of collagen VI was downregulated significantly in banded OFT vs. control ( $p=0.0390$ ). Expression of other genes were not significantly different in OFT tissue from banded vs. control hearts ( $\rho A$   $p=0.3003$ , collagen type I  $p=0.4346$ , periostin  $p=0.4935$ ,  $tgfbRIII$   $p=0.1219$ ,  $tgfbIII$   $p=0.2469$ ,  $mmp2$   $p=0.2547$ ,  $cdh11$   $p=0.2169$ ).

## CHAPTER 8

### DISCUSSION- MOLECULAR EFFECTS OF ALTERED INTRACARDIAC HEMODYNAMICS ON VALVE DEVELOPMENT<sup>6</sup>

As stated earlier, several studies have reported the fact that perturbation of hemodynamics in the embryonic heart leads to a spectrum of congenital heart / valve defects [46-54,63]. We recently showed that altering intracardiac hemodynamics by partial OFT constriction via banding, has consequences at the cellular and genetic level [52,63]. As a result, we have started to investigate the potential processes that go awry when normal hemodynamic stimuli are affected in the developing heart. Our banding model in the chick embryo mimics these other systems of altered hemodynamics while allowing a more rapid investigation of cellular / molecular perturbations that lead to these defects. Furthermore, it is plausible that disruption of blood flow is similar to that observed in valvular defects such as calcified aortic valves and/or bicuspid aortic valve disease [70,71]. While the long-term goal of our laboratory is to further examine our model system and decipher if the resulting genetic and cellular anomalies are parallel to those seen in the aforementioned adult etiologies, the purpose of this study was to alter

---

<sup>6</sup> Parts of this chapter have been excerpted from

- (1) Menon V; Eberth JF; Goodwin RL; JD, P. Altered hemodynamics in the embryonic heart affects outflow valve development. *J Cardiovasc Dev Dis.* **2015**, 2, 108-124. (Open access).
- (2) Menon V; Junor L; Eberth J; ford SM; McPheeters M; Jenkins M; Belhaj M; JD, P. Molecular consequences of cardiac valve development as a result of altered hemodynamics. *Microsc. Microanal.* **2017**, 23

the hemodynamics in the embryonic chicken heart by partially constricting the OFT, and to study the effects of this intervention on early valve developmental processes.

Hemodynamics in the chicken embryonic heart were altered by banding the OFT at the OVJ. This constriction led to a significant ‘jet effect’ at the OVJ as revealed by ultrasound-mediated flow velocity measurements and prolonged increased levels of wall shear stress. Despite the increased cardiac afterload, the volumetric flowrate and heart rate were similar between controls and banded hearts. This result is indicative of adequate distal tissue perfusion and little change to systemic cardiovascular physiology. A subsequent lumen narrowing was also experienced in the distal portions of the OFT and confirmed by AMIRA 3D reconstructions. This distal lumen narrowing is consistent with the findings of other researchers [72] who hypothesized that this effect may be due to paracrine factors released at the banding site. Regardless, at a consistent volumetric flow the narrowed lumen led to an increase in spatially averaged wall shear stresses and a concatenate increase in the differential pressure. Flow-induced wall shear stresses are a result of the viscous properties of flowing blood thereby creating physical signals that are sensed directly by the epithelial cell-lined lumen. Although pressure likely plays an important role in the EMT process, the differentiation, morphology and gene expression effects herein are attributed solely to changes in shear stress. The role of pressure in the EMT process is reserved for future work.

The control peak flow velocities measured for the OFT in our study ( $8.57 \pm 1.28$  cm/s) compare well to those of prior researchers, including Bharadwaj et al. for HH16 ( $9.2 \pm 0.09$  cm/s) and Liu et al. for HH18 ( $6.2 \pm 0.7$  cm/s) [73,74]. Liu et al. also reported a retrograde flow velocity of  $-2.0 \pm 2.0$  cm/s, and we found this value to be very close at

$-0.72 \pm 0.77$  cm/s. An estimation of time-averaged velocities from the full velocity profile of both of the aforementioned studies is also in the range of our measured value of  $2.54 \pm 0.68$  cm/s. Our banding model, however, has Doppler measured centerline velocities much greater than those presented by Midgett et al. [62]. Despite those differences, our results are reasonable when considering proportional changes in cross-sectional area caused by the banding process.

We found time-averaged ( $0.97 \pm 0.26$  Pa) and peak ( $3.30 \pm 0.50$  Pa) wall shear stress values to be near those found by Bharadwaj et al. for the HH16 chick (0.36 Pa and 0.97 Pa, respectively) [73]. Liu et al. also showed graphically the peak wall shear stress for the HH18 chick to be somewhere around 6 Pa [74]. Our values fall between these two estimates, and the differences could be attributed to the source tissue location, assumptions on the velocity profile, tissue fixation geometry or from spatially averaging across a larger tissue area. Without more advanced imaging modalities (e.g., micro-CT), we are unable to quantify cushion expansion in real time and require tissue fixed under physiological conditions for our geometric-based CFD analysis. These two factors contribute to error in our shear stress calculations and are acknowledged limitations to this work. Regardless, the results of our CFD study provide a reasonable comparison between control and banded tissues

Cushion volume and number of cells undergoing EMT were decreased by 39% and 69% respectively, in the OFT of the banded hearts relative to control hearts. These observations highlight the fact that hemodynamics plays a significant role in formation of the valve primordia during the initial stages of valve development that occur in HH16-17 embryos, the stage chosen for the OFT banding surgery. These reductions in OFT

cushion volume and cell number could potentially lead to the formation of abnormal, hypocellular OFT valves.

Aquaporins (aqp) are water channels that shuttle water across a concentration gradient [75,76]. Transcript levels of *aqp1* were significantly upregulated in the OFT tissue of banded hearts compared to that from control. This may be a compensatory mechanism to counteract the decrease in cushion volume resulting due to altered hemodynamics. The OFT cushion mesenchyme from the banded hearts also exhibited an increase in proliferative status, indicated by increased PCNA staining, relative to that of controls. This may be another compensatory mechanism in response to the banding insult to increase the number of cells in the cushion and attempt to achieve homeostasis.

As evidenced in the CFD model, there is a significant change in wall shear stress in, and distal to, the banding regions. However, for technical reasons, cushion tissues of the entire OFT were collected, which includes regions directly beneath/surrounding the band as well as regions post- and pre- constriction. Thus, the gene expression results reported in this study represent changes that occur in the whole OFT cushion tissue rather than at discrete locations. Since CFD simulations predicted spatially averaged wall shear stresses to be significantly higher in the banded model, we compared the entire tissue gene expression to the entire tissue shear stresses.

Endocardial cells, that line the lumen of the embryonic heart and the adult cardiovascular system, are the first to experience and respond to shear stress by mechanotransduction signaling pathways [77]. When comparing flow (therefore shear stress) to no flow (no shear) we have previously shown that *rhoA*, a small GTPase

involved in regulating the actin cytoskeleton, is upregulated in the presence of flow in in vitro cultures of AV [28] and OFT cushions [29], and is also an important mechanotransducer, in 3D cultured AV cushion explants [13]. At high levels of shear stress however, *rhoA* was shown to be down-regulated compared to physiological levels [14]. In the present study, we also observed a significant decrease in *rhoA* transcript levels in OFT cushions of the banded hearts. This decrease in *rhoA* transcription could potentially lead to inappropriate mechanotransduction and thus altered ECM production leading to abnormally formed OFT valves. Kruppel-like factor 2 (*klf2*) is an important shear-responsive transcription factor [78,79] and appears to have a role in normal valve development and regulates the EMT process [80]. We did not observe any significant change in the mRNA expression of this gene upon constricting the OFT. This may be a consequence of analyzing the expression of this gene in whole OFT cushion, and not just the region where shear stress is altered.

The mature OFT valve consists of three distinct ECM layers that confer special properties to valve function. The ventricularis offers elasticity to the OFT valves allowing them to extend and recoil, the middle spongiosa layer acts as a shock-absorber, and the collagen-rich fibrosa confers stiffness and strength [38,81]. The production / deposition of fibrous ECM proteins is important to maintain valvular integrity in order to allow valves to function efficiently and to prevent backflow of blood during the cardiac cycle; consequently aberrant expression and deposition of valve ECM proteins is associated with abnormalities in valve development and pathological states [38]. Collagen is the most abundant fibrous ECM protein in the mature valve with mutations in collagen1 $\alpha$ 1 leading to, among other conditions, aortic valve insufficiency that requires valve

replacement [38]. Tenascin C is a matricellular protein that is highly expressed during development and is associated with endocardial cushion tissue EMT. Elastin is found in the ventricularis, the aspect of the OFT valves that faces blood flow. It has been shown, in humans, that elastin content increases in the outflow valves from the fetal stage to adult [82]. In our study, we found a decreased expression of *coll* at the mRNA level and a downregulated trend in mRNA expression of *tenascinC* in OFT cushions from banded hearts relative to that from controls. We have previously shown that in the presence of flow and therefore shear stress, transcript levels of *coll* and *tenascinC* are decreased in in vitro 3D cultured HH25 OFT cushions compared to no flow controls [29]. Yet when compared to physiological levels of shear stress there were no observable differences when shear stresses were elevated to pathologically high levels (e.g., those generated from OVJ banding) [29]. Although the stage of the embryos in the present study subjected to banding surgery does not represent that stage at which there is complete expression of ECM genes, the reduction in *coll* may be attributed to the change in shear stress through the banded OFT. However, it appears that spatially averaged shear stress does not significantly influence expression of *elastin* and *vinculin* at least at the mRNA level at this embryonic stage. Importantly, it should be pointed out that the presence of flow did decrease mRNA expression of elastin in 3D cultured OFT cushions from HH 25 hearts and that pathologically high levels of shear stress also increased mRNA expression [29]. These differences are also likely attributable to the stage-dependent influence of hemodynamics on transcription of this gene. In the present study we observed increased transcript of *periostin* in the high shear stress model which are in parallel with our in vitro 3D OFT explant experiments [29] where transcript levels of periostin were upregulated in

OFT cushion tissue. Periostin is a product of TGF $\beta$ 3 signaling and has been shown to regulate chick AV valve maturation [83].

The coordinated signaling events between TGF $\beta$ , BMP and Notch pathways are important for EMT and thus formation of valve primordia and eventually the development of mature cardiac valves [84-86]. In the current study, we investigated the expression of a representative panel of genes important for EMT. The type III TGF $\beta$  receptor (TGF $\beta$ RIII) is the ligand presenting receptor and plays an important role in cushion EMT [87]. We observed a significant increase in gene expression of *tgfbRIII* and *tgfb3* in the OFT cushions of the banded hearts. However, there was no significant difference in expression levels of *tgfb2* between OFT of the banded and control hearts. *Snai2* is an important transcription factor of TGF $\beta$  signaling that induces EMT by decreasing expression of adhesion molecules including E-cadherin [5]. Even though we did not observe any alteration in gene expression of *snai2* in OFT tissue from the banded hearts, there was a significant decrease in the number of cells undergoing EMT and thus invading the cushion tissue. This may be due to the effect of altered hemodynamics on a *Snai2*-independent EMT process. Thus, there seems to be activation of only the upstream events of TGF $\beta$  signaling in OFT tissue by the change in hemodynamics in the heart. The increase in TGF $\beta$ 3 levels could partially contribute to the enhanced expression of periostin in OFT cushions of the banded heart. OFT banding did not lead to any significant alteration in hyaluronic acid synthetase 2 (*has2*) and *filamen A* mRNA in OFT tissue. *Has2* synthesizes hyaluronic acid, which is a major component of cushion ECM and is required for cushion EMT [88,89]; while *filamen A* is involved in cell migration. Thus, hemodynamics may not influence the expression of these genes at this site at least

at this early stage of valve development. Cadherin-11 (CDH11) is a type II classical cadherin that is found in the endothelium and mesenchyme of embryonic cushion tissue and may play a migratory role in populating the cardiac jelly [90]. OFT banding led to a significant downregulation in the expression of *cdh11* in OFT cushions. This indicates that changing cardiac hemodynamics in the embryonic heart could potentially affect the migration of endothelial cells, an important process of valve formation. Lastly, we found a significant increase in the expression of matrix metalloproteinase 2 (*mmp2*) in the OFT cushions of the banded hearts. MMP2 is required for degradation of the ECM and cell migration. However, it should be noted that MMP2 has to be proteolytically activated [91], which was not investigated in our study. Thus, we can only conclude that altered intracardiac hemodynamics seems to influence the expression of this gene at the mRNA level.

Of the 116 genes, revealed in global transcriptome analysis, that were differentially expressed in OFT cushion tissue from banded relative to that of control hearts, the expression of 11 genes was validated by qPCR. These genes were selected due to their specific roles in heart and valve development including migration of endothelial cells, valve leaflet formation and EMT [92-99]. Differential expression of these genes due to altered hemodynamics could have pathological consequences leading to the development of abnormal OFT valves with compromised function.

Both Herovici's collagen staining and IF revealed a decrease in the expression of type I collagen in cushions of OFT from banded vs. control hearts. There was also increased deposition of periostin and IST-9 in the banded cushions relative to that from control hearts. This abnormality in the expression and deposition of ECM proteins could

have pathological consequences. Thus, alteration of hemodynamic stimuli within the embryonic heart affects the mRNA and protein expression and localization of ECM in OFT cushions in vitro [29] and in vivo.

As mentioned above, message levels of *tgfb3* and *tgfbRIII* were upregulated in response to OFT banding. However, transcript levels of inhibitory smads (*smad6/7*) were also upregulated as a result of altered intracardiac hemodynamic loads. Moreover, there was decreased expression in EMT/mesenchymal markers – N cadherin, fibronectin and vimentin – in the OFT cushions from banded relative to control hearts. To definitively identify a decrease in EMT in response to altered hemodynamics, a collagen gel assay was performed by seeding OFT cushion explants from control and banded hearts on collagen gels. Although there was no significant change in the depth of the collagen invaded by mesenchymal cells from control and banded OFT explants, the number of cells were significantly lower from OFT explants from the banded hearts compared to explants from control hearts. Furthermore, as mentioned above, there was a reduction in cell number in the OFT cushions from banded hearts in relation to OFT cushions from controls (counted from H&E stained heart sections). Thus, we conclude that perturbation of hemodynamic stimuli through the embryonic heart leads to a decrease in EMT which could lead to the development of pathological OFT valves.

Serotonin is a neurotransmitter that also has exerts activity in the heart and vasculature [100-102]. Extracellular and intracellular activities of serotonin seem to be important for development and functioning of heart valves [103]. Transcript levels of the serotonin receptor (*htr1e*) were significantly downregulated in OFT cushion tissue from banded hearts compared to that from controls. Receptor binding was shown to activate

TGF $\beta$  signaling [103]. In our study, we did not see any noticeable change in the phosphorylation of ERK 1 / 2 in OFT from banded relative to control hearts. Thus, it is possible that OFT banding does not have an effect on non-canonical TGF $\beta$  signaling. While there was no significant change in mRNA levels of *smad4* in OFT tissue of banded vs. control (data not shown), SMAD phosphorylation status was not evaluated in response to altered hemodynamics in our banded system. However, as noted above, OFT banding did lead to a decrease in OFT cushion EMT as well as decreased expression of ECM proteins type I collagen and fibronectin.

It was recently shown that serotonin molecularly interacts with filamen A and this interaction is dependent on the activity of the enzyme transglutaminase 2 (TGM2) [104]. This TGM2-mediated serotonylation of filamin-A has been shown to be important in the organization of valve ECM layers [104]. In our study, there was no significant alteration in the mRNA level of *filamen A*; however, the serotonin transporter (*sert*) was significantly upregulated in OFT tissue from banded vs. that of control hearts. *tgm2* expression was increased, both at the mRNA and protein level. Even though our experiments were performed on embryos very early in development, abnormality in expression of these players could potentially affect future valve ECM stratification and thus lead to formation of diseased valves.

There was no significant loss of OFT cushion cells due to apoptosis in control and banded hearts as revealed by TUNEL staining, as would be expected at this stage of embryonic development [105].

OFT banding did not cause any significant change in transcript levels of genes in table 5.1 in AV cushion tissue relative to AV cushions of controls (data not shown). This

could probably indicate that altering hemodynamics in the OFT (by banding) causes changes in gene expression limited locally to OFT tissue, at least at this stage in embryonic development. However, IF experiments revealed differential expression and localization of EMT / ECM proteins in AV cushions from OFT banded hearts relative to AV cushions of non-banded controls. There seemed to be a decrease in deposition of ECM proteins, such as type I collagen and periostin, in AV cushions from banded vs. controls, there also seemed to be an increase in EMT markers fibronectin and vimentin. However, when AV cushion explants were seeded on collagen gels, no statistically significant differences were observed in the number of cells invading the gel from AV explants from banded and control groups, although there was a significant decrease in the depth of the gel invaded by cells from AV explants from OFT banded hearts. Thus, even though EMT markers seem to be upregulated in AV cushions from banded hearts, there is no difference in AV cushion mesenchymal cell number between the two groups, as revealed by collagen assay. These data suggest that perturbation of intracardiac hemodynamics by OFT banding, affects the secretory profile (decrease in ECM deposition) and migratory capacity of AV mesenchyme (decrease depth of collagen invaded). While the expression of EMT markers appears to be upregulated in AV cushions from banded hearts, OFT banding does not seem to affect the EMT process in the AV cushions (invading cell number in collagen assay), at least at this developmental stage and at this time point of analysis (24 hr post banding).

As in the banded OFT cushions, AV cushion mesenchyme from banded hearts revealed an increase in proliferation as seen by PCNA IF staining. Furthermore, AV sections from OFT banded hearts revealed a gap between the two AV cushions. At this

stage of development, the two AV cushions are close to fusing (as seen in control heart sections). This gap might be due to differential pressure created in the AV canal as a result of OFT banding. While studies have reported an increase in ventricular pressure as a result of OFT banding [72,106], real-time changes in pressure at different locations in our system due to OFT banding need to be determined.

## CHAPTER 9

### DISCUSSION- EFFECTS OF RELEASING THE CONSTRICTION AROUND THE OFT<sup>7</sup>

The focus of this study was to investigate if the altered cellular and molecular profile, due to changes in hemodynamics, could be reversed if the band around the OFT was released.

Morphological examination of hearts revealed that even after the band around the OFT was released, the OFT continued to show a deformed configuration relative to the controls. At the 24 hr PBR time point, the OFT of the recovery hearts was bent to a greater degree relative to that of the controls. In comparison, 48 hr PBR hearts displayed a couple of different altered phenotypes with the majority of those exhibiting an elongated phenotype with a narrower overall ventricle. Surprisingly, when the distance of the outer wall of the OFT was measured from the whole heart images, there was no persistent narrowing of the OFT (figure 6.2). These anomalous cardiac phenotypes are likely to affect immediate and future cardiac function.

Hemodynamics adapt to meet the evolving demands of the developing embryo. Accordingly, we observed that the blood flow velocity steadily increased with embryo maturity as expected, and was dramatically altered with the application of a fixed

---

<sup>7</sup> Parts of this chapter have been excerpted from Menon V; Eberth J; Junor L; Potts AJ; Belhaj M; DiPette DJ; Jenkins M; JD, P. Removing vessel constriction on the embryonic heart results in changes in valve gene expression, morphology, and hemodynamics. *Dev Dyn* **2017**

diameter band around the OVJ. The banding process creates a stenotic jet as documented previously and confirmed by others [52,62,107]. Our measured velocity is close to those reported by other investigators analyzing early stage embryos at the proximal outflow tract [44,62,73,74]. We note that at later time points, OFT septation has a dramatic effect on distal hemodynamic analysis and for simplicity purposes, we focused our attention on a consistent but proximal section of the OFT near the OVJ. As such we found that at 24 and 48 hr after removal of the band, blood flow velocity at this location had returned to levels near those of the stage- matched controls; a pattern repeated for the time averaged, peak, and retrograde flow velocities. For the 24 and 48 hr stage matched controls, our shear stress values were slightly lower than those described by other researchers [73]. but as noted earlier, this depends largely on the location of the analysis. Time averaged, peak, and retrograde wall shear stress were shown to be restored for the 24 hr PBR time point, but somewhat surprisingly, it was not restored at the 48 hr PBR time point when compared to stage-matched controls. Differences were minor but statistically significant. We note that these differences were likely caused by shape, rather than size effects. Two predominant morphological changes were observed in the PBR hearts represented by a thinner elongated ventral and a shorter wider heart with an increased flexure of the OFT. Regardless, failure to generate normalized shear stress could be due to pathological processes that occurred early on (as a result of banding) thereby creating altered tissue morphologies. This could potentially lead to a vicious cycle of growth and remodeling or complete restoration of a healthy phenotype. Future work will be needed to elucidate the long-term effects.

Overall, our gene expression data indicate that after releasing the band, transcript levels, of the key EMT and valve development genes analyzed in this study, vary in their response. Increased shear stress contributes to both immediate and delayed gene expression profiles so it is difficult to tease out cause-and-effect from this alone. Furthermore, there appears to be a gene-specific, rather than a process-specific, response to band removal. We speculate the one possible scenario is that 24 hr after banding, the heart undergoes a “first wave” of remodeling in response to altered intracardiac hemodynamics. For example, *colVI*, *tgfb3* and *periostin* were upregulated early following band removal (i.e. 24hr PBR). Then, some cellular and molecular processes do not immediately return to normal, instead the heart undergoes a “second wave” of remodeling which are represented by changes in *rho A*, *tgfbRIII* and *periostin*.

Genes known to play a role in mechanotransduction, ECM production and EMT showed varying responses to removal of the OFT band. An important mechanotransducer is rhoA. 24 hr after the band was removed, *rhoA* transcript levels in the OFT of the recovery hearts were normalized, which would indicate that any potential consequences of altered intracardiac hemodynamics on mechanotransduction, 24 hr after banding, were not observed. However, at the 48 hr PBR time point, *rhoA* message levels are downregulated, which may suggest inappropriate ECM production due to altered mechanotransduction which could lead to abnormal OFT valves.

ECM produced by cushion mesenchyme is pivotal for the formation of healthy cardiac valves with abnormal expression/deposition of ECM proteins leading to pathological conditions [38]. Transcript levels of both collagen I and VI showed similar expression patterns: upregulated at 24 hr PBR and then normalized at the 48 hr PBR time

point. In contrast, *periostin* mRNA is upregulated 24 hr PBR, but is then downregulated 48 hr PBR. The dysregulation observed in the expression of collagen and periostin 24 hr PBR suggests that the ECM remodeling is likely taking place and by 48 hr PBR the expression begins to taper back to normal levels. Even though collagen levels are normalized 48 hr PBR, the initial alterations may still have negative consequences on OFT valve development despite levels tending to normalize. It is possible that what is occurring is a change in the timing of the remodeling and despite normalizing of transcript levels, proper development of cushion is already altered.

Finally, the expression of a panel of important genes involved in EMT and cell migration showed a variety of responses. Transcript levels of the ligand-presenting type III tgf beta receptor (*tgfbRIII*) were normalized 24 hr PBR, but are downregulated 48 hr PBR. The type III tgf beta ligand (*tgfbIII*), in contrast, continued to stay upregulated 24 hr PBR and at the 48 hr PBR time point, levels normalized to those of stage-matched controls. *mmp2* and *cdh11* were normalized at the 24 hr PBR time point and continued to maintain expression levels similar to 48 hr stage matched controls.

As reported previously, OFT banding causes a significant decrease in the volume of the OFT cushion, 24 hr after surgery. We continue to see this decrease in OFT cushion volume 24 hr after releasing the band. This suggests that even once hemodynamic stimuli are restored, the OFT continues to exhibit a decrease in cushion volume. 48 hr PBR, cushion volume of the OFT in the recovery group is normalized; however, the OFT lumen still exhibits a malformed phenotype. Thus, with respect to cushion volume, it seems like the OFT cushion does recover from banding, but the cardiac pathological state caused by altered hemodynamics does not seem to improve even 48 hr after the band has

been removed. In addition, we also previously demonstrated that OFT cushions were hypocellular 24 hr post surgery. Here, we report that even though we do not see any significant differences in cell volume at either 24 or 48 hr PBR, we do see a significant decrease in the cushion to cell volume ratio at 24 hr PBR. This makes sense as our cushion volume is decreased and cell volume is not significantly decreased. This may be indicative of the cells slowing their secretory phenotype in response to the banding and increasing their proliferative capacity. In contrast, at 48hr PBR the cell volume is similar to control and the ratio of cushion to cell volume is no longer significant. This decrease in cushion volume early could lead to inappropriate ECM production and thus defective OFT cushion and eventually valve development. It is important to mention that we have observed no significant apoptosis in the OFT cushion mesenchyme from control or banded hearts 24 h after surgery.

A clear limitation to our hemodynamic analysis is the use of fixed geometries in CFD simulations. Although our H&E stained cross sections were fixed under physiological conditions, they represent a single time point in the changing cardiac cycle that involves both expansion and retraction of the tissue. On the other hand, the hemodynamic waveforms were recreated for the entire cardiac cycle. Banded and control wall dynamics have been examined by other groups and shown to play an important role in this model system, but requires more advanced imaging modalities than are available at our institution [107]. We acknowledge this to be a limitation in our current study, however, when considered with the genetic and cellular profiles in this dynamic tissue, the current work lends insight into these important and complicated relationships.

## CHAPTER 10

### DISCUSSION (PRELIMINARY STUDY) - MOLECULAR RESPONSES TO OFT BANDING AT DIFFERENT DEVELOPMENTAL STAGES

Optical pacing is another method used to alter hemodynamics though the developing heart which has been shown to cause several CHDs [53,108-110]. It was observed that pacing hearts only at a certain developmental stage resulted in the paced embryos exhibiting CHDs (Jenkins lab – personal communication). Thus, there seems to be a ‘window of vulnerability’ during embryonic development where the heart is more susceptible to changes in hemodynamics.

As mentioned in above sections, our data suggest that there is adaptation by the heart in response to the OFT banding. Once the constriction is released, the heart goes through another adjustment and subsequent molecular remodeling occurs. This preliminary study was designed to investigate if there exists such a developmental period of enhanced susceptibility of chick embryonic hearts to OFT banding. HH 14 represents the developmental stage before which cushion EMT begins and at HH 20 OFT cushions undergo active EMT. Gene expression was profiled 24 hr after banding at HH 14 and HH 20 from OFTs of banded relative to control embryos at these stages.

There was no significant change in the expression of genes analyzed in OFT cushion tissue from banded compared to that from control hearts at HH 14 except for

type I collagen, which was upregulated. Type VI collagen showed a decreased expression, at the mRNA level, in banded OFTs at HH 20. As described above, transcript levels of type I and type VI collagen were downregulated in OFTs obtained 24 hr after banding at HH 17. These data suggest that expression of collagen is sensitive to changes in flow through the embryonic heart. Thus, for most of the genes analyzed, expression seems to be affected only if hemodynamic stimuli are altered at that developmental stage at which EMT commences. However, the differential mRNA expression of collagen in response to OFT banding at early and late embryonic developmental periods could potentially lead to anomalous OFT valve development with a compromise in function.

## CHAPTER 11

### CONCLUSIONS

We have developed a novel ex ovo OFT banding method of altering hemodynamics through the developing chick heart. Using this method, it is now possible to investigate the cellular and molecular biology of perturbed hemodynamics, which had not been done previously. Ultrasound imaging and CFD analysis confirmed that banding the OFT at the OVJ caused an increase in blood flow velocity and a corresponding increase in shear stress without any significant compromise on cardiovascular function thereby validating the banding protocol. Using this model, we have shown for the first time, that altered intracardiac hemodynamics has consequences at the cellular and molecular level which could potentially lead to the formation of abnormal cardiac valves. OFT EMT and ECM production were negatively affected by the banding intervention. OFT banding also influenced the secretory profile and migratory capacity of AV cushion cells.

Banding the OFT and its subsequent release results in continued morphologically altered hearts. In addition, perturbed hemodynamic stimuli persist once the OFT is no longer constricted. Moreover, some aspects of the genetic/cellular profiles, affected by altered hemodynamics, seem to normalize, especially 48 hr after band release. However, not all processes normalize in response to band removal (e.g., cushion volume). Moreover, this suggests that at this time in development, the heart is very susceptible to changes in hemodynamics. Cardiac defects due to changes in hemodynamic stimuli may

be the result of a short perturbation that is then resolved. However, this would need to be verified by examining older hearts that have had early perturbations for a short period. It could well be that the time in which the band is placed is more crucial than the length in which the band is maintained.

## CHAPTER 12

### FUTURE STUDIES

One of the advantages of the ex ovo banding model described here is that it allows for molecular analysis of acute effects of altered intracardiac hemodynamics. However, an important next step is to evaluate the chronic defects induced by perturbing hemodynamics through the heart by banding at early developmental stages and studying the pathways and cellular responses at later stages. This will allow for identification of potential mechanisms that go awry due to altered hemodynamic stimuli leading to congenital valvular defects.

It is well known that OFT banding changes the pressure within the heart. However, due to limitations in the availability of pressure sensors, we were not able to obtain real-time pressure changes in response to banding. It would be important to determine these variations in pressure especially in the AV canal, which would conclusively explain the gap seen between the AV cushions of the OFT banded heart.

Studies from our laboratory have so far shown EMT to be altered due to OFT banding. This has been demonstrated at the cellular as well as genetic levels. It is then crucial to identify epigenetic markers that are altered due to banding. Towards this end, ChiP-Seq will be performed to identify alteration of chromatin marks specific to EMT in response to changing intracardiac hemodynamics.

While we have shown OFT banding to alter molecular processes, it is imperative to determine if other methods used to change blood flow through the embryonic heart

lead to CHDs by affecting similar pathways. Towards this end, chick embryos will be optically paced and the resulting molecular pathways dissected.

## REFERENCES

1. Whitteridge, G. William harvey on the circulation of the blood and on generation. *Am J Med* **1978**, *65*, 888-890.
2. Auffray, C.; Noble, D. Origins of systems biology in william harvey's masterpiece on the movement of the heart and the blood in animals. *Int J Mol Sci* **2009**, *10*, 1658-1669.
3. Hinton, R.; Yutzey, K. Heart valve structure and function in development and disease. *Annu Rev Physiol* **2011**, *73*, 29-46.
4. Neeb, Z.; Lajiness, J.; Bolanis, E.; Conway, S. Cardiac outflow tract anomalies. *Wiley Interdiscip Rev Dev Biol* **2013**, *2*, 499-530.
5. von Gise, A.; Pu, W. Endocardial and epicardial epithelial to mesenchymal transitions in heart development and disease. *Circ Res* **2012**, *110*, 1628-1645.
6. Person, A.; Klewer, S.; Runyan, R. Cell biology of cardiac cushion development. *Int Rev Cytol* **2005**, *243*, 287-335.
7. de Vlaming, A.; Sauls, K.; Hajdu, Z.; Visconti, R.; Mehesz, A.; Levine, R.; Slangenaupt, S.; Hagège, A.; Chester, A.; Markwald, R., *et al.* Atrioventricular valve development: New perspectives on an old theme. *Differentiation* **2012**, *84*, 103-116.
8. Webb, S.; Qayyum, S.; Anderson, R.; Lamers, W.; Richardson, M. Septation and separation within the outflow tract of the developing heart. *J Anat* **2003**, *202*, 327-342.

9. de Lange, F.; Moorman, A.; Anderson, R.; Männer, J.; Soufan, A.; de Gier-de Vries, C.; Schneider, M.; Webb, S.; van den Hoff, M.; Christoffels, V. Lineage and morphogenetic analysis of the cardiac valves. *Circ Res* **2004**, *95*, 645-654.
10. Restivo, A.; Piacentini, G.; Placidi, S.; Saffirio, C.; Marino, B. Cardiac outflow tract: A review of some embryogenetic aspects of the conotruncal region of the heart. *Anat Rec A Discov Mol Cell Evol Biol* **2006**, *288*, 936-943.
11. Okamoto, N.; Akimoto, N.; Hidaka, N.; Shoji, S.; Sumida, H. Formal genesis of the outflow tracts of the heart revisited: Previous works in the light of recent observations. *Congenit Anom (Kyoto)* **2010**, *50*, 141-148.
12. Anderson, R.; Webb, S.; Brown, N.; Lamers, W.; Moorman, A. Development of the heart: (3) formation of the ventricular outflow tracts, arterial valves, and intrapericardial arterial trunks. *Heart* **2003**, *89*, 1110-1118.
13. Nakaya, Y.; Sheng, G. Emt in developmental morphogenesis. *Cancer Lett.* **2013**, *341*, 9-15.
14. Nakaya, Y.; Sheng, G. An amicable separation: Chick's way of doing emt. *Cell Adh Migr* **2009**, *3*, 160-163.
15. Icardo, J. Changes in endocardial cell morphology during development of the endocardial cushions. *Anat Embryol (Berl)* **1989**, *179*, 443-448.
16. Bernanke, D.; Markwald, R. Migratory behavior of cardiac cushion tissue cells in a collagen-lattice culture system. *Dev Biol* **1982**, *91*, 235-245.
17. Runyan, R.; Markwald, R. Invasion of mesenchyme into three-dimensional collagen gels: A regional and temporal analysis of interaction in embryonic heart tissue. *Dev Biol* **1983**, *95*, 108-114.

18. Mjaatvedt, C.; Lepera, R.; Markwald, R. Myocardial specificity for initiating endothelial-mesenchymal cell transition in embryonic chick heart correlates with a particulate distribution of fibronectin. *Dev Biol* **1987**, *119*, 59-67.
19. Armstrong, E.; Bischoff, J. Heart valve development: Endothelial cell signaling and differentiation. *Circ Res* **2004**, *95*, 459-470.
20. Zeisberg, M.; Neilson, E. Biomarkers for epithelial-mesenchymal transitions. *J Clin Invest*. **2009**, *119*, 1429-1437.
21. Rugonyi, S. Cardiac mechanics, hemodynamics, and embryonic heart development. *The FASEB Journal* **2016**, *30*.
22. Culver, J.; Dickinson, M.E. The effects of hemodynamic force on embryonic development. *Microcirculation* **2010**, *17*, 164-178.
23. Davies, P. Flow-mediated endothelial mechanotransduction. *Physiol Rev* **1995**, *75*, 3.
24. Butcher, J.; McQuinn, T.; Sedmera, D.; Turner, D.; Markwald, R. Transitions in early embryonic atrioventricular valvular function correspond with changes in cushion biomechanics that are predictable by tissue composition. *Circ Res* **2007**, *100*, 1503-1511.
25. Hove, J.; Köster, R.; Forouhar, A.; Acevedo-Bolton, G.; Fraser, S.; Gharib, M. Intracardiac fluid forces are an essential epigenetic factor for embryonic cardiogenesis. *Nature* **2003**, *421*, 127-127.
26. Egorova, A.; Khedoe, P.; Goumans, M.; Yoder, B.; Nauli, S.; ten Dijke, P.; Poelmann, R.; Hierck, B. Lack of primary cilia primes shear- induced endothelial-to-mesenchymal transition. *Circ Res* **2011**, *108*, 1093-1101.

27. Sewell-Loftin, M.; DeLaughter, D.; Peacock, J.; Brown, C.; Baldwin, H.; Barnett, J.; Merryman, W. Myocardial contraction and hyaluronic acid mechanotransduction in epithelial-to-mesenchymal transformation of endocardial cells. *Biomaterials* **2014**, *35*, 2809-2815.
28. Tan, H.; Biechler, S.; Junor, L.; Yost, M.; Dean, D.; Li, J.; Potts, J.; Goodwin, R. Fluid flow forces and rhoa regulate fibrous development of the atrioventricular valves. *Dev Biol* **2013**, *374*, 345-356.
29. Biechler, S.; Junor, L.; Evans, A.; Eberth, J.; Price, R.; Potts, J.; Yost, M.; Goodwin, R. The impact of flow-induced forces on the morphogenesis of the outflow tract. *Front Physiol* **2014**, *5*.
30. Hoffman, J.; Kaplan, S. The incidence of congenital heart disease. *J Am Coll Cardiol* **2002**, *39*, 1890-1900.
31. Yang, Q.; Chen, H.; Correa, A.; Devine, O.; Mathews, T.; Honein, M. Racial differences in infant mortality attributable to birth defects in the united states, 1989-2002. *Birth Defects Res A Clin Mol Teratol* **2006**, *76*, 706-713.
32. Hoffman, J. Incidence of congenital heart disease: Ii. Prenatal incidence. *Pediatr Cardiol* **1995**, *16*, 155-165.
33. Bruneau, B. The developmental genetics of congenital heart disease. *Nature* **2008**, *451*, 943-948.
34. Goldstein, S. Embryonic death in early pregnancy: A new look at the first trimester. *Obstetrics and gynecology. Obstet Gynecol* **1994**, *84*, 294-297.
35. Mäkikallio, K.; Jouppila, P.; Räsänen, J. Human fetal cardiac function during the first trimester of pregnancy. *Heart* **2005**, *91*.

36. Gittenberger-de Groot, A.; Bartelings, M.; Deruiter, M.; Poelmann, R. Basics of cardiac development for the understanding of congenital heart malformations. *Pediatr Res* **2005**, *57*, 169-176.
37. Russo, C.; Elixhauser, A. Hospitalizations for birth defects, 2004: Statistical brief #24,” in healthcare cost and utilization project (hcup) statistical briefs. *Rockville, MD: Agency for Healthcare Research and Quality US* **2007**.
38. Combs, M.; Yutzey, K. Heart valve development: Regulatory networks in development and disease. *Circ Res* **2009**, *105*, 408-421.
39. Midgett, M.; Rugonyi, S. Congenital heart malformations induced by hemodynamic altering surgical interventions. *Front Physiol* **2014**, *5*, 287.
40. Jenkins, M.; Adler, D.; Gargesha, M.; Huber, R.; Rothenberg, F.; Belding, J.; Watanabe, M.; Wilson, D.; Fujimoto, J.; Rollins, A. Ultrahigh-speed optical coherence tomography imaging and visualization of the embryonic avian heart using a buffered fourier domain mode locked laser. *Opt Express* **2007**, *15*, 6251-6267.
41. Jenkins, M.; Peterson, L.; Gu, S.; Gargesha, M.; Wilson, D.; Watanabe, M.; Rollins, A. Measuring hemodynamics in the developing heart tube with four-dimensional gated doppler optical coherence tomography. *J Biomed Opt* **2010**, *15*.
42. Jenkins, M.W.; Watanabe, M.; Rollins, A.M. Longitudinal imaging of heart development with optical coherence tomography. *IEEE J Sel Top Quantum Electron* **2012**, *18*, 1166-1175.
43. Midgett, M.; Rugonyi, S. Analysis of 4d myocardial wall motion during early stages of chick heart development. *Methods Mol Biol* **2015**, *1299*, 191-212.

44. Goenezen, S.; Chivukula, V.; Midgett, M.; Phan, L.; Rugonyi, S. 4d subject-specific inverse modeling of the chick embryonic heart outflow tract hemodynamics. *Biomech Model Mechanobiol* **2016**, *15*, 723-743.
45. Ho, S.; Tan, G.; Foo, T.; Phan-Thien, N.; Yap, C. Organ dynamics and fluid dynamics of the hh25 chick embryonic cardiac ventricle as revealed by a novel 4d high-frequency ultrasound imaging technique and computational flow simulations. *Ann Biomed Eng* **2017**.
46. Hu, N.; Clark, E. Hemodynamics of the stage 12 to stage 29 chick embryo. *Circ Res* **1989**, *65*, 1665-1670.
47. Hogers, B.; DeRuiter, M.; Gittenberger-de Groot, A.; Poelmann, R. Unilateral vitelline vein ligation alters intracardiac blood flow patterns and morphogenesis in the chick embryo. *Circ Res* **1997**, *80*, 473-481.
48. Hogers, B.; DeRuiter, M.; Gittenberger-de Groot, A.; Poelmann, R. Extraembryonic venous obstructions lead to cardiovascular malformations and can be embryolethal. *Cardiovasc Res* **1999**, *41*, 87-99.
49. Reckova, M.; Rosengarten, C.; deAlmeida, A.; Stanley, C.; Wessels, A.; Gourdie, R.; Thompson, R.; Sedmera, D. Hemodynamics is a key epigenetic factor in development of the cardiac conduction system. *Circ Res* **2003**, *93*, 77-85.
50. Stekelenburg-de Vos, S.; Ursem, N.; Hop, W.; Wladimiroff, J.; Gittenberger-de Groot, A.; Poelmann, R. Acutely altered hemodynamics following venous obstruction in the early chick embryo. *J Exp Biol* **2003**, *206*, 1051-1057.

51. Lucitti, J.; Tobita, K.; Keller, B. Arterial hemodynamics and mechanical properties after circulatory intervention in the chick embryo. *J Exp Biol* **2005**, *208*, 1877-1885.
52. Menon, V.; Eberth, J.; Goodwin, R.; Potts, J. Altered hemodynamics in the embryonic heart affects outflow valve development. *J Cardiovasc Dev Dis.* **2015**, *2*, 108-124.
53. Ford, S.; McPheeters, M.; Wang, Y.; Ma, P.; Gu, S.; Strainic, J.; Snyder, C.; Rollins, A.; Watanabe, M.; Jenkins, M. Increased regurgitant flow causes endocardial cushion defects in an avian embryonic model of congenital heart disease. *Congenit Heart Dis* **2017**, *12*, 322-331.
54. Midgett, M.; López, C.; David, L.; Maloyan, A.; Rugonyi, S. Increased hemodynamic load in early embryonic stages alters endocardial to mesenchymal transition. *Front Physiol* **2017**, *8*.
55. Menon, V.; Eberth, J.; Junor, L.; Potts, A.; Belhaj, M.; DiPette, D.; Jenkins, M.; Potts, J. Removing vessel constriction on the embryonic heart results in changes in valve gene expression, morphology, and hemodynamics. *Dev Dyn* **2017**.
56. Pang, K.; Parnall, M.; Loughna, S. Effect of altered haemodynamics on the developing mitral valve in chick embryonic heart. *J Mol Cell Cardiol* **2017**, *108*, 114-126.
57. Broekhuizen, M.; Hogers, B.; DeRuiter, M.; Poelmann, R.; Gittenberger-de Groot, A.; Wladimiroff, J. Altered hemodynamics in chick embryos after extraembryonic venous obstruction. *Ultrasound Obstet Gynecol* **1999**, *13*, 437-445.

58. deAlmeida A; McQuinn T; D, S. Increased ventricular preload is compensated by myocyte proliferation in normal and hypoplastic fetal chick left ventricle. *Circ Res* **2007**, *100*, 1363-1370.
59. Menon, V.; Junor, L.; Balhaj, M.; Eberth, J.; Potts, J. A novel ex ovo banding technique to alter intracardiac hemodynamics in an embryonic chicken system. *J Vis Exp* **2016**, *13*.
60. McQuinn, T.; Bratoeva, M.; Dealmeida, A.; Remond, M.; Thompson, R.; Sedmera, D. High-frequency ultrasonographic imaging of avian cardiovascular development. *Dev Dyn* **2007**, *236*, 3503-3513.
61. Kain, K.; Miller, J.; Jones-Paris, C.; Thomason, R.; Lewis, J.; Bader, D.; Barnett, J.; Zijlstra, A. The chick embryo as an expanding experimental model for cancer and cardiovascular research. *Dev Dyn* **2014**, *243*, 216-228.
62. Midgett, M.; Goenezen, S.; Rugonyi, S. Blood flow dynamics reflect degree of outflow tract banding in hamburger-hamilton stage 18 chicken embryos. *J R Soc Interface* **2014**, *11*.
63. Menon, V.; Junor, L.; Eberth, J.; Ford, S.; McPheeters, M.; Jenkins, M.; Belhaj, M.; Potts, J. Molecular consequences of cardiac valve development as a result of altered hemodynamics. *Microsc. Microanal.* **2017**, *23*.
64. Lin, C.; Lin, C.; Chen, C.; Zhou, B.; Chang, C. Partitioning the heart: Mechanisms of cardiac septation and valve development. *Development* **2012**, *139*, 3277-3299.
65. Hamburger, V.; Hamilton, H. A series of normal stages in the development of the chick embryo. 1951. *Dev Dyn* **1992**, *195*, 231-272.

66. Schneider, C.; Rasband, W.; Eliceiri, K. Nih image to imagej: 25 years of image analysis. *Nat Methods* **2012**, *9*, 671-675.
67. McDonald, D.A.; Edward Arnold, L. Blood flow in arteries *Experimental Physiology* **1974**.
68. Pfaffl, M.W. A new mathematical model for relative quantification in real-time rt-pcr. *Nucleic Acids Res* **2001**, *29*, e45.
69. Ye, J.; Coulouris, G.; Zaretskaya, I.; Cutcutache, I.; Rozen, S.; Madden, T. Primer-blast: A tool to design target-specific primers for polymerase chain reaction. *BMC Bioinformatics* **2012**, *13*.
70. Weiss, R.M.; Miller, J.D.; Heistad, D.D. Fibrocalcific aortic valve disease: Opportunity to understand disease mechanisms using mouse models. *Circ Res* **2013**, *113*, 209-222.
71. Siu, S.; Silversides, C. Bicuspid aortic valve disease. *J Am Coll Cardiol* **2010**, *55*, 2789-2800.
72. Shi, L.; Goenezen, S.; Haller, S.; Hinds, M.; Thornburg, K.; Rugonyi, S. Alterations in pulse wave propagation reflect the degree of outflow tract banding in hh18 chicken embryos. *Am J Physiol Heart Circ Physiol* **2013**, *305*, H386-396.
73. Bharadwaj, K.; Spitz, C.; Shekhar, A.; Yalcin, H.; Butcher, J. Computational fluid dynamics of developing avian outflow tract heart valves. *Ann Biomed Eng* **2012**, *40*, 2212-2227.
74. Liu, A.; Nickerson, A.; Troyer, A.; Yin, X.; Cary, R.; Thornburg, K.; Wang, R.; Rugonyi, S. Quantifying blood flow and wall shear stresses in the outflow tract of chick embryonic hearts. *Comput Struct* **2011**, *89*, 855-867.

75. Yong, J.; He, L.; Wen-jing, L.; Hai-bin, T.; Chang-jun, C.; Fu-gui, L.; Yan-hang, Z.; Xiao-zhen, Q.; Zeng-bin, W.; Yu, W., *et al.* Endothelial aquaporin-1 (aqp1) expression is regulated by transcription factor mef2c. *Mol Cells* **2016**, *39*, 292-298.
76. Liu, H.; Wintour, M.E. Aquaporins in development – a review. *Reprod Biol Endocrinol* **2005**, *3*.
77. Haack, T.; Abdelilah-Seyfried, S. The force within: Endocardial development, mechanotransduction and signalling during cardiac morphogenesis. *Development* **2016**, *143*, 373-386.
78. Groenendijk, B.; Van der Heiden, K.; Hierck, B.; Poelmann, R. The role of shear stress on et-1, klf2, and nos-3 expression in the developing cardiovascular system of chicken embryos in a venous ligation model. *Physiology (Bethesda)* **2007**, *22*, 380-389.
79. Huddleson, J.; Ahmad, N.; Srinivasan, S.; Lingrel, J. Induction of klf2 by fluid shear stress requires a novel promoter element activated by a phosphatidylinositol 3-kinase-dependent chromatin-remodeling pathway. *J Biol Chem* **2005**, *280*, 23371-23379.
80. Chiplunkar, A.; Lung, T.; Alhashem, Y.; Koppenhaver, B.; Salloum, F.; RC, K.; Haar, J.; Lloyd, J. Krüppel-like factor 2 is required for normal mouse cardiac development. *PLoS One* **2013**, *8*.
81. Gross, L.; Kugel, M. Topographic anatomy and histology of the valves in the human heart. *Am J Pathol.* **1931**, *7*, 445-474.

82. Aikawa, E.; Whittaker, P.; Farber, M.; Mendelson, K.; Padera, R.; Aikawa, M.; Schoen, F. Human semilunar cardiac valve remodeling by activated cells from fetus to adult: Implications for postnatal adaptation, pathology, and tissue engineering. *Circulation* **2006**, *113*, 1344-1352.
83. Norris, R.; Potts, J.; Yost, M.; Junor, L.; Brooks, T.; Tan, H.; Hoffman, S.; Hart, M.; Kern, M.; Damon, B., *et al.* Periostin promotes a fibroblastic lineage pathway in atrioventricular valve progenitor cells. *Dev Dyn* **2009**, *238*, 1052-1063.
84. Garside, V.; Chang, A.; Karsan, A.; Hoodless, P. Co-ordinating notch, bmp, and tgf- $\beta$  signaling during heart valve development. *Cell Mol Life Sci* **2013**, *70*, 2899-2917.
85. Lencinas, A.; Tavares, A.; Barnett, J.; Runyan, R. Collagen gel analysis of epithelial-mesenchymal transition in the embryo heart: An in vitro model system for the analysis of tissue interaction, signal transduction, and environmental effects. *Birth Defects Res C Embryo Today* **2011**, *93*, 298-311.
86. Lim, J.; Thiery, J. Epithelial-mesenchymal transitions: Insights from development. *Development* **2012**, *139*, 3471-3486.
87. Brown, C.; Boyer, A.; Runyan, R.; Barnett, J. Requirement of type iii tgf-beta receptor for endocardial cell transformation in the heart. *Science* **1999**, *283*, 2080-2082.
88. Rodriguez, K.J.; Piechura, L.M.; Masters, K.S. Regulation of valvular interstitial cell phenotype and function by hyaluronic acid in 2-d and 3-d culture environments. *Matrix Biol* **2011**, *30*, 70-82.

89. Armstrong, E.; Bischoff, J. Heart valve development endothelial cell signaling and differentiation. *Circ Res* **2004**, *95*, 459-470.
90. Zhou, J.; Bowen, C.; Lu, G.; Knapp Iii, C.; Recknagel, A.; Norris, R.; Butcher, J. Cadherin-11 expression patterns in heart valves associate with key functions during embryonic cushion formation, valve maturation and calcification. *Cells Tissues Organs* **2013**, *198*, 300-310.
91. Alexander, S.; Jackson, K.; Bushnell, K.; McGuire, P. Spatial and temporal expression of the 72-kda type iv collagenase (mmp-2) correlates with development and differentiation of valves in the embryonic avian heart. *Dev Dyn* **1997**, *209*, 261-268.
92. Wang, C.; Chen, I.; Kuo, M.; Su, P.; Lai, Z.; Wang, C.; Huang, W.; Hoffman, J.; Kuo, C.; You, M., *et al.* Zebrafish thsd7a is a neural protein required for angiogenic patterning during development. *Dev Dyn* **2011**, *240*, 1412-1421.
93. Li, J.; Yue, Y.; Zhao, Q. Retinoic acid signaling is essential for valvulogenesis by affecting endocardial cushions formation in zebrafish embryos. *Zebrafish* **2016**, *13*, 9-18.
94. Clay, M.; Halloran, M. Cadherin 6 promotes neural crest cell detachment via f-actin regulation and influences active rho distribution during epithelial-to-mesenchymal transitioncadherin 6 promotes neural crest cell detachment via f-actin regulation and influences active rho distribution during epithelial-to-mesenchymal transition. *Development* **2014**, *141*, 2506-2515.
95. Wessels, A.; van den Hoff, M.; Adamo, R.; Phelps, A.; Lockhart, M.; Sauls, K.; Briggs, L.; Norris, R.; van Wijk, B.; Perez-Pomares, J., *et al.* Epicardially derived

- fibroblasts preferentially contribute to the parietal leaflets of the atrioventricular valves in the murine heart. *Dev Biol* **2012**, *366*, 111-124.
96. Kang, J.; Gu, Y.; Li, P.; Johnson, B.; Sucov, H.; Thomas, P. Pdgf-a as an epicardial mitogen during heart development. *Dev Dyn* **2008**, *237*, 692-701.
97. Plageman TF Jr; KE, Y. T-box genes and heart development: Putting the "t" in heart. *Dev Dyn* **2005**, *232*, 11-20.
98. Braitsch, C.; Yutzey, K. Transcriptional control of cell lineage development in epicardium-derived cells. *J Dev Biol* **2013**, *1*, 92-111.
99. Chen, H.; Shi, S.; Acosta, L.; Li, W.; Lu, J.; Bao, S.; Chen, Z.; Yang, Z.; Schneider, M.; Chien, K., *et al.* Bmp10 is essential for maintaining cardiac growth during murine cardiogenesis. *Development* **2004**, *131*, 2219-2231.
100. Nebigil, C.; Maroteaux, L. A novel role for serotonin in heart. *Trends Cardiovasc Med* **2001**, *11*, 329-335.
101. Maurer-Spurej, E. Serotonin reuptake inhibitors and cardiovascular diseases: A platelet connection. *Cell Mol Life Sci* **2005**, *62*, 159-170.
102. Watts, S.; Morrison, S.; Davis, R.; Barman, S. Serotonin and blood pressure regulation. *Pharmacol Rev* **2012**, *64*, 359-388.
103. Pavone, L.; Norris, R. Distinct signaling pathways activated by "extracellular" and "intracellular" serotonin in heart valve development and disease. *Cell Biochem Biophys* **2013**, *67*, 819-828.
104. Sauls, K.; de Vlaming, A.; Harris, B.; Williams, K.; Wessels, A.; Levine, R.; Slaughter, S.; Goodwin, R.; Pavone, L.; Merot, J., *et al.* Developmental basis

- for filamin-a-associated myxomatous mitral valve disease. *Cardiovasc Res* **2012**, 96, 109-119.
105. BJ, M. Reference guide to the stages of chick heart embryology. *Dev Dyn* **2005**, 233, 1217-1237.
106. Tobita, K.; Schroder, E.; Tinney, J.; Garrison, J.; Keller, B. Regional passive ventricular stress-strain relations during development of altered loads in chick embryo. *Am J Physiol Heart Circ Physiol* **2002**, 282, H2386-2396.
107. Chivukula, V.; Goenezen, S.; Liu, A.; Rugonyi, S. Effect of outflow tract banding on embryonic cardiac hemodynamics. *J Cardiovasc Dev Dis.* **2016**, 3.
108. Ford, S.; Watanabe, M.; Jenkins, M. A review of optical pacing with infrared light. *J Neural Eng* **2017**.
109. Jenkins, M.; Duke, A.; Gu, S.; Chiel, H.; Fujioka, H.; Watanabe, M.; Jansen, E.; Rollins, A. Optical pacing of the embryonic heart. *Nat Photonics* **2010**, 4, 623-626.
110. Peterson, L.; McPheeters, M.; Barwick, L.; Gu, S.; Rollins, A.; Jenkins, M. Altering embryonic cardiac dynamics with optical pacing. *Conf Proc IEEE Eng Med Biol Soc* **2012**, 2012, 1382-1385.

## APPENDIX A – PERMISSION TO REPRINT

For chapters 1, 2, 5, 8

### **Altered Hemodynamics in the Embryonic Heart Affects Outflow Valve Development**

Vinal Menon<sup>1</sup> , John F. Eberth<sup>1,2</sup> , Richard L. Goodwin<sup>3</sup>  and Jay D. Potts<sup>1,2,\*</sup> 

<sup>1</sup> Department of Cell Biology and Anatomy, School of Medicine, University of South Carolina, Columbia, SC 29209, USA

<sup>2</sup> Biomedical Engineering Program, College of Engineering and Computing, University of South Carolina, Columbia, SC 29208, USA

<sup>3</sup> Biomedical Sciences, School of Medicine, University of South Carolina, Greenville, SC 29605, USA

\* Author to whom correspondence should be addressed.

Academic Editors: Cheryl L. Maslen and Russell Norris

Received: 10 March 2015 / Revised: 7 May 2015 / Accepted: 8 May 2015 / Published: 15 May 2015

(This article belongs to the Special Issue *Genetics and Cardiovascular Development and Disease*)

 [View Full-Text](#) |  [Download PDF](#) [3929 KB, uploaded 19 May 2015] |  [Browse Figures](#)

#### **Abstract**

Cardiac valve structure and function are primarily determined during early development. Consequently, abnormally-formed heart valves are the most common type of congenital heart defects. Several adult valve diseases can be backtracked to abnormal valve development, making it imperative to completely understand the process and regulation of heart valve development. Epithelial-to-mesenchymal transition (EMT) plays an important role in the development of heart valves. Though hemodynamics is vital to valve development, its role in regulating EMT is still unknown. In this study, intracardiac hemodynamics were altered by constricting the outflow tract (OFT)/ventricle junction (OVJ) of HH16–17 (Hamilton and Hamburger (HH) Stage 16–17) chicken embryos, *ex ovo* for 24 h. The constriction created an increase in peak and time-averaged centerline velocity along the OFT without changes to volumetric flow or heart rate. Computational fluid dynamics was used to estimate the level of increased spatially-averaged wall shear stresses on the OFT cushion from AMIRA reconstructions. OFT constriction led to a significant decrease in OFT cushion volume and the number of invaded mesenchyme in the OFT cushion. qPCR analysis revealed altered mRNA expression of a representative panel of genes, vital to valve development, in the OFT cushions from banded hearts. This study indicates the importance of hemodynamics in valve development. [View Full-Text](#)

**Keywords:** valvular disease; cardiac valve development; endocardial cushions; EMT; hemodynamics

This is an open access article distributed under the [Creative Commons Attribution License](#) which permits unrestricted use, distribution, and reproduction in any medium, provided the original work is properly cited. (CC BY 4.0).

For chapter 2:

← REPLY   ←← REPLY ALL   → FORWARD   ...



Adria Gottesman-Davis <adria.gottesman-davis@jove.com>

Wed 9/27/2017 11:58 AM

Mark as unread

To: Vinal Menon;

• You replied on 9/27/2017 12:05 PM.

Hello Vinal,

This letter is to confirm that you have permission from the Journal of Visualized Experiments to use your JoVE article, ID 53955, "**A Novel Ex Ovo Banding Technique to Alter Intracardiac Hemodynamics in an Embryonic Chicken System,**" as part of your PhD dissertation for the University of South Carolina School of Medicine-Columbia.

Best wishes,  
Adria

**CAMBRIDGE UNIVERSITY PRESS LICENSE  
TERMS AND CONDITIONS**

Sep 29, 2017

This Agreement between Mr. Vinal Menon ("You") and Cambridge University Press ("Cambridge University Press") consists of your license details and the terms and conditions provided by Cambridge University Press and Copyright Clearance Center.

License Number	4198250903399
License date	Sep 29, 2017
Licensed Content Publisher	Cambridge University Press
Licensed Content Publication	Microscopy and Microanalysis
Licensed Content Title	Molecular Consequences of Cardiac Valve Development as a Result of Altered Hemodynamics
Licensed Content Author	Vinal Menon, Lorain Junor, John Eberth, Stephanie Ford, Matt McPheeters, Michael Jenkins, Marwa Belhaj, Jay Potts
Licensed Content Date	Aug 4, 2017
Licensed Content Volume	23
Licensed Content Issue	S1
Start page	1330
End page	1331
Type of Use	Dissertation/Thesis
Requestor type	Author
Portion	Full article
Author of this Cambridge University Press article	Yes
Author / editor of the new work	Yes
Order reference number	
Territory for reuse	North America Only
Title of your thesis / dissertation	Hemodynamic regulation of cardiac valve development
Expected completion date	Nov 2017
Estimated size(pages)	130
Requestor Location	Mr. Vinal Menon 6439 Garners Ferry Road Bldg-1, Rm C-36  COLUMBIA, SC 29209 United States

Attn: Mr. Vinal Menon  
Publisher Tax ID GB823847609  
Billing Type Invoice  
Billing Address Mr. Vinal Menon  
6439 Garners Ferry Road  
Bldg-1, Rm C-36  
COLUMBIA, SC 29209  
United States  
Attn: Mr. Vinal Menon  
Total 0.00 USD

## Terms and Conditions

**TERMS & CONDITIONS**

Cambridge University Press grants the Licensee permission on a non-exclusive non-transferable basis to reproduce, make available or otherwise use the Licensed content 'Content' in the named territory 'Territory' for the purpose listed 'the Use' on Page 1 of this Agreement subject to the following terms and conditions.

1. The License is limited to the permission granted and the Content detailed herein and does not extend to any other permission or content.
2. Cambridge gives no warranty or indemnity in respect of any third-party copyright material included in the Content, for which the Licensee should seek separate permission clearance.
3. The integrity of the Content must be ensured.
4. The License does extend to any edition published specifically for the use of handicapped or reading-impaired individuals.
5. The Licensee shall provide a prominent acknowledgement in the following format:  
author/s, title of article, name of journal, volume number, issue number, page references, , reproduced with permission.

Other terms and conditions:

v1.0

Questions? [customercare@copyright.com](mailto:customercare@copyright.com) or +1-855-239-3415 (toll free in the US) or +1-978-646-2777.

**JOHN WILEY AND SONS LICENSE  
TERMS AND CONDITIONS**

Oct 04, 2017

This Agreement between Mr. Vinal Menon ("You") and John Wiley and Sons ("John Wiley and Sons") consists of your license details and the terms and conditions provided by John Wiley and Sons and Copyright Clearance Center.

License Number	4201940155649
License date	Oct 04, 2017
Licensed Content Publisher	John Wiley and Sons
Licensed Content Publication	Developmental Dynamics
Licensed Content Title	Removing vessel constriction on the embryonic heart results in changes in valve gene expression, morphology, and hemodynamics
Licensed Content Author	Vinal Menon,John F. Eberth,Lorain Junor,Alexander J. Potts,Marwa Belhaj,Donald J. Dipette,Michael W. Jenkins,Jay D. Potts
Licensed Content Date	Oct 4, 2017
Licensed Content Pages	1
Type of use	Dissertation/Thesis
Requestor type	Author of this Wiley article
Format	Electronic
Portion	Full article
Will you be translating?	No
Title of your thesis / dissertation	Hemodynamic regulation of cardiac valve development
Expected completion date	Nov 2017
Expected size (number of pages)	130
Requestor Location	Mr. Vinal Menon 6439 Garners Ferry Road Bldg-1, Rm C-36  COLUMBIA, SC 29209 United States Attn: Mr. Vinal Menon
Publisher Tax ID	EU826007151
Billing Type	Invoice
Billing Address	Mr. Vinal Menon 6439 Garners Ferry Road Bldg-1, Rm C-36

COLUMBIA, SC 29209  
United States  
Attn: Mr. Vinal Menon

Total 0.00 USD

[Terms and Conditions](#)

### TERMS AND CONDITIONS

This copyrighted material is owned by or exclusively licensed to John Wiley & Sons, Inc. or one of its group companies (each a "Wiley Company") or handled on behalf of a society with which a Wiley Company has exclusive publishing rights in relation to a particular work (collectively "WILEY"). By clicking "accept" in connection with completing this licensing transaction, you agree that the following terms and conditions apply to this transaction (along with the billing and payment terms and conditions established by the Copyright Clearance Center Inc., ("CCC's Billing and Payment terms and conditions"), at the time that you opened your RightsLink account (these are available at any time at <http://myaccount.copyright.com>).

#### Terms and Conditions

- The materials you have requested permission to reproduce or reuse (the "Wiley Materials") are protected by copyright.
- You are hereby granted a personal, non-exclusive, non-sub licensable (on a stand-alone basis), non-transferable, worldwide, limited license to reproduce the Wiley Materials for the purpose specified in the licensing process. This license, **and any CONTENT (PDF or image file) purchased as part of your order**, is for a one-time use only and limited to any maximum distribution number specified in the license. The first instance of republication or reuse granted by this license must be completed within two years of the date of the grant of this license (although copies prepared before the end date may be distributed thereafter). The Wiley Materials shall not be used in any other manner or for any other purpose, beyond what is granted in the license. Permission is granted subject to an appropriate acknowledgement given to the author, title of the material/book/journal and the publisher. You shall also duplicate the copyright notice that appears in the Wiley publication in your use of the Wiley Material. Permission is also granted on the understanding that nowhere in the text is a previously published source acknowledged for all or part of this Wiley Material. Any third party content is expressly excluded from this permission.
- With respect to the Wiley Materials, all rights are reserved. Except as expressly granted by the terms of the license, no part of the Wiley Materials may be copied, modified, adapted (except for minor reformatting required by the new Publication), translated, reproduced, transferred or distributed, in any form or by any means, and no derivative works may be made based on the Wiley Materials without the prior permission of the respective copyright owner. **For STM Signatory Publishers clearing permission under the terms of the [STM Permissions Guidelines](#) only, the terms of the license are extended to include subsequent editions and for editions in other languages, provided such editions are for the work as a whole in situ and does not involve the separate exploitation of the permitted figures or extracts,**

You may not alter, remove or suppress in any manner any copyright, trademark or other notices displayed by the Wiley Materials. You may not license, rent, sell, loan, lease, pledge, offer as security, transfer or assign the Wiley Materials on a stand-alone basis, or any of the rights granted to you hereunder to any other person.

- The Wiley Materials and all of the intellectual property rights therein shall at all times remain the exclusive property of John Wiley & Sons Inc, the Wiley Companies, or their respective licensors, and your interest therein is only that of having possession of and the right to reproduce the Wiley Materials pursuant to Section 2 herein during the continuance of this Agreement. You agree that you own no right, title or interest in or to the Wiley Materials or any of the intellectual property rights therein. You shall have no rights hereunder other than the license as provided for above in Section 2. No right, license or interest to any trademark, trade name, service mark or other branding ("Marks") of WILEY or its licensors is granted hereunder, and you agree that you shall not assert any such right, license or interest with respect thereto
- NEITHER WILEY NOR ITS LICENSORS MAKES ANY WARRANTY OR REPRESENTATION OF ANY KIND TO YOU OR ANY THIRD PARTY, EXPRESS, IMPLIED OR STATUTORY, WITH RESPECT TO THE MATERIALS OR THE ACCURACY OF ANY INFORMATION CONTAINED IN THE MATERIALS, INCLUDING, WITHOUT LIMITATION, ANY IMPLIED WARRANTY OF MERCHANTABILITY, ACCURACY, SATISFACTORY QUALITY, FITNESS FOR A PARTICULAR PURPOSE, USABILITY, INTEGRATION OR NON-INFRINGEMENT AND ALL SUCH WARRANTIES ARE HEREBY EXCLUDED BY WILEY AND ITS LICENSORS AND WAIVED BY YOU.
- WILEY shall have the right to terminate this Agreement immediately upon breach of this Agreement by you.
- You shall indemnify, defend and hold harmless WILEY, its Licensors and their respective directors, officers, agents and employees, from and against any actual or threatened claims, demands, causes of action or proceedings arising from any breach of this Agreement by you.
- IN NO EVENT SHALL WILEY OR ITS LICENSORS BE LIABLE TO YOU OR ANY OTHER PARTY OR ANY OTHER PERSON OR ENTITY FOR ANY SPECIAL, CONSEQUENTIAL, INCIDENTAL, INDIRECT, EXEMPLARY OR PUNITIVE DAMAGES, HOWEVER CAUSED, ARISING OUT OF OR IN CONNECTION WITH THE DOWNLOADING, PROVISIONING, VIEWING OR USE OF THE MATERIALS REGARDLESS OF THE FORM OF ACTION, WHETHER FOR BREACH OF CONTRACT, BREACH OF WARRANTY, TORT, NEGLIGENCE, INFRINGEMENT OR OTHERWISE (INCLUDING, WITHOUT LIMITATION, DAMAGES BASED ON LOSS OF PROFITS, DATA, FILES, USE, BUSINESS OPPORTUNITY OR CLAIMS OF THIRD PARTIES), AND WHETHER OR NOT THE PARTY HAS BEEN ADVISED OF THE POSSIBILITY OF SUCH DAMAGES. THIS LIMITATION SHALL APPLY NOTWITHSTANDING ANY

**FAILURE OF ESSENTIAL PURPOSE OF ANY LIMITED REMEDY PROVIDED HEREIN.**

- Should any provision of this Agreement be held by a court of competent jurisdiction to be illegal, invalid, or unenforceable, that provision shall be deemed amended to achieve as nearly as possible the same economic effect as the original provision, and the legality, validity and enforceability of the remaining provisions of this Agreement shall not be affected or impaired thereby.
- The failure of either party to enforce any term or condition of this Agreement shall not constitute a waiver of either party's right to enforce each and every term and condition of this Agreement. No breach under this agreement shall be deemed waived or excused by either party unless such waiver or consent is in writing signed by the party granting such waiver or consent. The waiver by or consent of a party to a breach of any provision of this Agreement shall not operate or be construed as a waiver of or consent to any other or subsequent breach by such other party.
- This Agreement may not be assigned (including by operation of law or otherwise) by you without WILEY's prior written consent.
- Any fee required for this permission shall be non-refundable after thirty (30) days from receipt by the CCC.
- These terms and conditions together with CCC's Billing and Payment terms and conditions (which are incorporated herein) form the entire agreement between you and WILEY concerning this licensing transaction and (in the absence of fraud) supersedes all prior agreements and representations of the parties, oral or written. This Agreement may not be amended except in writing signed by both parties. This Agreement shall be binding upon and inure to the benefit of the parties' successors, legal representatives, and authorized assigns.
- In the event of any conflict between your obligations established by these terms and conditions and those established by CCC's Billing and Payment terms and conditions, these terms and conditions shall prevail.
- WILEY expressly reserves all rights not specifically granted in the combination of (i) the license details provided by you and accepted in the course of this licensing transaction, (ii) these terms and conditions and (iii) CCC's Billing and Payment terms and conditions.
- This Agreement will be void if the Type of Use, Format, Circulation, or Requestor Type was misrepresented during the licensing process.
- This Agreement shall be governed by and construed in accordance with the laws of the State of New York, USA, without regards to such state's conflict of law rules. Any legal action, suit or proceeding arising out of or relating to these Terms and Conditions or the breach thereof shall be instituted in a court of competent jurisdiction in New

York County in the State of New York in the United States of America and each party hereby consents and submits to the personal jurisdiction of such court, waives any objection to venue in such court and consents to service of process by registered or certified mail, return receipt requested, at the last known address of such party.

#### **WILEY OPEN ACCESS TERMS AND CONDITIONS**

Wiley Publishes Open Access Articles in fully Open Access Journals and in Subscription journals offering Online Open. Although most of the fully Open Access journals publish open access articles under the terms of the Creative Commons Attribution (CC BY) License only, the subscription journals and a few of the Open Access Journals offer a choice of Creative Commons Licenses. The license type is clearly identified on the article.

##### **The Creative Commons Attribution License**

The [Creative Commons Attribution License \(CC-BY\)](#) allows users to copy, distribute and transmit an article, adapt the article and make commercial use of the article. The CC-BY license permits commercial and non-

##### **Creative Commons Attribution Non-Commercial License**

The [Creative Commons Attribution Non-Commercial \(CC-BY-NC\) License](#) permits use, distribution and reproduction in any medium, provided the original work is properly cited and is not used for commercial purposes.(see below)

##### **Creative Commons Attribution-Non-Commercial-NoDerivs License**

The [Creative Commons Attribution Non-Commercial-NoDerivs License](#) (CC-BY-NC-ND) permits use, distribution and reproduction in any medium, provided the original work is properly cited, is not used for commercial purposes and no modifications or adaptations are made. (see below)

##### **Use by commercial "for-profit" organizations**

Use of Wiley Open Access articles for commercial, promotional, or marketing purposes requires further explicit permission from Wiley and will be subject to a fee.

Further details can be found on Wiley Online Library

<http://olabout.wiley.com/WileyCDA/Section/id-410895.html>

#### **Other Terms and Conditions:**

**v1.10 Last updated September 2015**

**Questions? [customercare@copyright.com](mailto:customercare@copyright.com) or +1-855-239-3415 (toll free in the US) or +1-978-646-2777.**